DEVELOPMENT OF A METHOD FOR CORRELATING INTEGRIN BETA 1 EXPRESSION AND SURFACE CHARACTERISTICS UNDER INDIVIDUAL CELLS

A Thesis
Presented to
The Academic Faculty

By

Meredith A. Myers

In Partial Fulfillment
Of the Requirements for the Degree
Master of Science in Materials Science and Engineering

Georgia Institute of Technology

December 2011

Development of a Method for Correlating Integrin Beta 1 Expression and Surface Characteristics Under Individual Cells

Approved by:

Dr. Barbara D. Boyan, Advisor
School of Materials Science and Engineering, Wallace H. Coulter Department of Biomedical Engineering
Georgia Institute of Technology

Dr. Zvi Schwartz
Wallace H. Coulter Department of Biomedical Engineering
Georgia Institute of Technology

Dr. Ken H. Sandhage
School of Materials Science and Engineering
Georgia Institute of Technology

Date Approved: August 11, 2011

ACKNOWLEDGEMENTS

I would like to thank my advisors, Dr. Barbara Boyan and Dr. Zvi Schwartz, as well as my committee member, Dr. Ken Sandhage, for their guidance and support as I worked to complete my Master's degree. I am appreciative of my fellow Boyan/Schwartz lab members for their friendship and help during the past two years. I am also grateful for my friends in the Clemson family, who have always been there for me to lean on during the hard times and laugh with when times are good. Finally, I would like to especially thank my parents, Mark and Marvine Myers, for their love and support that they have given me throughout my time at Georgia Tech and my entire life. I could not have made it to this point without them, and I am very blessed to have them as a constant in my life. This research was funded by a grant from the National Institutes of Health.

TABLE OF CONTENTS

Page

LIST OF TABLES

LIST OF FIGURES

SUMMARY

Osseointegration, or the direct integration of an implant into bone tissue, is necessary for implant success. Titanium is commonly used clinically in dental and orthopaedic implants because of its passivating oxide layer, which facilitates osseointegration, and its mechanical properties such as a modulus of elasticity similar to bone. Diverse studies have shown that surface microtopography, chemistry, and surface energy affect osteoblast behavior. The problem with these studies is that they access the average behavior of a culture in response to a substrate and not the behavior of individual cells. The objective of this study was to develop a method for correlating the behavior of individual cells with the characteristics of the surface underneath them. More specifically, this work developed a method to correlate integrin beta-1 (β1) expression with the surface characteristics under individual cells. Integrins are cell surface receptors that bind to specific proteins in the extracellular matrix adsorbed on the implant surface. Previous work has shown that expression of certain integrins is increased when osteoblasts on titanium substrates develop a more differentiated phenotype, and that integrin β1 is necessary for osteoblast response to roughness on titanium substrates.

This study used molecular beacons specific to integrin β1 to quantify integrin β1 expression of MG63 cells cultured on titanium disks. A template was designed to coordinate the location of cells using fluorescence microscopy and scanning electron microscopy (SEM) in reference to laser etchings on the disks. After live cell imaging, cells were fixed, dried, and critical point dried for focused ion beam (FIB) milling. Transmission electron microscopy (TEM) sections of cells identified with high and low integrin β1 molecular beacon intensity were milled, and cells with high and low integrin β1 molecular beacon intensity were also serial sectioned. While our TEM results were

inconclusive, SEM images from serial sectioning showed contact points between the cell body and the substrate, consistent with previous results. Cells cultured on pretreatment (PT) or sandblasted acid etched (SLA) titanium surfaces were also serial sectioned, showing that cells on SLA surfaces have more regions of contact between the cells and the substrate than cells on PT surfaces.

This work is significant as it is the first study to develop a method to correlate individual cell behavior with the substrate surface characteristics under the individual cells. Previous studies have reported the average cell behavior in response to their substrates, while this work allows for the study of substrate surface characteristics that positively affect integrin β1 expression in individual cells. Further optimization of the fluorescence imaging process and FIB milling process could be done, and the method developed in this study could be used in future studies to investigate surface characteristics after using other fluorescent analyses of cell behavior, such as immunocytochemistry.

CHAPTER 1

INTRODUCTION

Titanium Implants and Integrins

Integration of implants and bone is necessary for implant success. Osseointegration was first described by Brånemark et al. as an implant's "direct anchorage to the bone tissue".[1] In this study, edentulous jaw implants were allowed at least three months of healing prior to loading and then subsequently observed in a ten year study. Osseointegrated implants showed a greater implant stability and functionality.[1-3] Bone-to-implant contact for osseointegrated implants in canines was approximately 70% after 15 months of healing and 12 months of loading.[4] Clinical studies have shown that implants have a success rate of approximately 99%,[5] and this rate is significantly lower when implants are placed in patients with chronic periodontitis.[6] Titanium is clinically used in dental and orthopaedic implants because of the biocompatibility of its passivating oxide layer, which facilitates osseointegration, and specific mechanical properties such as its modulus of elasticity, which is comparable to bone.[2,7,8]

Studies show that surface microtopography, surface energy, and chemistry affect osteoblast (bone-forming cell) behavior.[9-11] As a result, many modifications to implant titanium have been studied. Changes on the implant surface affect protein adsorption, which can then affect the cells' focal adhesion formation and gene expression.[9,12-14] For example, Olivares-Navarrete et al. demonstrated that the expression of genes such as osteocalcin and transforming growth factor β-1 (TGF-β1) changes on titanium substrates

with varying roughness.[14] *In vitro* studies of MG63 cells, a human osteoblast-like cell line, on titanium with micro- and sub-micro- scale roughness show a decrease in proliferation and an increase in local factor production (alkaline phosphatase, osteocalcin, TGF-β1, and prostaglandin E2 [PGE_2]), indicating that cells become more mature osteoblasts on increasingly rough titanium surfaces.[9,12,13] A similar study using mesenchymal stem cells (MSCs) also showed a more differentiated osteoblastic phenotype as roughness of the titanium surfaces increased.[14] Additionally, cells grown on microrough surfaces produce an osteogenic environment that induces osteoblast differentiation in cells that are not in direct contact with the substrate.[9,14] A modification was developed to create nanoscale surface features on substrates with micro- and submicro- scale roughness.[15] Nanomodified surfaces with microscale roughness caused osteoblasts to have a more differentiated phenotype compared to cells on unmodified surfaces. Microtextured surfaces have also been manufactured under a nitrogen environment to prevent contact with air, creating a hydrophilic surface.[11,16] This change in the surfaces led to an increase in differentiation of cells and an increase in release of factors that stimulate osteogenesis. Titanium implants have also been coated with ceramics to affect cell behavior.[17,18] Hydroyapatite coatings have been extensively explored because of its ability to directly bond with bone.[2] Hydroxyapatite coated microstructured implants increased markers of osteoblast differentiation.[17] Other hydroxyapatite coated titanium beads showed a higher amount of bone bound to them than noncoated titanium beads, as well as an increase in push-out strength, indicating a stronger fixation.[18]

These changes in cellular behavior as the substrate surface changes are largely mediated by integrin binding to the adsorbed proteins on the implant surface.[10,14,19] Integrins form transmembrane heterodimers of alpha and beta subunits that function as

receptors. The extracellular domains of the integrins bind to specific proteins in the extracellular matrix. Different alpha and beta pairs recognize specific amino acid sequences on proteins within the extracellular matrix, stimulating intracellular signaling pathways.[20] Integrin expression varies with the surface characteristics of the culture substrate and the developmental stage of the cell.[20] Osteoblasts on titanium substrates express the α2, α5, αv, β1, and β3 integrin subunits on polished and rough titanium.[21,22] A study by Raz et al. showed the expression of α2 and β1 mRNA to be higher on titanium compared to plastic, while α5 was lower on titanium than plastic.[23] Expression of αv and β3 was the same on both surfaces. The β1 integrin subunit pairs with the α2 and α5 integrin subunits on titanium.[20,23] The α2β1 integrin pair recognizes collagen in the extracellular matrix[24] and is necessary for osteoblast differentiation on microrough titanium surfaces,[10,25] while the α5β1 integrin pair binds fibronectin[26] and is involved with cell attachment and proliferation.[27] Several studies indicate that the integrin β1 is important in mediating the cellular response to titanium by showing that the integrin β1 expression is greater on titanium substrates than plastic and that the expression is higher on titanium substrates with a rough microtopography.[10,19,23] Also, in one of the studies, when the integrin β1 subunit was silenced, osteoblasts lost their ability to detect surface roughness.[19] These findings demonstrate that the integrin β1 subunit is necessary for osteoblast response to roughness of titanium surfaces.

Molecular Beacons

Molecular beacons are used for real-time investigation of mRNA expression in individual live cells. Molecular beacons are hairpin oligonucleotide probes with a fluorophore at one end and a quencher at the other. The loop of the hairpin structure is composed of a sequence complementary to the target mRNA while the stem is composed of two complementary sequences that will not bind to the target.[28] The

hairpin structure forms in absence of the molecular beacon's target, and the fluorophore is quenched in this conformation. Binding of the molecular beacon to its target opens the hairpin structure; the fluorophore is no longer covered by the quencher and is able to emit a fluorescent signal upon excitation.[28] Each MB is designed for a target gene, giving the ability to quantify real-time changes in mRNA in living cells.[29]

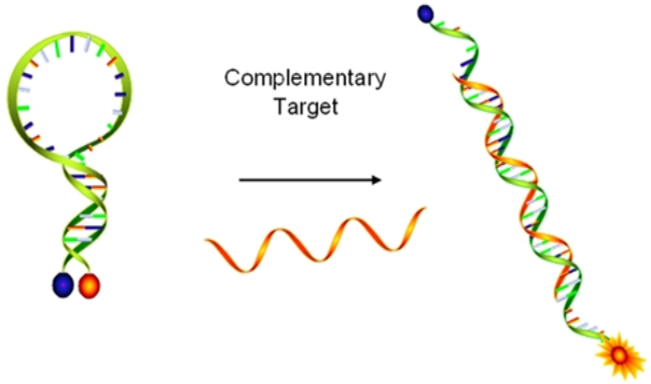

Figure 1: Molecular beacon mechanism. Molecular beacons remain in the closed conformation until they are in the presence of their complementary target. Binding to this target opens the hairpin structure so that the quencher (blue) does not cover the fluorophore (orange), allowing it to emit a signal upon excitation.[30]

Several methods for delivering molecular beacons exist, including those based on transfection, reversible permeabilization, peptide linking, electroporation, and microninjection.[31,32] Transfection is a technique traditionally used to introduce DNA into cells; however, it is not considered to be highly efficient because of possible DNA degradation by lysosomes.[33] Peptide linking conjugates a peptide with the capability to pass through the cell membrane to the molecular beacon.[32] This technique increases the complexity of beacon synthesis and may also lead to endocytosis and beacon degradation.[31] Electroporation requires high-intensity electric pulses to be delivered to

cells, which may damage the cells.[34] Microninjection may also damage the cells, and is also not useful for studying large numbers of cells.[35] Reversible permeabilization offers high delivery efficiency in a non-endocytic manner, and in a shorter time than other methods.[36] Streptolysin O (SLO) is used for reversible permeabilization of cells for molecular beacon delivery.[36,37] This bacterial toxin attaches to the cell membrane and forms pores within the membrane, allowing the beacons to diffuse into the cytosol.[37] Cells are incubated in serum containing media with SLO and the molecular beacon for 10-15 minutes, and then cells are resealed in a further incubation in serum containing media.[36]

Molecular beacons are advantageous tools for gene expression analysis due to their ability to monitor specific mRNA expression in individual live cells. Immunocytochemistry cannot be used to study mRNA expression in live cells because of the necessity to fix cells before probe delivery and to remove unhybridized probes.[28] While real-time PCR and Western blot may also be used to assess integrin mRNA expression and protein presence, these techniques do not allow for single cell analysis or analysis at early culture time points, as they require a large number of cell lysates. Single cell PCR techniques allow for gene analysis in single cells, however this technique does not allow for live cell analysis or for cells to be localized on their substrates for further study.[38]

Lennon et al. designed a molecular beacon specific to the β1 integrin subunit mRNA and developed a method for imaging molecular beacons on opaque substrates showing that integrin β1 expression at early culture time points, in pre-confluent MG63 cells, is substrate-dependant.[39] The specificity of this molecular beacon has been confirmed by real-time PCR, immunofluorescence, and *in-situ* hybridization of integrin β1 silenced cells. Molecular beacons in individual, living cells could be imaged and

quantified on titanium substrates. Through single cell quantification of molecular beacon intensity, integrin β1 expression increased significantly in these pre-confluent studies as surface roughness increased, indicating that integrin β1 is involved in the cell response to its substrate at pre-confluent and confluent time points.[19,39]

The Use of FIB in Material Characterization

Before becoming extensively used in materials research, the semiconductor industry used focused ion beam (FIB) microscopes for circuit repair and failure analysis.[40,41] More recently, the FIB technique has been used to examine cross sections of materials and prepare site-specific transmission electron microscope (TEM) samples.[42,43] FIBs use a source of gallium ions at high currents for milling; dual beam FIBs have a scanning electron beam column integrated in one machine for simultaneous imaging and milling.[42]

FIB milling has been used for characterizing biomaterials; the oxide layer on a titanium dental screw has been analyzed using bright field and high-resolution TEM.[44] On *in situ* prepared TEM samples, the titanium oxide layer and deposited platinum layers were clearly seen and mapped, and the oxide layer was determined to be TiO_2 by x-ray photon spectroscopy (XPS). Lattice fringe imaging was also performed using high-resolution TEM, and the oxide layer was rutile TiO_2. It was demonstrated that the FIB would be a useful tool for investigating biomaterials, including those with irregular surface geometry.

The first reports of using FIB on biological samples came in late 2004 and early 2005 when the digestive gland system and gland epithelial cells of terrestrial isopods were observed.[45,46] These two studies by Drobne et al. demonstrated that it was possible to perform site-specific serial sectioning and imaging of gland and cell

ultrastructure in non-embedded samples. Further studies examined the interface between cells and various substrates, such as poly(methyl methacrylate) (PMMA),[47] coated glass coverslides,[48] hydroxyapatite,[49] and titanium films.[50] When MG63 cells were cultured on nanopatterned PMMA, focal contacts between the cells and the surfaces and non-soluble extracellular matrix components were seen on milled samples.[47] This observation confirmed that FIB could be a valuable tool in the study of cell-substrate interfaces. Neural cells were cultured and observed on protein adsorbed platinum coated glass coverslips and poly(lactic acid-co-glycolic acid) fiber coated glass slides, and serial sectioning through the cells showed changes in cell attachment and allowed for cell-substrate interface analysis.[48] However, subcellular structures could not be seen clearly enough for investigation. The FIB was used to prepare TEM samples of monocyte-like cells cultured on hydroxyapatite disks.[49] Despite the material differences between the ceramic substrate and the cell, the FIB milled samples of uniform thickness, and the cell-substrate boundary was visible. We believe that this would leave the interfaces available for further analysis. MSCs and osteoblasts have been studied on titanium foils.[50] Top-down milling was used to mill single cells while side-on milling was used to produce sections of cells; both preserved the cell morphology. During TEM analysis, little of the cell ultrastructure could be seen; however, the titanium oxide layer at the interface was clearly visible and was mapped using energy-dispersive x-ray spectroscopy (EDS). All of these studies show that the FIB is a useful tool for studying individual cells and the interactions between cells and their substrates.

When observing the behavior of cells cultured on a given substrate, most studies look at the average cell behavior of the culture and not the behavior of individual cells. This study develops a method to use molecular beacons to assess integrin β1 expression in individual cells and FIB mill the substrate of these cells, allowing for the

cell specific correlation of substrate surface characteristics with cells that have high and low integrin β1 expression. From this, we will see how titanium surface characteristics will affect the integrin β1 expression of individual cells.

SPECIFIC AIMS AND EXPERIMENTAL DESIGN

The **objective** of this project is to develop a method to correlate surface properties with integrin β1 expression of individual cells and to determine how surface properties affect integrin β1 expression of individual cells.

The overall **hypothesis** is that cell-specific surface characteristics such as microtopography and chemistry will affect integrin β1 expression.

Aim 1: Develop a method to identify individual cells using fluorescence microscopy and scanning electron microscopy (SEM).

Aim 1.1: Design a template to locate individual cells on the fluorescence microscope and on the SEM. The **objective** of this aim was to create a reference system so that the locations of cells could be coordinated on the fluorescence microscope and on the SEM and to fluorescently stain the cell membranes so that cell morphology could be seen and imaged to allow for confirmation of cell identity on the SEM.

Aim 1.2: Use FIB to interrogate substrate characteristics under individual cells. The **objective** of this study was to use FIB milling to create samples of the titanium substrates so that surface characteristics of the substrate under individual cells may be investigated.

Aim 2: Correlate integrin β1 expression with substrate surface chemistry and microtopography in individual cells. The **hypothesis** is that surface characteristics will affect integrin β1 expression of individual cells.

CHAPTER 2

METHODOLOGY

Disk Preparation and Coordinate Validation

All disks were fabricated by Institut Straumann AG as part of their responsibilities in a collaborative project funded by United States Public Health Service Project AR052102. PT, or pretreatment, disks, with a R_a<0.2µm, were notched using a Dremel® tool (Mt. Prospect, IL). Using the clock system as a reference, notches were cut in the disks at 12 o'clock, 3 o'clock, 6 o'clock, and 9 o'clock, with the notch at 12 o'clock being larger than the other three notches. Disks were then indented at the corners of each of the four notches using a DM 400F LECO hardness tester (St. Joseph, MI) with 1kg of weight for 15 seconds (Figure 2A). The notches and indents were observed on a Leo 1530 SEM and the DeltaVision Deconvolution microscope (Applied Precision LLC, Issaquah, WA). The indents were used as coordination points to find cells on the disks. The disks were then cleaned in sequential ultrasonic baths of Micro-90 (International Products Corporation, Burlington, NJ), acetone, isopropyl alcohol, ethanol, and deionized water. The disks were the sterilized by autoclave before cell plating. An insert for the two well chamber slides was designed to hold the disk in place and stabilize the system during imaging (Figure 2B, D).

PT and sandblasted acid etched (SLA) disks were also laser etched in collaboration with Institut Straumann AG (Figure 2C). Laser etchings were observed on a Hitachi S800 SEM (Tokyo, Japan) and the DeltaVision Deconvolution microscope. The corners of the etchings were used as coordination points to find the cells on the disks. The laser etching coordinate system was validated by first FIB milling a mark near the middle of one of the laser etched PT disks. The location of this trench on the

DeltaVision was recorded, and the coordinate system was used to locate the trench subsequently on the FIB. The distance the mark was from the center of the viewing space was recorded, and after the disk was moved within the FIB chamber, the mark was subsequently located. This was repeated six times to determine the error of the laser etching coordinate system.

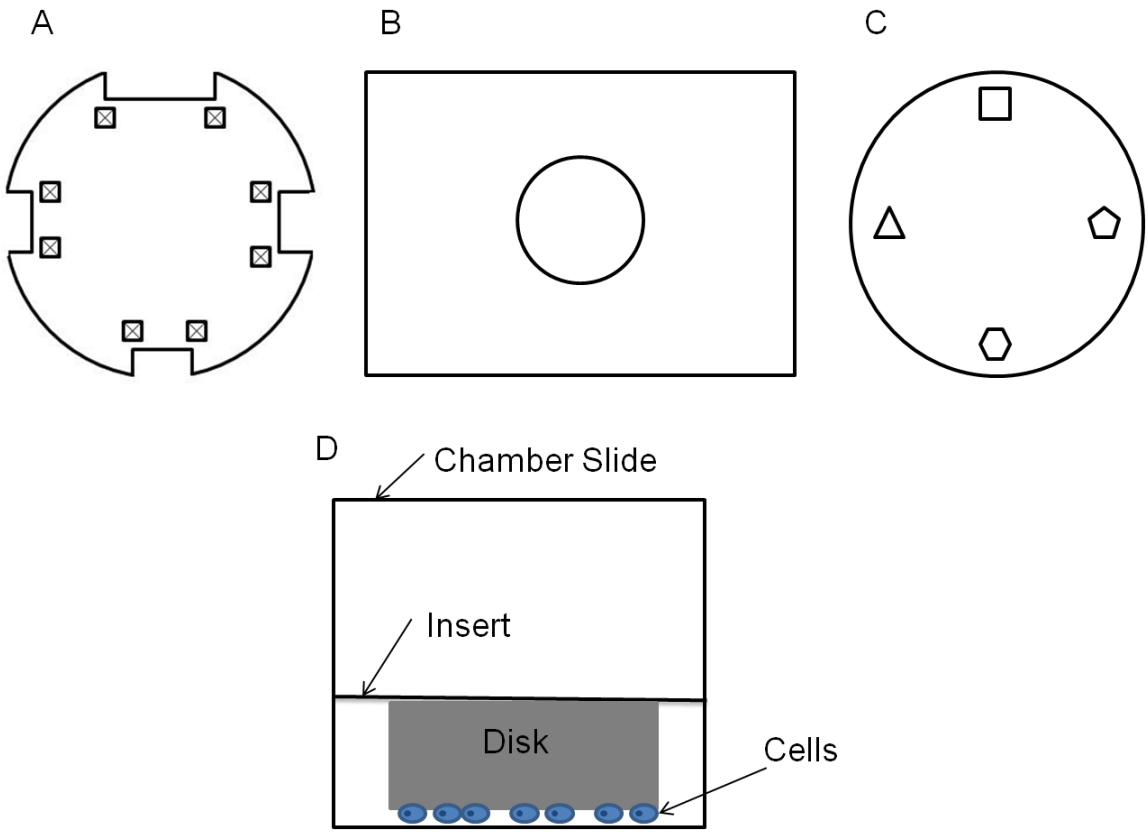

Figure 2: Schematic of system for referencing specific cells on titanium disks. **(A)** Schematic of the notch and indent referencing system. **(B)** Schematic of the two well chamber slide insert. **(C)** Schematic of the laser etching referencing system. **(D)** Schematic of setup for fluorescence imaging.

Cell Culture

Human osteoblast-like MG63 cells (American Type Culture Collection) were plated at a density of 10,000 cells/cm^2 on titanium disks or glass four well chamber

slides (Nalge Nunc, Rochester, NY) and cultured for 72 hours. The cells were fed with Dulbecco's modified Eagle medium (DMEM) (Cellgro, Manassas, VA) supplemented with 10% fetal bovine serum and 1% penicillin-streptomycin (Invitrogen, Carlsbad, CA) 24 and 48 hours after plating. At 72 hours after plating, the molecular beacons were delivered to the cells for imaging according to one of the protocols described below.

Molecular Beacon Delivery

A molecular beacon, MB639, that was previously shown to be specific for the beta-1 subunit was used for this study.[39] The molecular beacon, sequence cgacgAGTAATCCTCCTCATTTCAcgtcg (Biosearch Technologies), was delivered to the cells via Streptolysin O (SLO) reversible permeabilization. SLO, 2U/mL, (Sigma Aldrich, St. Louis, MO) was activated with 5mM tris(2-carboxyethyl)phosphine (TCEP) (Sigma Aldrich) for 30 minutes – 1 hour at 37^{o}C. The cells were incubated for 15 minutes in 500µL of phenol red free serum free media (Invitrogen) containing 0.1 U/mL of the activated SLO and 1µM of the MB639 solution. Post delivery, cells were washed three times with phenol red free serum containing media (Invitrogen). Cell membranes were allowed to reseal during a 30-minute incubation at 37^{o}C in 500µL of serum containing media with 1µg/mL Hoechst 33342 for staining the cell nuclei (Invitrogen). Live cell fluorescence imaging was performed using the DeltaVision Deconvolution Microscope with an Olympus 60X Plan Apo N lens (Center Valley, PA), numerical aperture 1.42, and a CoolSNAP_HQ2/ICX285 camera. Images were collected at 0.2 µm z intervals with an exposure time of 0.05 seconds with the Hoechst 33342-DAPI filter 350/460nm for the nuclear staining and an exposure time of 0.7 seconds with the Quasar570-Cy3 filter 545/570nm for the molecular beacon imaging. The molecular beacon intensity was quantified by making a projection of the cell and summing the intensity from each projection in the image stack and removing the background signal[39].

Staining the Cell Membrane

Two stains were tested to allow the cell morphology to be seen fluorescently. First, three dilutions of the Alexa Fluor® 350 phalloidin stain (Invitrogen) and Hoescht nuclear stain were tested: 1µg/mL phalloidin stain only, 1µg/mL phalloidin stain with 1µg/mL nuclear stain, and 0.1µg/mL phalloidin stain with 0.1µg/mL nuclear stain. After molecular beacons were delivered to cells cultured on glass or PT disks, the phalloidin staining was done with the addition of 1µg/mL of Oregon Green® 488 phalloidin stain (Invitrogen) after the nuclear staining/membrane resealing step in serum free media.

The Vybrant® Alexa Fluor® 488 Lipid Raft Labeling Kit (Invitrogen) was also tested for staining the cell membrane. The staining was done prior to beacon delivery. The fluorescent cholera toxin subunit B (CT-B) conjugate was delivered to the cells 1µg/mL in serum free media for 10 minutes. Cells were washed three times with serum free media before a 15-minute incubation with the anti-CT-B antibody in serum free medium. Cells were washed three times with serum free media prior to beacon delivery.

The Oregon Green® 488 Phalloidin stain and the Vybrant® Alexa Fluor® 488 Lipid Raft stain were imaged on the DeltaVision using the green fluorescent protein (GFP) filter 470/525nm with an exposure time of 0.5 seconds. The Alexa Fluor® 350 phalloidin stain was imaged using the Hoechst 33342-DAPI filter 350/460nm with an exposure time of 0.05 seconds.

Studying the Effects of Culture Time on the Cells

Cells were cultured on PT disks for 48, 72, and 120 hours. At the end of the culture period, molecular beacons were delivered to the cells and the cell membranes were stained using the lipid raft stain. Samples were imaged on the DeltaVision Deconvolution Microscope and then prepared for SEM as described below. Samples were imaged on an Ultra 60 field emission SEM (Zeiss, Peabody, MA).

Studying the Effects of the Dehydration Medium on the Cells

Cells were either stained and permeabilized with SLO or left with no treatment. After fixation, cells were dehydrated in ethanol or acetone, 15%, 30%, 45%, 60%, 75%, 90%, and 100% for 24 hours at each concentration. Samples were then dried in a dessicator and gold coated for SEM.

Studying the Effects of SLO, Lipid Raft Stain, and Temperature on the Cells

Cells were either stained with the lipid raft stain, permeabilized with SLO, or stained and permeabilized. After staining/permeabilization, the cells were fixed and prepared for SEM as described below. Another set of samples were treated in the same three groups and then re-incubated for 24 hours at 37^{o}C. After re-incubation, the cells were fixed and prepared for SEM as described below.

Another set of samples was tested to see how temperature affected cells with the other treatments. Cells with no treatment, lipid raft staining only, SLO permeabilization only, or lipid raft staining and SLO permeabilization were left at room temperature for 1.5 hours. Other cells were stained, permeabilized and re-incubated at 37^{o}C for 1.5 hours or stained, permeabilized, or fixed immediately after the membrane resealing step. After the 1.5 hours in room temperature or re-incubation, the cells were fixed and prepared for SEM as described below.

Studying the Effects of Cell Fixation Prior to Imaging

GFP transfected MG63 cells were cultured on a PT disk. After 72 hours, MB639 was delivered to these cells and they were imaged on the DeltaVision Deconvolution Microscope. The sample was then prepared for and imaged on the SEM.

MB639 or a random molecular beacon (RMB), sequence cgtcgCAGATACACTTCAGATAGGATcgacg (Biosearch Technologies), was delivered to the cells. Samples were then washed three times with phosphate buffered saline (PBS) and fixed for one hour at 4^{o}C with Karnovsky's Fixative Solution (Electron Microscopy

Sciences, Hatfield, PA) or for ten minutes at -20°C with 50:50 v/v methanol:acetone. After fixation, lipid raft staining was done in PBS. The cells were then imaged on the DeltaVision Deconvolution Microscope. Samples were prepared for and imaged on the SEM after fluorescence imaging.

MB639 or RMB were also delivered to cells cultured on glass disks. After molecular beacon delivery, samples were washed three times with PBS, fixed at room temperature for 10 minutes in 95% ethanol, 10% buffered formalin, or 4% paraformaldehyde. After fixation, lipid raft staining was done in PBS and the cells were imaged on the DeltaVision Deconvolution Microscope.

Studying Cell Adhesion during Imaging

Cells were cultured on laser etched disks for 72 hours. MB639 was delivered to the cells, and coordinates of cells and the corners of the laser etchings were found on the DeltaVision Deconvolution Microscope. Samples were then prepared for SEM and FIB as described below. When preparing for fixation, rinsing the sample with PBS only once instead of three times was also tested. Other samples were fixed in the imaging set-up (insert and disk in a two well chamber slide) for 30 minutes before the disk was removed from the chamber slide and fixed overnight. To test how to prevent cells from attaching to the glass chamber slide during imaging, chamber slides were sprayed with Teflon® spray (Miller-Stephensen, Danbury, CT) or coated with Sigmacote® (Sigma-Aldrich) prior to fluorescence imaging.

Studying the Effects of Using a Spacer during Fluorescence Imaging

Aluminum foil, 10 µm thick, and polycarbonate, 200 µm thick, were tested as spacers to raise the insert and disk off the chamber slide glass during imaging. To initially test if the spacers would work, the laser etchings were viewed using the 60X

Plan Apo N lens and the Olympus 40X and 60X LUC Plan FLN lenses, numerical apertures 0.6 and 0.7, respectively. Cells were then cultured on laser etched disks for 72 hours. MB639 was delivered to the cells, and cells were imaged using 40X and 60X Plan FLN lenses. Coordinates of cells and the corners of the laser etchings were found on the DeltaVision Deconvolution Microscope. Samples were then prepared for SEM as described below.

Scanning Electron Microscopy, Focused Ion Beam Milling, and Transmission Electron Microscopy

Cells were washed three times with PBS and fixed overnight in 1mL Karnovsky's fixative solution (Electron Microscopy Sciences). Cells were then washed three times with PBS and dehydrated in a sequential acetone, isopropyl alcohol, or ethanol dehydration with samples being dehydrated in each concentration (15%, 30%, 45%, 60%, 75%, 90%, and 100%) for 1-2 hours. Samples were then dried over the critical point of CO_2 in an E3000 Critical Point Dryer (Quorum Technologies, Ontario, Canada) using acetone, in an Automegasamdri - 915B Critical Point Dryer (Tousimis, Rockville, MD) using isopropyl alcohol, or in an EMS850 Critical Point Dryer (Electron Microscopy Sciences) using ethanol. After drying, samples were gold coating using a SC7640 Polaron Sputter Coater (Quorum Technologies) for 2 minutes with a current of 18mA and a voltage of 2.2V. Cells were imaged using a Hitachi S800 SEM unless otherwise noted.

Once a method for cell preparation was finalized, samples were milled using a Nova Nanolab 200 FIB/SEM (FEI, Hillsboro, OR). Individual cells imaged on the DeltaVision were found on the FIB/SEM using the notch and indent or laser etching referencing system. This was done using an affine transformation implemented in Matlab (version R2010a, Mathworks, Natick, MA). The affine transformation allowed for corrections of differences in magnification of the two microscopes, inversion between the

fluorescence microscope and the SEM, and rotation of the disk going between the two microscopes. The sample was tilted 52^{o} and milling was done with gallium ions with a beam current between 0.1nA and 1.0nA. Cells were serial sectioned with milling steps of 500nm – 2µm to observe how the cell attached to the disk. Three-dimensional (3D) reconstructions of the cells were done using Matlab (Mathworks). Analysis of the number of contact points between the cells and the surfaces and the distance of contact between the cells and the surfaces in the serial sectioning images was performed using Image J (National Institutes of Health, Bethesda, MD).

For TEM sections to be milled on the FIB, a thin layer of platinum was first deposited at 0.5nA for sample protection (Figure 3A). Regular cross sections were milled on both sides of the region of interest using a beam current of 20nA, and then cleaning cross sections were milled at 3nA (Figure 3B). All cross sections were milled at 52^{o}. The sides and bottom of the sample were milled using a current of 1nA (Figure 3C) before the micromanipulator (Omniprobe®, Dallas, TX) was welded to the sample using platinum at 0.1nA. The remaining attachments connecting the section to the disk were milled at 0.5nA before the sample was lifted out (Figure 3D). The sample was then welded to a three post copper TEM grid (Omniprobe®), using platinum at 0.5nA (Figure 3E, F). After welding, the section was thinned to approximately 500nm using decreasing currents of 3nA, 1nA, and 0.5nA. Electron transparent TEM sections were examined using a Jeol JEM 100CX-II TEM (JEOL, Ltd., Tokyo, Japan) at 100kV.

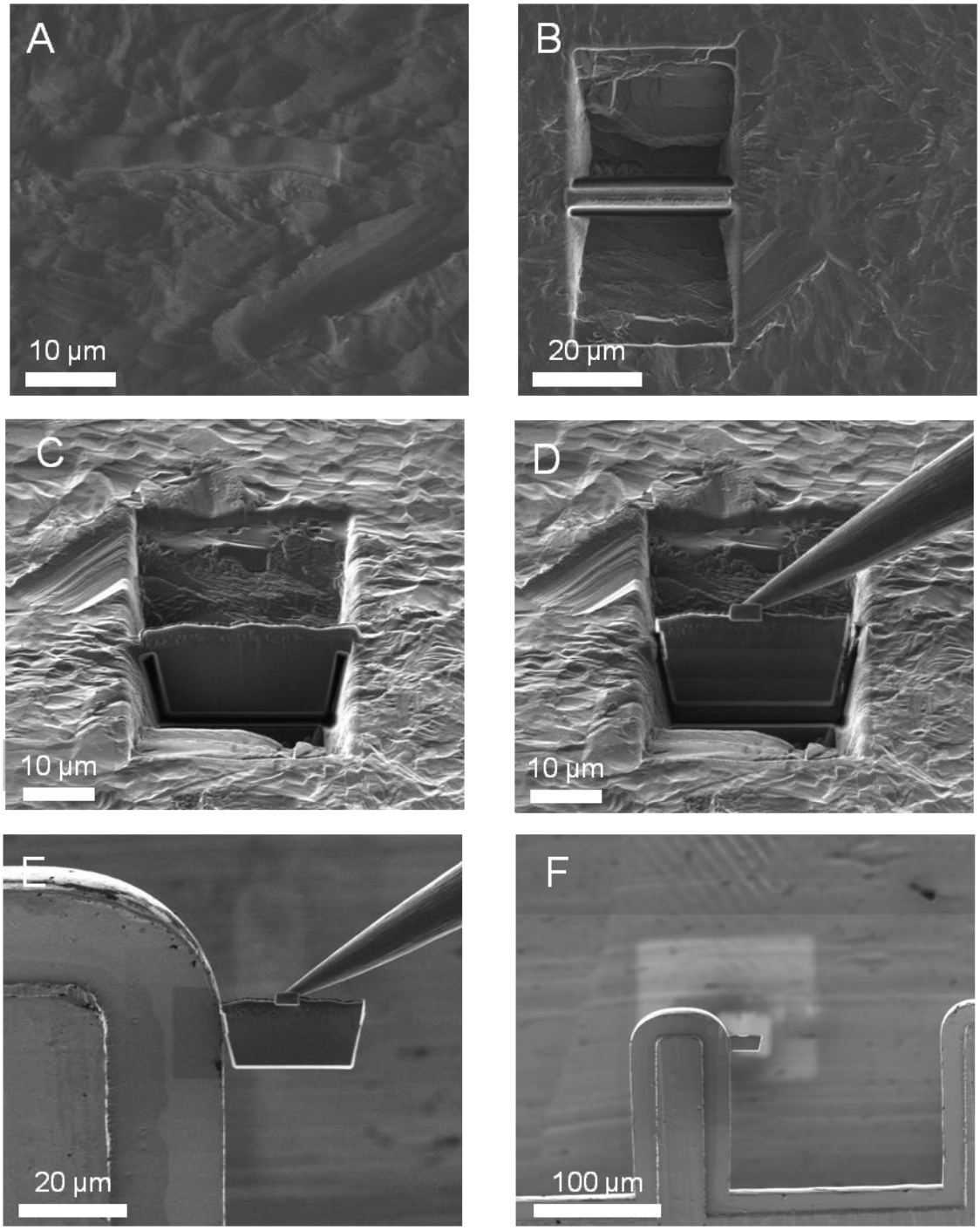

Figure 3: FIB milling a TEM cross section. **(A)** Protective platinum layer at the area of interest. **(B)** Trenches milled on opposing sides of the sectioned area of interest. **(C)** Section attached to the bulk sample prior to lift out. **(D)** Section welded to the micromanipulator for lift out. **(E)** Section before welding to a TEM grid. **(F)** Section attached to a TEM grid.

CHAPTER 3

RESULTS AND DISCUSSION

In the present study, a method for correlating integrin β1 expression with surface characteristics under individual cells was developed. We began by developing a template to coordinate the location of individual cells on the fluorescence microscope and on the FIB/SEM. Fluorescent stains for staining the cell membrane and the process of fluorescence imaging were studied to optimize the system prior to FIB milling TEM sections and serial sectioning high β1 molecular beacon intensity cells, low β1 molecular beacon intensity cells, and cells cultured on PT and SLA surfaces. While most studies look at the average behavior of cells cultured on a given substrate, this study created a method to allow for observing cell behavior of individual cells with respect to the surface characteristics of the substrate under these cells.

Disk Preparation and Coordinate Validation

Titanium disks were either (1) notched and indented, or (2) laser etched to allow for coordination of individual cells on the disks. The indents measured approximately 60-80 μm along the side, and the indents were seen and imaged on both the SEM and the DeltaVision Deconvolution Microscope (Figure 4A-C). The notches that were cut into the disks were easily located on the SEM (Figure 4B). Around the notches, debris from cutting the notches with the Dremel® was seen, and this debris cast a shadow on the disk surface when viewing on the SEM (Figure 4D). When the disks were laser etched, the corners of the etchings were easily identified on the DeltaVision (Figure 4E) and on the SEM (Figure 4F). After a mark was FIB milled on one of the PT disks

(Figure 5A), this mark was located on the fluorescence microscope (Figure 5B) before using the coordinate system for subsequent location on the FIB (Figure 5C). The coordinate validation showed that the mark was 109.54 +/- 14.65 μm (SEM) from the coordinates obtained with the referencing system and Matlab program; this distance is approximately one and a half times the length of a well-spread MG63 cell. The accuracy of this system could be improved by having the reference points closer to the cells instead of hundreds of microns away from the cells. Instead of placing four laser etchings near the edge of the disks, smaller etchings could placed closer together, and cells within this smaller area could be coordinated.

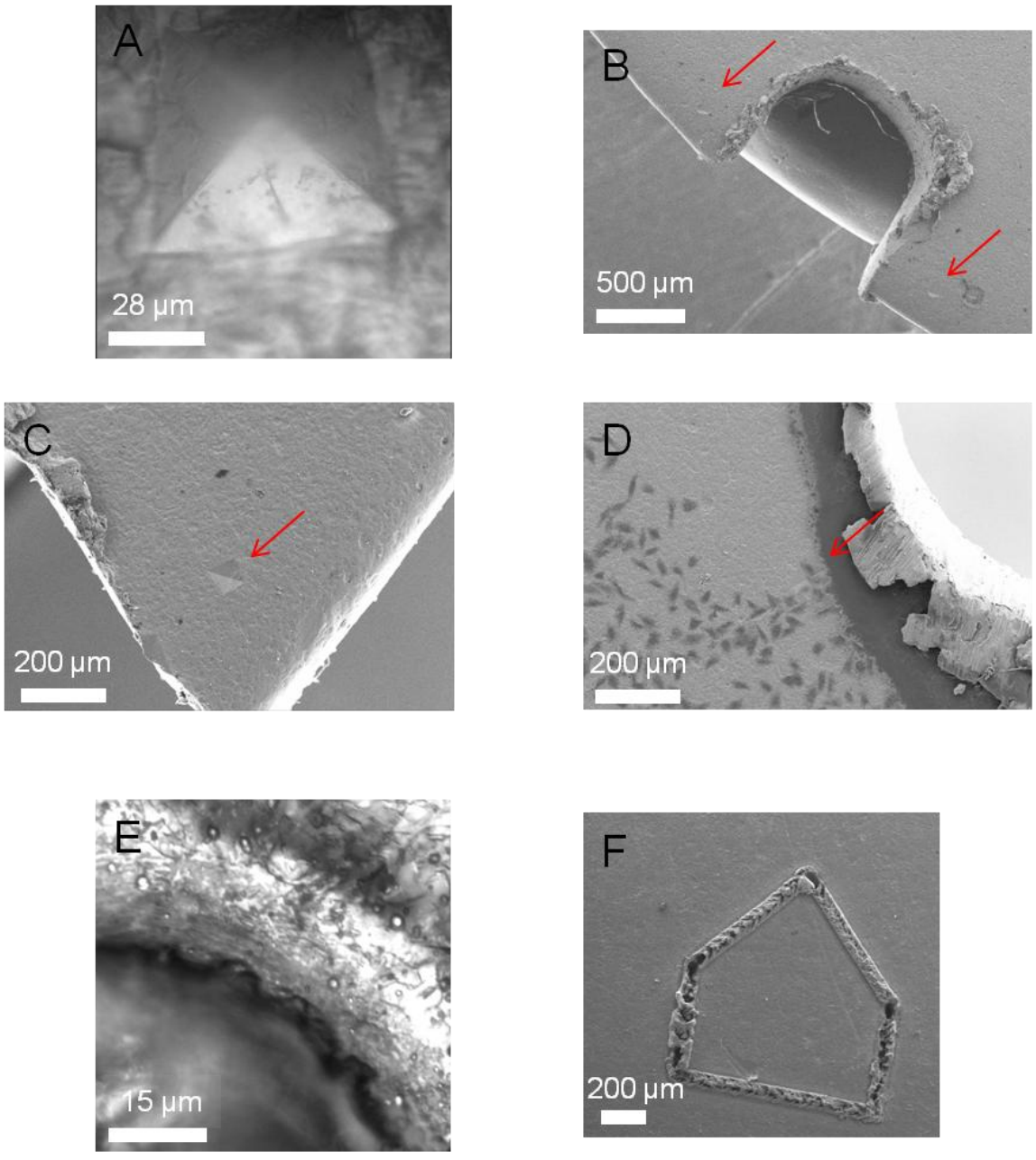

Figure 4: Visualization of the disk coordination system. **(A)** Indent as seen on the DeltaVision Deconvolution Microscope. **(B)** Notch as seen on the SEM. Indents are indicated by the arrows. **(C)** Indent on the SEM, indicated by an arrow. **(D)** Debris from cutting the notch seen on the SEM. Indent indicted by an arrow. **(E)** Corner of an etching as seen on the DeltaVision Deconvolution Microscope. **(F)** Laser etching as seen on SEM.

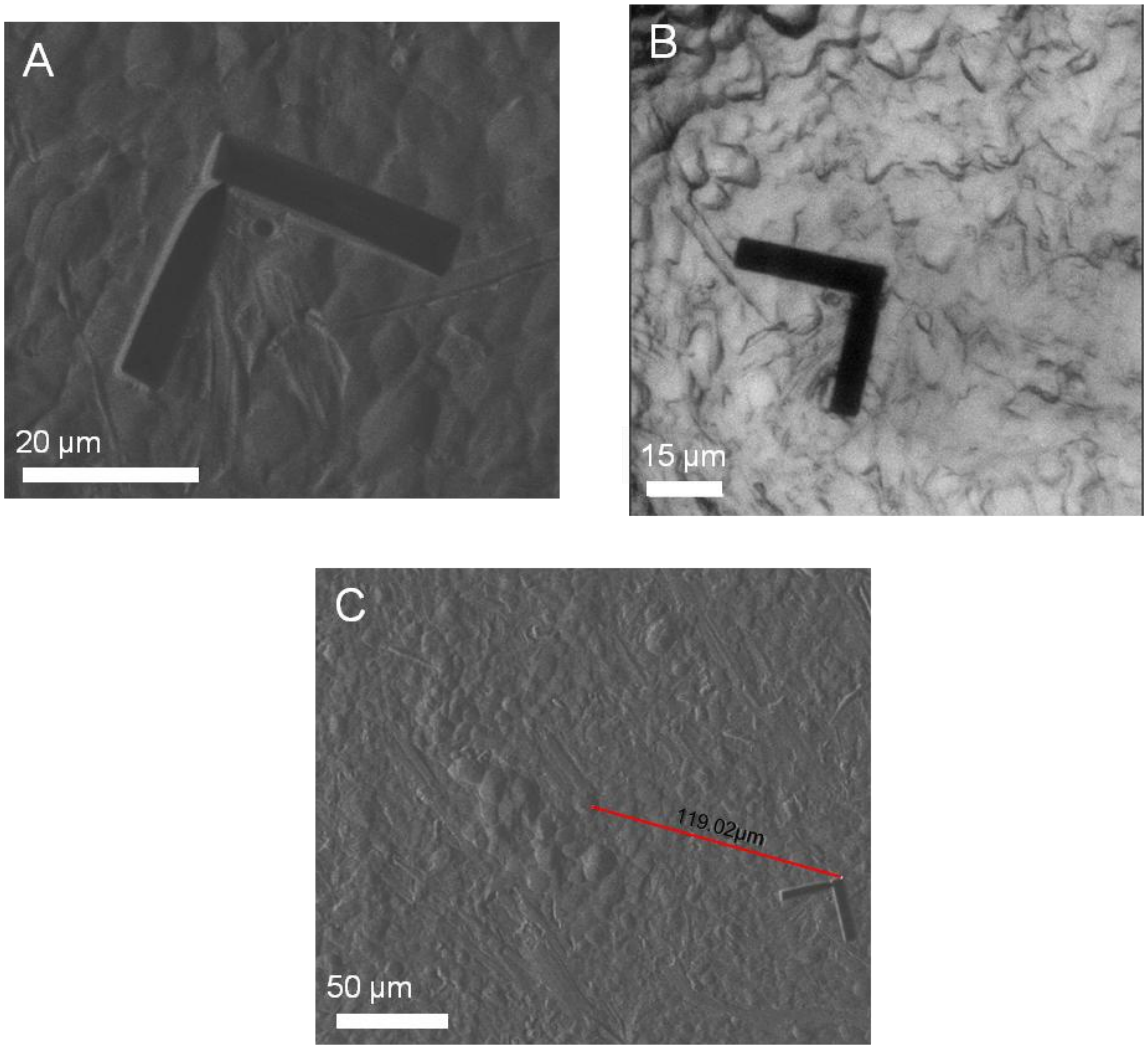

Figure 5: Laser etching coordinate system validation. **(A)** Test mark milled on the FIB. **(B)** Mark as seen on the DeltaVision Deconvolution Microscope. **(C)** Location of the mark compared to point coordinated from the laser etching template and Matlab program.

Staining the Cell Membrane

Alexa Fluor® 350 Phalloidin stain and the Vybrant® Alexa Fluor® 488 Lipid Raft Labeling Kit were tested to determine which showed the cell morphology most clearly on the DeltaVision. Using 1µg/mL of the phalloidin stain, the cell shape was seen, however the lack of contrast between the signal and the background did not allow the cell shape to be seen clearly (Figure 6A). Using 1µg/mL of phalloidin stain and nuclear stain, the

cell morphology was seen and the contrast between the membrane and the background was higher than using 1µg/mL phalloidin stain or 0.1µg/mL phalloidin stain and nuclear stain (Figure 6B). When 0.1µg/mL phalloidin stain and nuclear stain was used, the cell morphology was not seen at all (Figure 6C). When 1µg/mL Oregon Green® 488 Phalloidin stain was used after molecular beacon delivery, the cell membrane was not seen when cells were cultured on glass (Figure 6D – F) or PT disks (Figure 6G – I).

Staining was also done before molecular beacon delivery using the Vybrant® Alexa Fluor® 488 Lipid Raft Labeling Kit, and the cells were imaged on glass and PT disks using this method. On glass, the lipid raft stain showed whether the cells were round or well spread with filopodia attaching to the surfaces; the beacons could also be seen (Figure 6J – L). On PT, the beacons could be seen along with the lipid raft stain (Figure 6M – O). Cells imaged on PT appeared to be less spread than on glass, with only a few extensions to the surface.

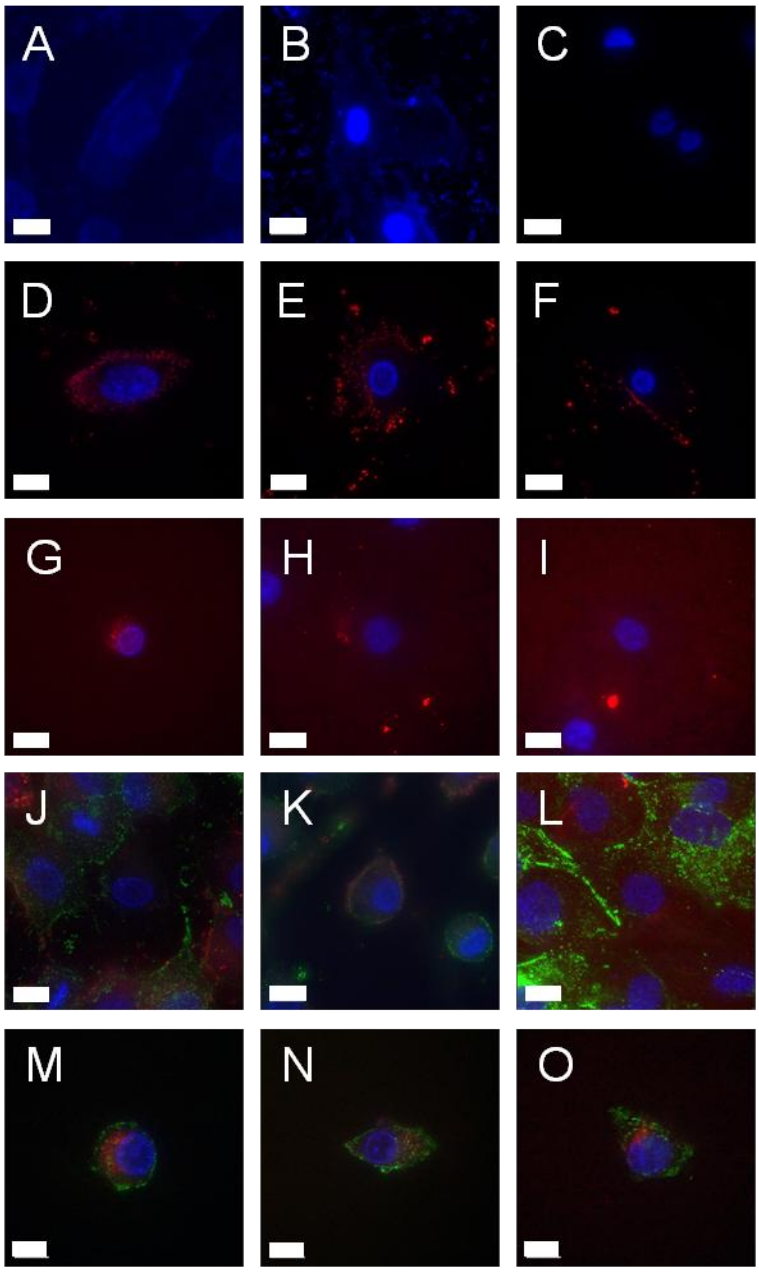

Figure 6: Staining the cell membrane using phalloidin stain and lipid raft labeling. Scale bar represents 15µm. **(A)** MG63 cells cultured on glass stained with Alexa Fluor® 350 Phalloidin Stain:1µg/mL phalloidin stain, 1µg/mL phalloidin stain and 1µg/mL Hoechst 33342 nuclear stain, and 0.1µg/mL phalloidin stain and 0.1µg/mL Hoechst 33342 nuclear stain. **(D)-(F)** MG63 cells cultured on glass stained with 1µg/mL phalloidin stain and 1µg/mL Hoechst 33342 nuclear stain and with MB639. **(G)-(I)** MG63 cells cultured on glass and PT disks stained with 1µg/mL phalloidin stain and 1µg/mL Hoechst 33342 nuclear stain and with MB639. **(J)-(L)** MG63 cells cultured on glass stained with Vybrant® Alexa Fluor® 488 Lipid Raft Labeling Kit and MB639. **(M)-(O)** MG63 cells cultured on PT disks stained with Vybrant® Alexa Fluor® 488 Lipid Raft Labeling Kit and MB639.

Fluorescent phalloidin derivatives, such as Alexa Fluor® 350 and Oregon Green® 488, exist for staining actin in fixed and living cells.[51,52] However, because of phalloidins inability to permeate cell membranes and their toxicity, they are not frequently used in live cells.[51] Previous studies have used phalloidin staining in live cells, where the phalloidin was delivered via cell permeabilization; however, only approximately 33% of the cells remained viable one hour after staining.[52] Our results showed that the phalloidin stains did not work when combined with the beacon delivery and imaging. Even though phalloidin stain has been shown to work in live cells previously,[52] we believe the phalloidin stain did not work when combined with molecular beacons because of the toxic nature of phalloidins[51] and because the stain was in the cell approximately two hours during fluorescence imaging. The stain was also delivered during the resealing step after beacon delivery instead of during the permeabilizing step to minimize the stain's time within the cell. In the fluorescence imaging system used in this study, it was necessary for cells to remain viable during imaging, because molecular beacons have been tested and designed for use in living cells.[28,35]

Several studies have shown that lipid raft labeling has been done using a fluorescently tagged cholera toxin subunit B in live cells that were fixed before fluorescence imaging[53] or for live cell imaging.[54] Lipid raft stain was used in live cell laser scanning confocal microscopy when cells were cultured on coverslips and imaged in a live cell perfusion chamber.[54] Despite differences in the imaging system, our results showed that lipid raft staining was also successful at allowing the cell morphology to be seen fluorescently with molecular beacons.

FIB Method Test

After fluorescence imaging and preparation for SEM, a disk was observed and milled on the FIB/SEM using the notch and indent referencing system to find the desired cell. A cell that was imaged fluorescently was identified on the FIB using the coordinates from the notch/indent system and the identity was confirmed from the fluorescent image (Figure 7A). When imaged using the FIB/SEM, this cell was rounded and not spread out on the disk (Figure 7B). Serial sectioning through the cell showed that the cell was not in continual contact with the surface but instead contacted the surface through extensions or filopodia (Figure 7C-F).

Previous studies showed that after 3 days of culture, MG63 cells on PT disks should be relatively flat with a few extensions.[16] However, the cell sectioned on the FIB was rounded. After making this observation, thorough testing began to see what was causing the cells to not appear spread when imaged on the SEM and how this could be prevented.

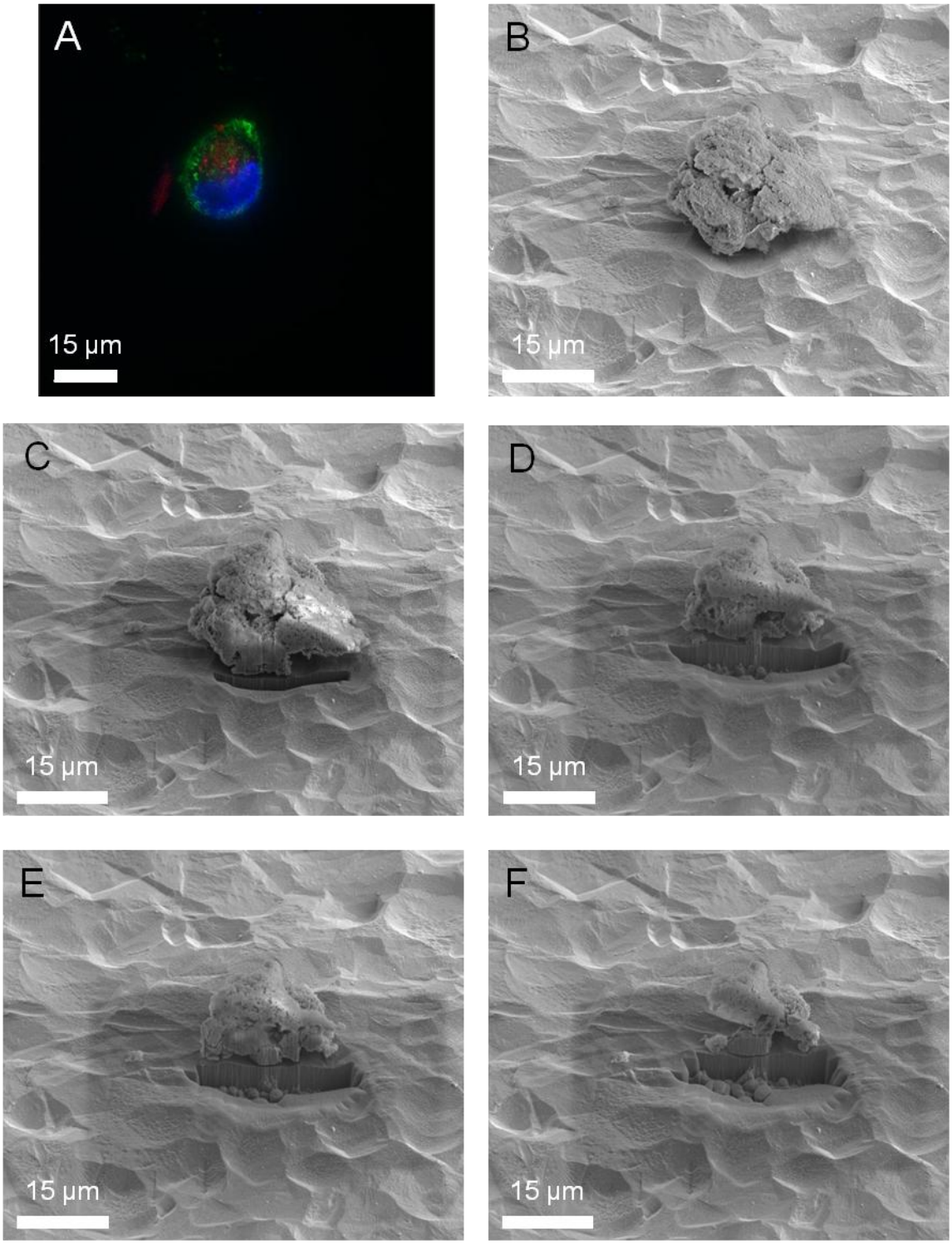

Figure 7: FIB serial sectioning through a cell. **(A)** MG63 cell image fluorescently. **(B)** The same cell identified on the FIB using the coordinates system. **(C)-(F)** Serial sectioning through the cell.

Studying the Effects of Culture Time on the Cells

Cells were cultured for 2, 3, and 5 days to determine how culture time affected cell spreading. After 2 days of culture, cells did not appear to be spread when imaged on the fluorescence microscope, as the lipid raft stain did not show any cell extensions (Figure 8A - C). After 3 days of culture, the cells were more spread than after 2 days, and this was seen by the fluorescent staining showing that the cells took up a larger area of the surface (Figure 8F - H). After 5 days of culture, cells had nearly grown to confluence, and it was difficult to see the cell morphology and image individual cells on the fluorescence microscope (Figure 8K - M). For each time point, no cells were apparent when the samples were observed on the SEM at lower magnifications (Figure 8D, E, I, J, N, O). At high magnifications, cell debris was seen and imaged.

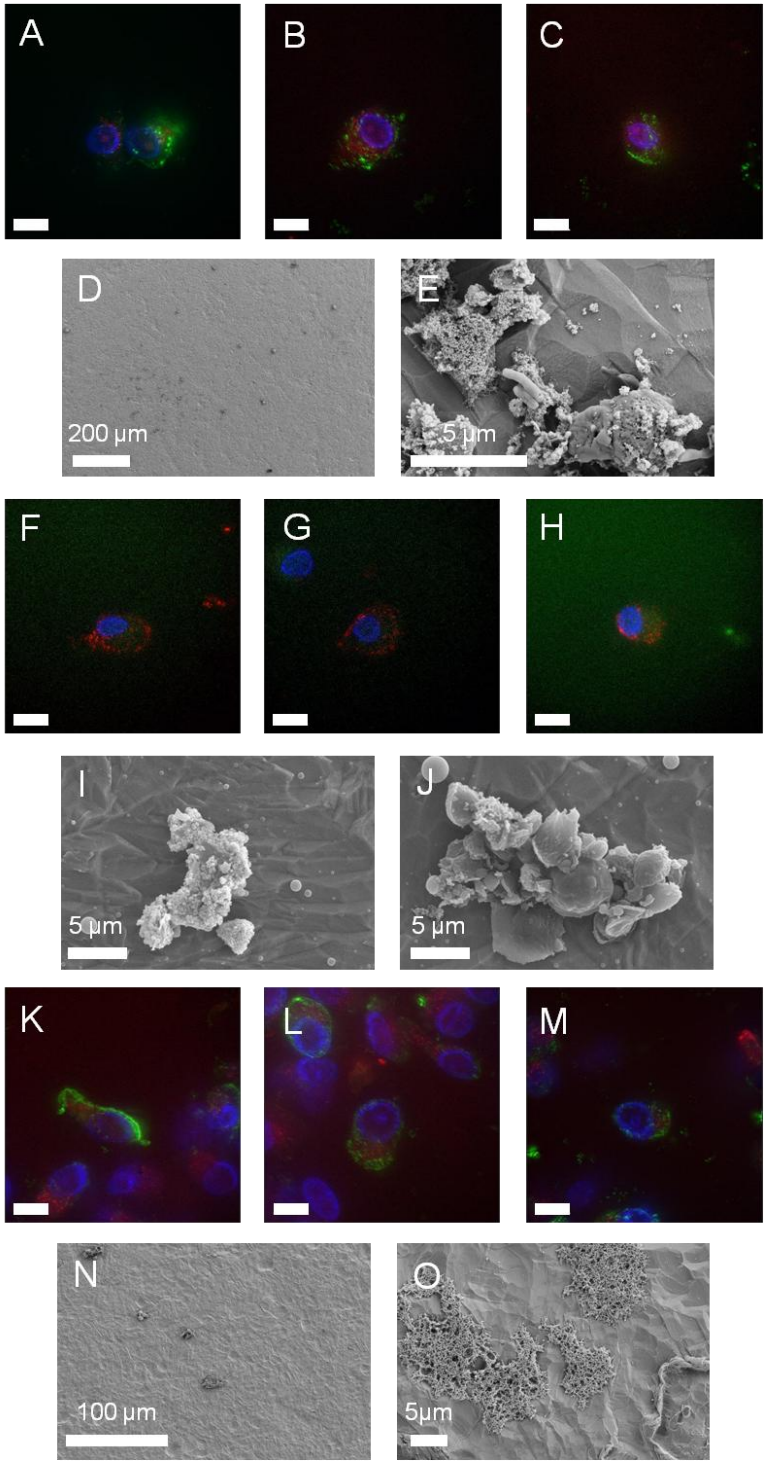

Figure 8: Studying the effects of culture time on the cells. At the end of the culture time, molecular beacon delivery and lipid raft staining was done prior to fluorescence imaging and SEM imaging. **(A)-(C)** Two day culture time fluorescent images. Scale bar represents 15µm. **(D)-(E)** Two day culture time SEM images. **(F)-(H)** Three day culture time fluorescent images. Scale bar represents 15µm. **(I)-(J)** Two day culture time SEM images. **(K)-(M)** Five day culture time fluorescent images. Scale bar represents 15µm. **(N)-(O)** Five day culture time SEM images.

When molecular beacons were previously imaged in MG63 cells on titanium, a three day culture time was used,[39] and our fluorescent results confirmed that this was the best time for fluorescence imaging in this system. Although cells did not appear to be rounded when imaged fluorescently, when samples were imaged on the SEM, there was only cell debris on the surface. After three days of culture, Zhao et al. showed that MG63 cells on PT disks should appear to be flat on the surface with a few extensions from the cell body.[16] However, cells in imaged on titanium substrates in previous studies were not subject to the beacon imaging process prior to cell fixation and SEM imaging.[9,13,16] Therefore, the fact that debris, not spread cells, was found on the surface may be caused by a part of the beacon imaging procedure prior to SEM imaging.

Studying the Effects of the Dehydration Medium on the Cells

After determining that the rounded or detaching cells were not due to the culture time, dehydration medium was tested. Cells were stained and premeabilized before dehydration in graded ethanol or acetone dehydrations and drying to see if the dehydration medium affects cell morphology. On control samples, there was an abundance of cells on both disks (Figure 9A - D). Regardless of the dehydration medium, the cells were well spread and polygonal in shape. However, for samples that were stained and permeabilized prior to fixation, few cells were seen on the surfaces (Figure 9E - H). On the sample dehydrated with ethanol and the one dehydrated with acetone, only rounded cells or cell debris was seen on the disks.

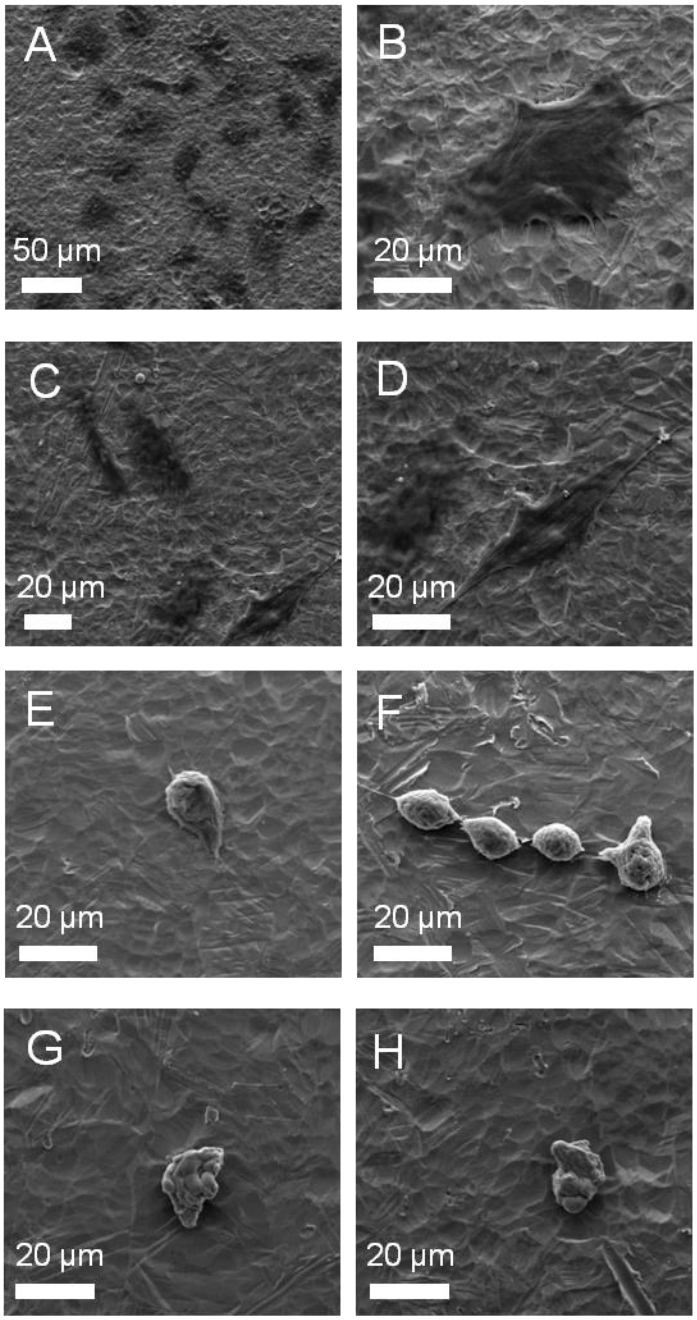

Figure 9: Studying the effects of dehydration medium on the cells. **(A)-(B)** MG63 cells dehydrated in ethanol. **(C)-(D)** MG63 cells dehydrated in acetone. **(E)-(F)** MG63 cells dehydrated in ethanol after lipid raft staining and SLO permeabilization. **(G)-(H)** MG63 cells dehydrated in acetone after lipid raft staining and SLO permeabilization.

Previously, graded acetone, ethanol, and 2,2-dimethoxypropane have been tested for dehydrating tissue sections followed by critical point drying.[55] This study showed no change in sample morphology with dehydration medium. Critical point drying has also been proved as a useful technique for preserving morphology of cells or tissues for SEM.[55,56] Therefore, our results showing that using ethanol versus acetone did not affect cell morphology were consistent with previous results.[55,56]

Studying the Effects of SLO, Lipid Raft Stain, and Temperature on the Cells

Determining that the cell spreading and attachment problems were not due to culture time or dehydration medium led to the study of the steps in fluorescent staining, molecular beacon delivery, and beacon imaging. Cells were treated to see the effects of lipid raft stain and SLO alone, their combination, and if effects could be recovered by a 24 hour re-incubation. On the control sample, an abundance of well spread, polygonal shaped cells were seen on SEM (Figure 10A, B). When only lipid raft staining was done, most cells on the surface were well spread while few cells appeared to be detaching from the surface or have a rounded morphology (Figure 10C, D). When cells were only permeabilized with SLO, there were more rounded cells than on the control sample or the sample where only lipid raft staining was done (Figure 10E, F). When lipid raft staining and SLO permeabilization was both done, there were more rounded cells on the surface than any of the other three samples (Figure 10G, H). Even so, the majority of the cells on this sample appeared to be spread and polygonal shaped.

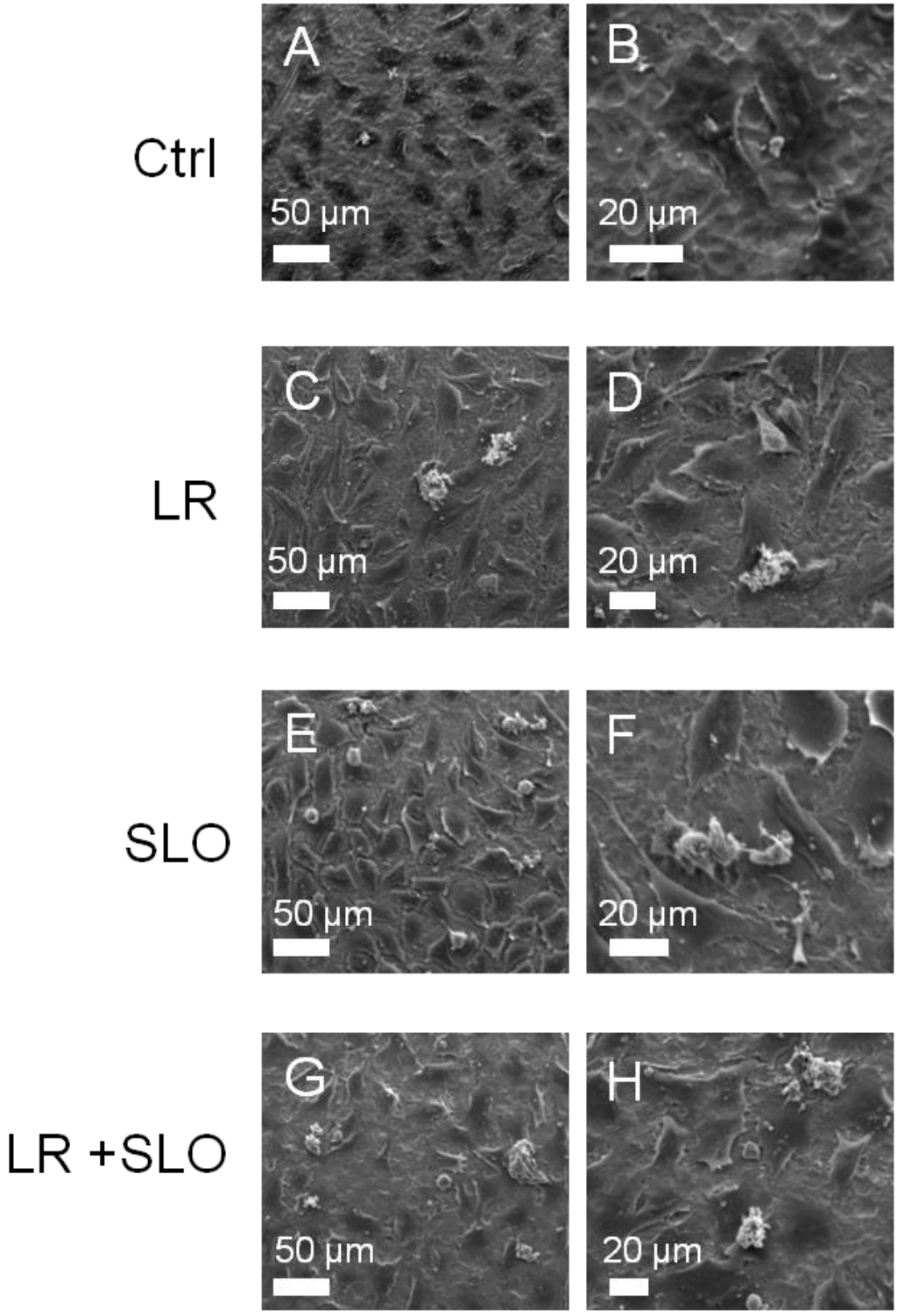

Figure 10: Studying the effects of lipid raft labeling, SLO permeabilization on the cells. **(A)-(B)** Control MG63 cells were fixed after culture. **(C)-(D)** MG63 cells were fixed after lipid raft staining. **(E)-(F)** MG63 cells were fixed after SLO permeabilization. **(G)-(H)** MG63 cells were fixed after lipid raft staining and SLO permeabilization.

Samples that were re-incubated for 24 hours after treatment showed a similar pattern in the number of rounded cells as samples that were fixed directly after treatment. For all of the re-incubated samples, cells were confluent and it was difficult to distinguish individual cells on these samples (Figure 11A - H). On the re-incubated control sample, very few rounded cells were seen; most cells were spread and polygonal shaped (Figure 11A, B). On the re-incubated sample with only lipid raft stain, more rounded cells were seen than on the re-incubated control sample or the lipid raft sample that was fixed after staining (Figure 11C, D). For the sample permeabilized with SLO and re-incubated, more rounded cells were seen than on the control or lipid raft stain re-incubated samples or the permeabilized sample that was fixed after permeabilization (Figure 11E, F). For the sample that was stained, permeabilized, and re-incubated, there were more round cells than on any of the other re-incubated samples or the sample that was stained, permeabilized, and fixed (Figure 11G, H).

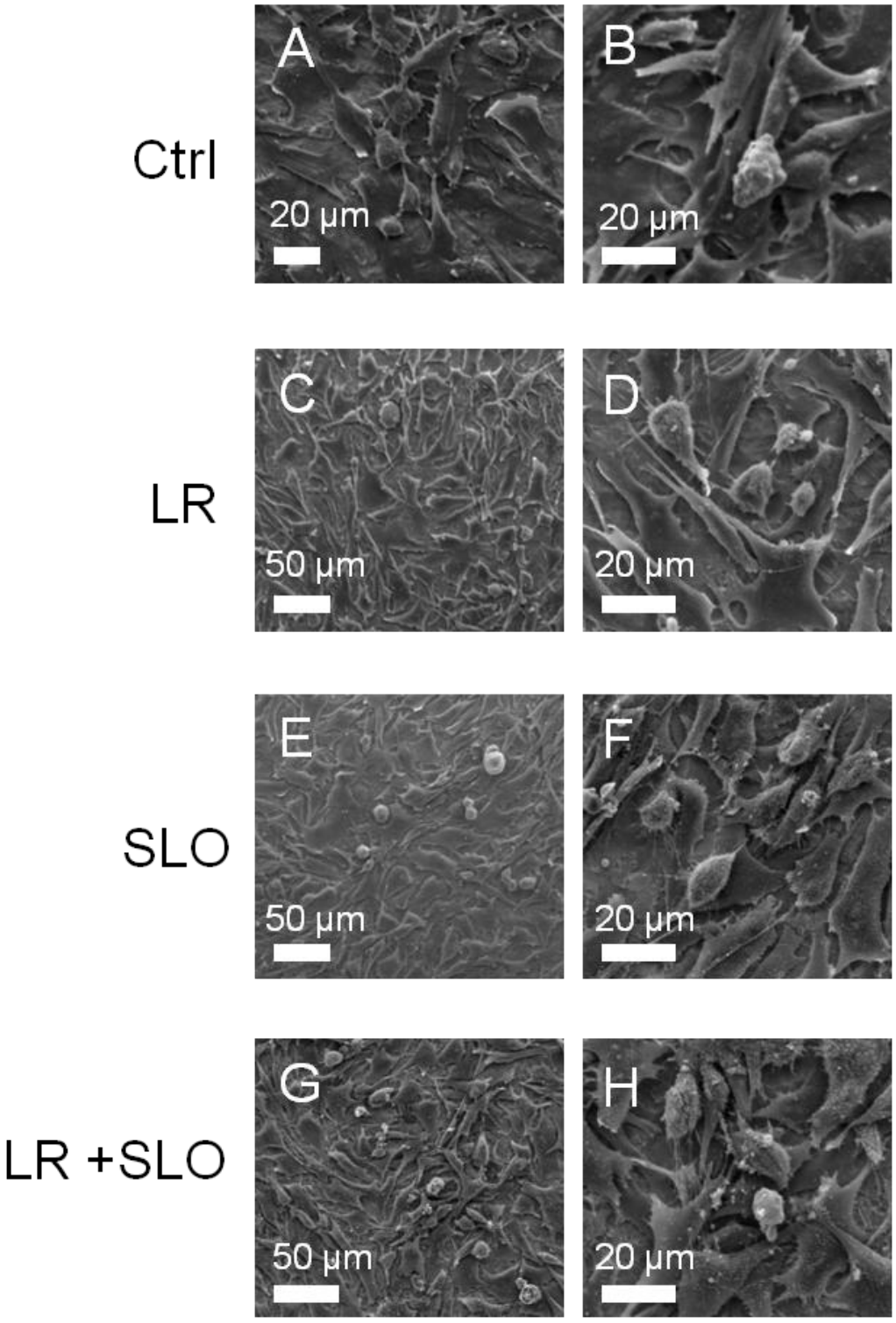

Figure 11: Studying the effects of re-incubation after lipid raft staining and SLO permeabilization. **(A)-(B)** Control MG63 cells were fixed 24 hours after three days of culture. **(C)-(D)** MG63 cells were re-incubated for 24 hours after lipid raft staining. **(E)-(F)** MG63 cells were re-incubated for 24 hours after SLO permeabilization. **(G)-(H)** MG63 cells were re-incubated for 24 hours after lipid raft staining and SLO permeabilization.

Other samples were tested to see how being at room temperature during imaging affected cells in combination with the lipid raft stain and SLO. The sample that was left at room temperature for 1.5 hours showed a few rounded cells, but most cells on this disk were well spread with a polygon shape and several extensions (Figure 12A, B). Samples where cells were stained or permeabilized and left 1.5 hours at room temperature showed an increasing number of rounded cells compared to the sample that was only left for 1.5 hours at room temperature (Figure 12C - F). Cells that were fixed directly after cell staining and permeabilization were well spread, with the polygonal morphology and extensions consistent with previous results (Figure 12G, H). Cells that were re-incubated for 1.5 hours after staining and permeabilization showed more rounded cells than when cells were fixed after staining and permeabilization (Figure 12I, J). The stained, permeabilized, and re-incubated sample also showed an increased number of rounded cells compared to samples that were stained or permeabilized and left at room temperature for 1.5 hours (Figure 12K, L). The sample that was left at room temperature for 1.5 hours after staining and permeabilization only shoed a small number of rounded cells or cell debris on the surface.

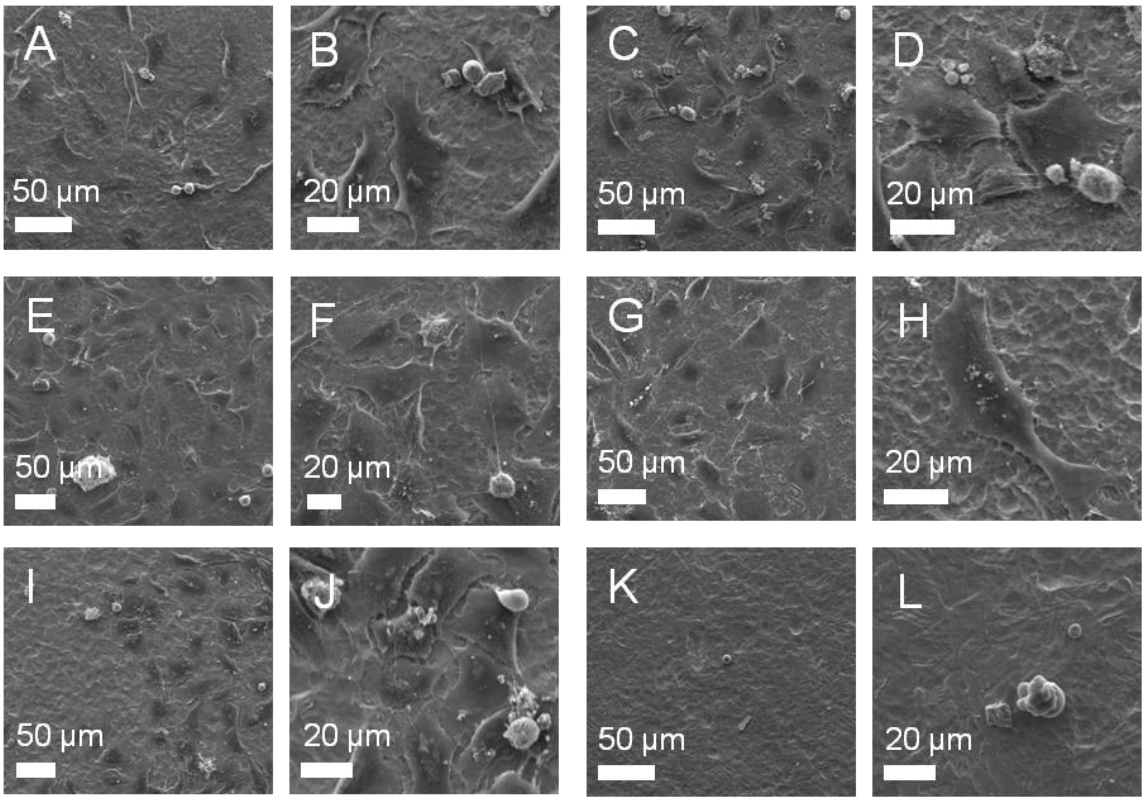

Figure 12: Studying the effects of lipid raft labeling, SLO permeabilization, and time at room temperature on the cells. **(A)-(B)** MG63 cells were left at room temperature for 1.5 hours. **(C)-(D)** MG63 cells were left at room temperature for 1.5 hours after lipid raft staining. **(E)-(F)** MG63 cells were left at room temperature for 1.5 hours after SLO permeabilization. **(G)-(H)** MG63 cells were fixed after lipid raft staining and SLO permeabilization. **(I)-(J)** MG63 cells were re-incubated for 1.5 hours after lipid raft staining and SLO permeabilization. **(K)-(L)** MG63 cells were left at room temperature for 1.5 hours after lipid raft staining and SLO permeabilization.

Initially the effects of SLO and lipid raft staining were tested independently and when the two were combined. Although lipid raft staining has been performed in live cells,[54] cells are often fixed prior to fluorescence imaging,[53] and when live cell imaging was performed, cells were cultured on coverslips and mounted in a perfusion chamber during imaging.[54] While Milev et al. successfully imaged lipid raft staining in live cells, further studies were not performed to determine if the staining had a negative effect on cells through the duration of the imaging time.[54] SLO has been shown to be an effective method for probe delivery through reversible permeabilization.[36,37] While the cell

membrane recovers from permeabilization upon incubation with serum containing media and cells remain viable after resealing, this repair is dependent upon the concentration of SLO used for permeabilization.[57] Molecular beacons have not been used with other staining methods and while the combination of lipid raft staining and SLO permeabilization in this study did negatively affect some of the cells, our results confirmed that lipid raft staining and SLO permeabilization could be done with live cells.

During fluorescence imaging, the cells were also subject to room temperature hypothermia as there was no temperature control on the DeltaVision. Hypothermia has been shown to decrease integrin β1 expression in extravasated neutrophils,[58] and room temperature hypothermia can increase cell apoptosis.[59] Results in this study were consistent with previous findings, as lipid raft staining and SLO permeabilization had a negative effect on the cells, combining this with room temperature hypothermia ultimately led to cell detachment.

Studying the Effects of Cell Fixation Prior to Imaging

To reduce the negative effects of the LR stain, SLO, and time at room temperature, GFP transfected MG63s were tested, and normal MG63 cells were fixed after MB delivery and before LR staining and imaging. Molecular beacons were delivered to GFP transfected MG63 cell, and these cells appeared well spread on the fluorescence microscope (Figure 13A - C). SEM results were similar to cells that were stained, permeabilized, and left at room temperature for 1.5 hours (Figure 13D - F). Few cells were observed on the surface, and anything present on the surface was either rounded cells or cell debris.

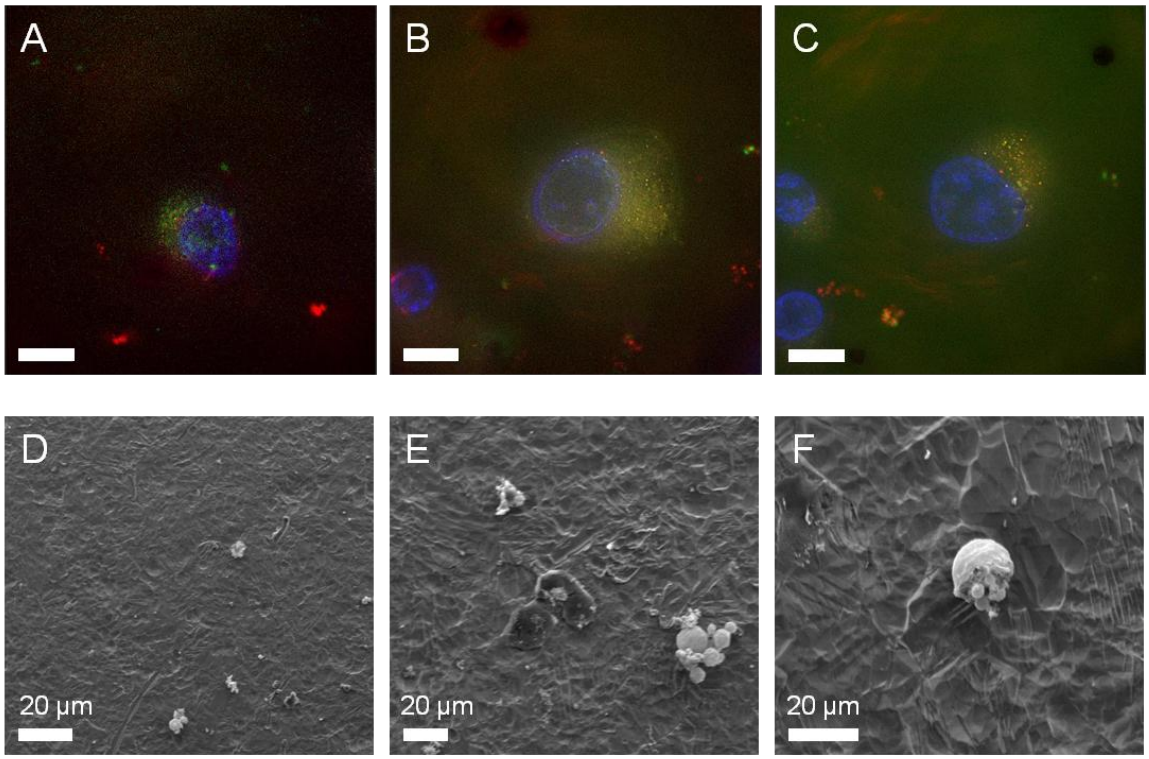

Figure 13: Visualizing the cell morphology using GFP transfected MG63 cells. Scale bar represents 15µm. **(A)-(C)** GFP transfected MG63 cells after molecular beacon delivery imaged fluorescently. **(D)-(F)** SEM imaging after fluorescence microscopy.

Cells that were fixed with Karnovsky's fixative after beacon delivery and before lipid raft staining showed a well spread morphology when imaged fluorescently with MB639 (Figure 4A - C) and with RMB (Figure 14D – F). Regardless of which beacon (MB639 or RMB) was delivered to the sample, filopodia and extensions could be seen from the cells. There did not appear to be any differences in the beacon intensity between cells in which MB639 or RMB were delivered, and for both beacons, the signal showed up as a haze across the cells. Scaling the fluorescent images for comparison (Figure 14G - L) and quantifying the beacon intensity (Figure 15) showed that there was no difference in the total beacon intensity of the cells with MB639 and the cells with RMB. On SEM, an abundance of cells were seen on the surface, and while rounded

cells were seen, the majority of the cells were well spread with visible filopodia (Figure 14M - O). Using the same method, cells were also fixed with 50:50 v/v methanol:acetone. When this was done, no cells were seen fluorescently, and SEM showed only cell debris on the disk regardless of which beacon was delivered to the cells (Figure 16A - F).

Cells were also cultured on glass disks, and 95% ethanol, 10% buffered formalin, and 4% paraformaldehyde were tested to fix the cells after beacon delivery and before lipid raft staining and fluorescence imaging. When cells were fixed with 95% ethanol after MB639 delivery and before lipid raft staining, the cell membranes could not be seen or imaged fluorescently (Figure 17A - C). The beacon signal in cells fixed with ethanol appeared as a haze across the cells. Cells fixed with 10% buffered formalin appeared well spread fluorescently, and cell extensions were seen and imaged (Figure 17D - F). Beacon signal in cells fixed with formalin also appeared as a haze across the cells. When 4% paraformaldehyde was used as a fixative, cells showed a well spread morphology where extensions could be seen fluorescently (Figure 17G - I). In these cells, the beacon signal was a haze across the cells as with cells fixed with ethanol or formalin.

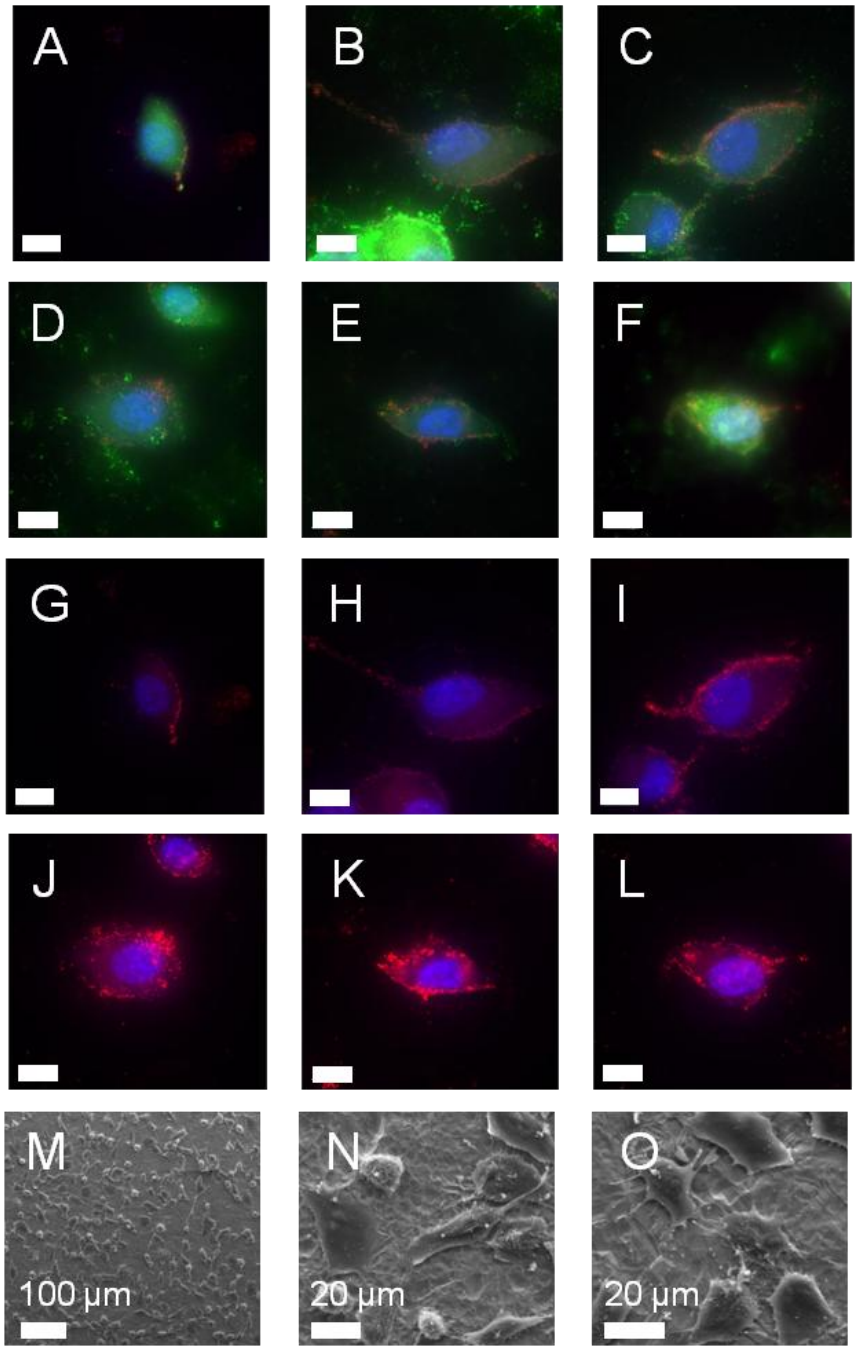

Figure 14: Studying the effect of Karnovsky's fixation before fluorescence imaging. MG63 cells were fixed with Karnovsky's fixative after molecular beacon delivery and prior to lipid raft labeling. Scale bar represents 15µm unless otherwise noted. **(A)-(C)** MG63 cells imaged fluorescently with MB639. **(D)-(F)** MG63 cells imaged fluorescently with RMB. **(G)-(I)** Fluorescent images from (A)-(C) scaled for comparison of the molecular beacon intensity. **(J)-(L)** Fluorescent images from (D)-(F) scaled for comparison of the molecular beacon intensity. **(M)-(O)** SEM imaging of MG63 cells fixed with Karnovsky's fixative before fluorescence imaging.

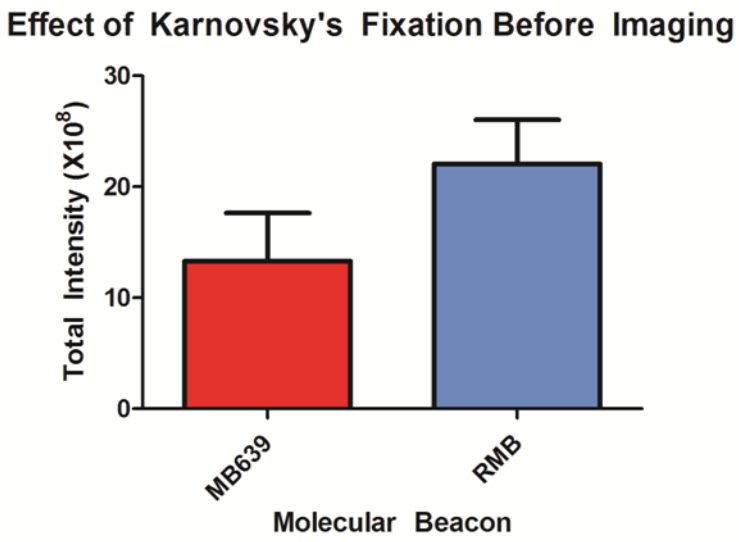

Figure 15: Image quantification of cells fixed with Karnovsky's before fluorescence imaging.

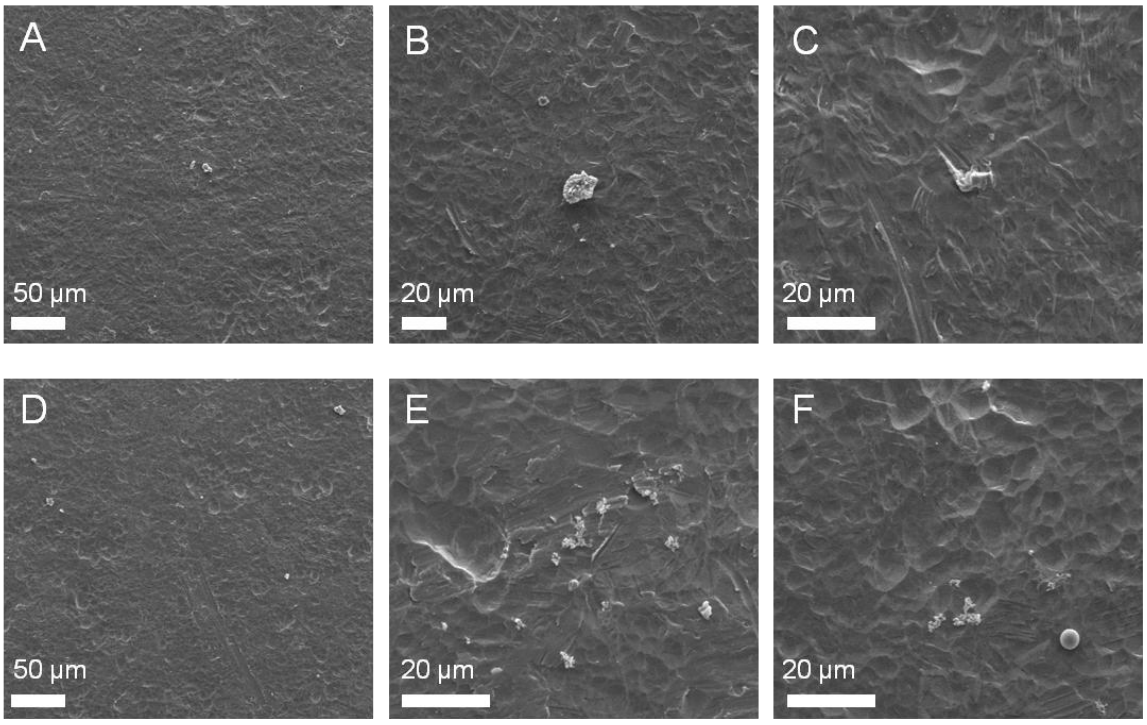

Figure 16: Studying the effect of methanol:acetone fixation before fluorescence imaging. **(A)-(C)** SEM imaging of MG63 cells after MB639 delivery. **(D)-(F)** SEM imaging of MG63 cells after RMB delivery.

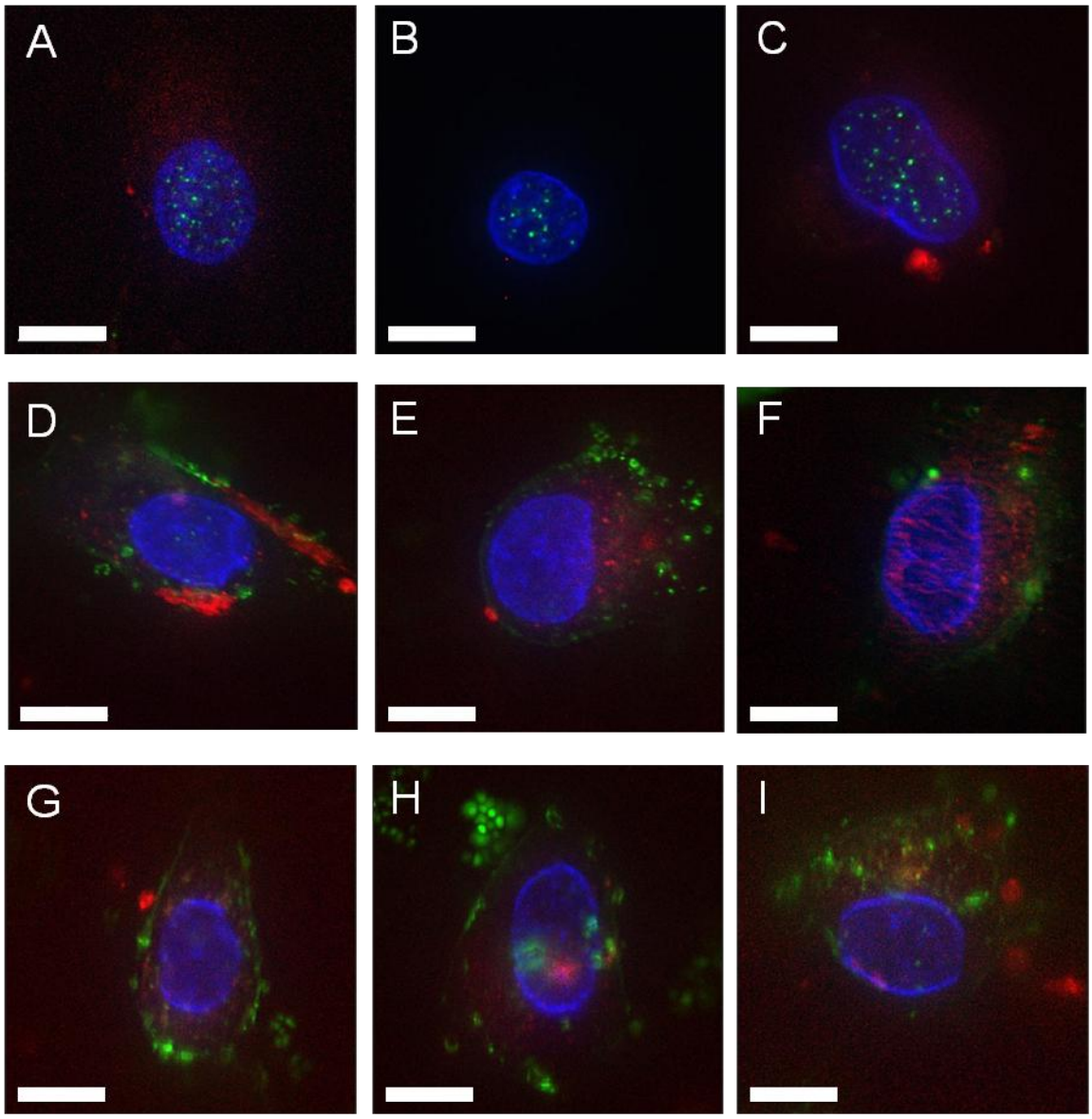

Figure 17: Studying the effect of ethanol, formalin, and paraformaldehyde fixation before fluorescence imaging. MG63 cells were fixed after molecular beacon delivery and prior to lipid raft staining. Scale bar represents 15μm. **(A)-(C)** MG63 cells imaged fluorescently after 95% ethanol fixation. **(D)-(F)** MG63 cells imaged fluorescently after 10% buffered formalin fixation. **(G)-(I)** MG63 cells imaged fluorescently after 4% paraformaldehyde fixation.

Five fixatives were tested to fix the samples after molecular beacon delivery and prior to lipid raft staining in attempt to eliminate the negative effects of the lipid raft stain on the live cells. As there have been no reports of molecular beacons imaged in fixed cells, fixatives commonly used for SEM and *in* situ hybridization were chosen. For *in situ* hybridization, a variety of crosslinking and alcohol fixatives can be used to maintain cell morphology and RNA quality.[60] Karnovsky's fixative was first tested, as it is a mixture of paraformaldehyde and glutaraldehyde, which are commonly used for SEM and TEM sample preparation.[61] Cells with MB639 and RMB were imaged and compared to determine if the fixation affected the molecular beacons. The imaged intensity from RMB should have been significantly less than that of MB639 to indicate that no non-specific binding or beacon degradation occurred.[39] As no difference in beacon intensity was found, it was concluded that Karnovsky's fixative affected the beacons and would not work in this system. Ethanol as a fixative in *in situ* hybridization dissolves the cell membrane for probe delivery,[62] and this membrane dissolution was observed fluorescently in cells fixed with 95% ethanol as the cell membrane could not be seen or imaged. MB639 imaged in cells fixed with 95% ethanol, 10% buffered formalin, and 4% paraformaldehyde appeared as a haze across the cells, which can be indicative of non—specific fluorescence.[63] Other chemical fixatives were either chemically similar to these five fixatives, or combinations of one or more of the fixatives,[60] so further testing with cell fixation before imaging were not pursued.

Studying Cell Adhesion during Imaging

Cell adhesion to the glass chamber slide during fluorescence imaging and several methods for preventing this were tested. After MB639 delivery, cells on laser etched PT disks were imaged on the DeltaVision Deconvolution Microscope (Figure 18A - C). On the SEM, cell debris was seen on the disk, and few cells remained on the

surface (Figure 18D - F). Of the few cells that were seen on the disk, they did not appear to be well spread, as their morphology was not elongated and most of the cells did not have extensions. When the disk was taken to the FIB/SEM, none of the cells that were fluorescently identified and imaged were seen (Figure 18G - I). Using the coordinates to find cells on the FIB, there were no cells present in these areas and only cell debris was seen. After fluorescence microscopy for imaging the molecular beacons (Figure 19A - C), cells were only rinsed one time with PBS before fixation, instead of three times as in the original protocol. When this sample was observed on the SEM, no more cells were seen on the SEM than with the original rinsing protocol (Figure 19D - F). Mostly cell debris was seen on the disk, and any cells still on the surface were rounded. It was then hypothesized that cells may be adhering to the chamber slide during fluorescence imaging, so that when the disk is removed from the chamber slide, the cells begin to break apart (Figure 20A, B). Cells on another sample were fixed after molecular beacon imaging for 30 minutes before the disk was removed from the chamber slide/insert imaging set up (Figure 21A - C). On this sample, there were still a small number of cells on the disk on the SEM, and all cells that were found on this sample were rounded (Figure 21D - F).

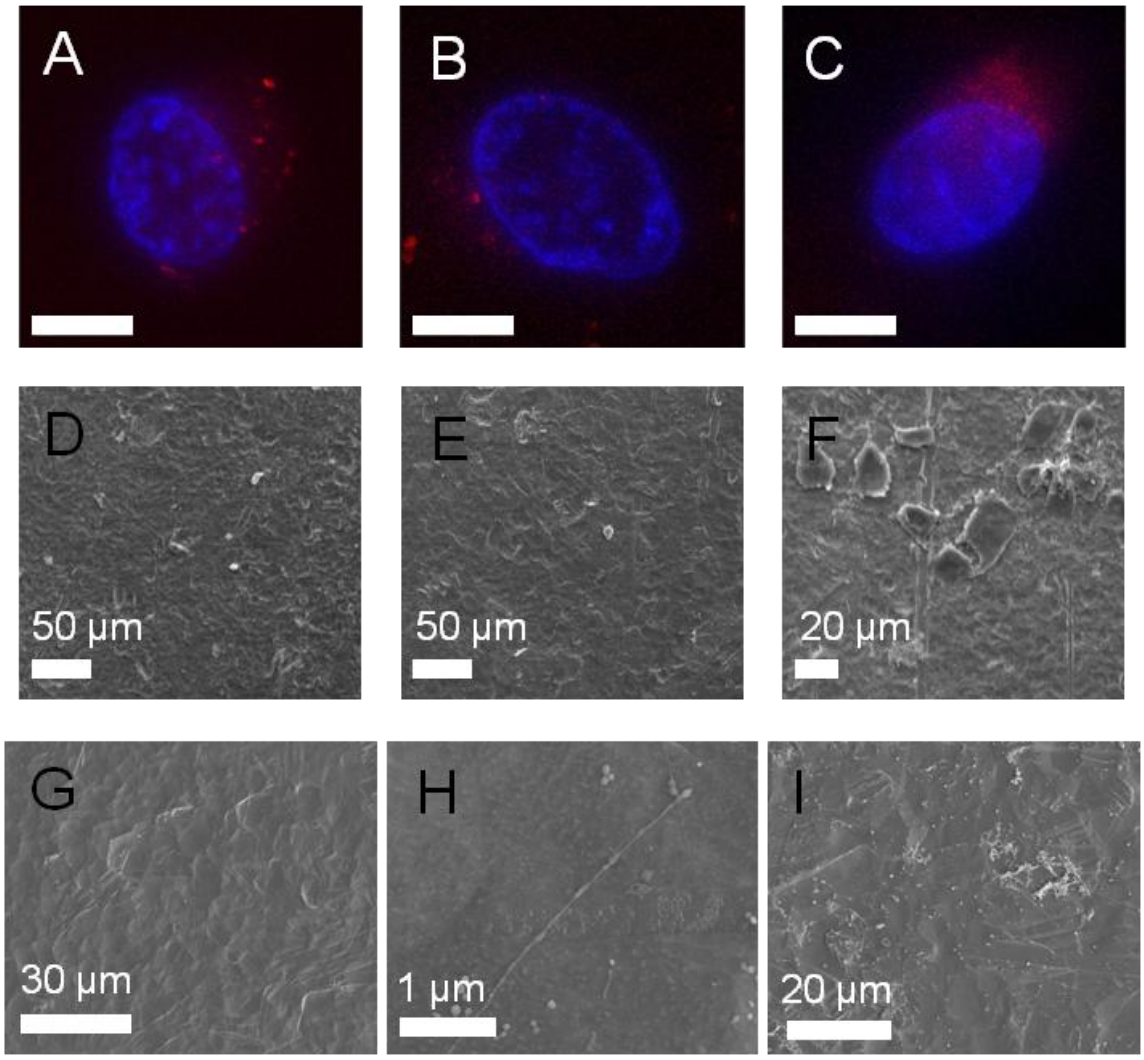

Figure 18: Visualizing cells for FIB milling after fluorescence imaging. **(A)-(C)** Fluorescence MB639 imaging of MG63 cells. Scale bar represents 15µm. **(D)-(F)** SEM imaging of the fluorescently imaged sample. **(G)-(I)** FIB/SEM imaging of the fluorescently imaged sample.

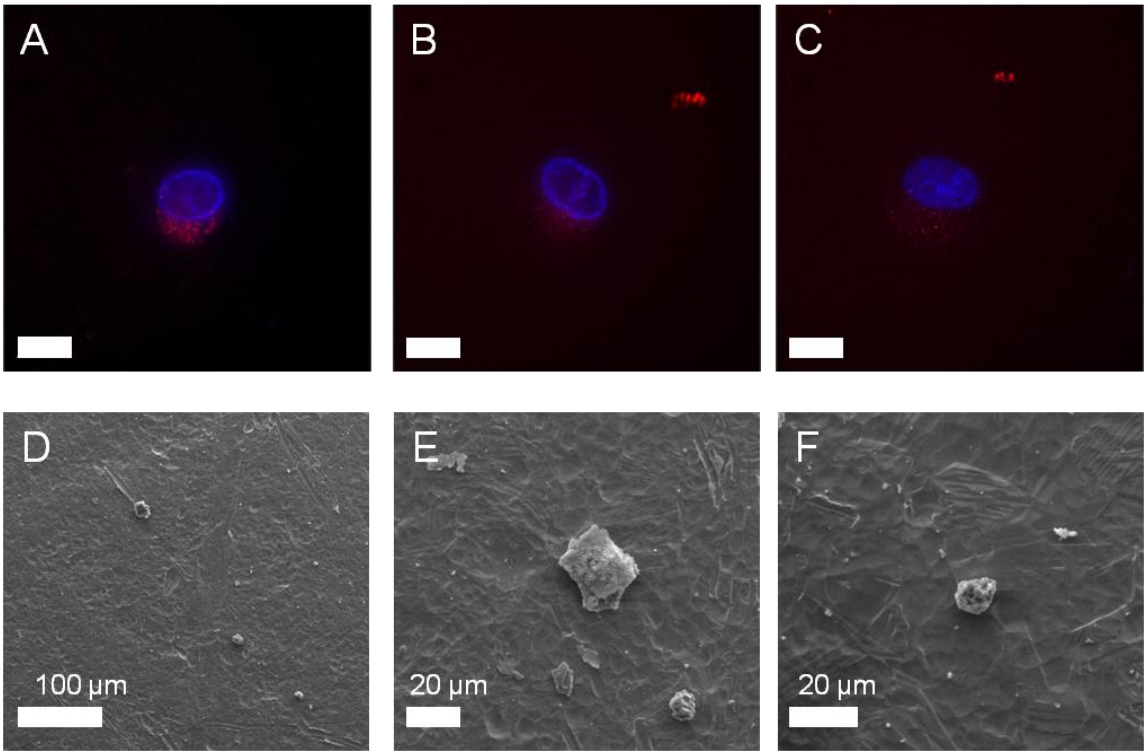

Figure 19: Studying the effect of less washing after fluorescence imaging and before fixation. MG63 cells were rinsed one time with PBS after fluorescence imaging and prior to fixation. **(A)-(C)** Fluorescence MB639 imaging of MG63 cells. Scale bar represents 15µm. **(D)-(F)** SEM imaging of the fluorescently imaged sample.

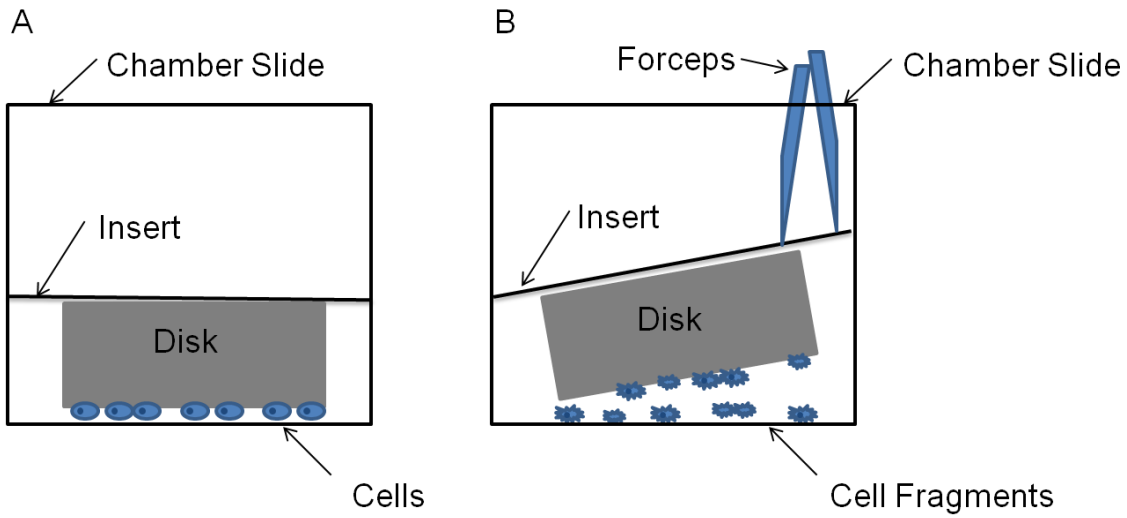

Figure 20: Schematic of fluorescence imaging set up. **(A)** During fluorescence imaging, the disk is inverted in a glass chamber slide so that the cells are in contact with the chamber slide. **(B)** When the disk is removed, cells may break apart or detach from the titanium disk.

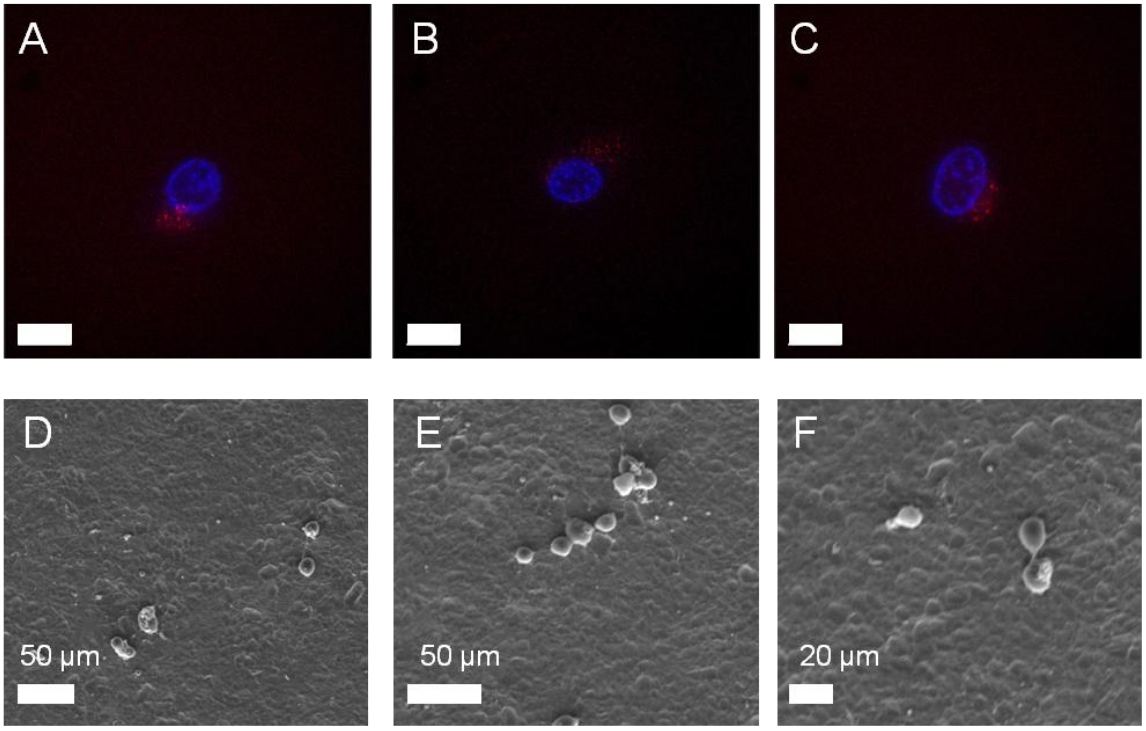

Figure 21: Studying the effect of fixing the cells in the imaging set up. MG63 cells were fixed prior to removing the disk and insert from the chamber slide. **(A)-(C)** Fluorescence MB639 imaging of MG63 cells. Scale bar represents 15µm. **(D)-(F)** SEM imaging of the fluorescently imaged sample.

We also tried coating the chamber slides with non-fouling coatings to prevent cell adhesion to the glass during molecular beacon imaging. Chamber slides were coated with Teflon® and Sigmacote® prior to use to prevent cells from adhering to the glass during fluorescence imaging. When molecular beacon imaging was done for a sample in a Teflon® coated chamber slide (Figure 22A - C), nuclear staining showed that many clusters of cells were attached to the glass after the disk was removed from the imaging set up (Figure 22D - F). On the SEM, there were still not a large number of cells on the disk (Figure 22G - I). Any cells that were seen on the SEM were rounded; very few extensions were seen from these cells. Cells were also imaged in a Sigmacote® coated chamber slide (Figure 23A - C). For this sample, some cells still attached to the glass

after the disk was removed from the imaging set up, but fewer cells were visible on the glass than when Teflon® was used to coat the chamber slide (Figure 23D - F). When imaged on the SEM, clusters of cells and cell debris were seen (Figure 23G - I). The cells still appeared rounded, however there were many more present than had been seen on samples in previous experiments. On the FIB/SEM, none of the cells located fluorescently were still on the surface (Figure 23J - L). Only cell debris was seen in the areas where cells were when imaged fluorescently.

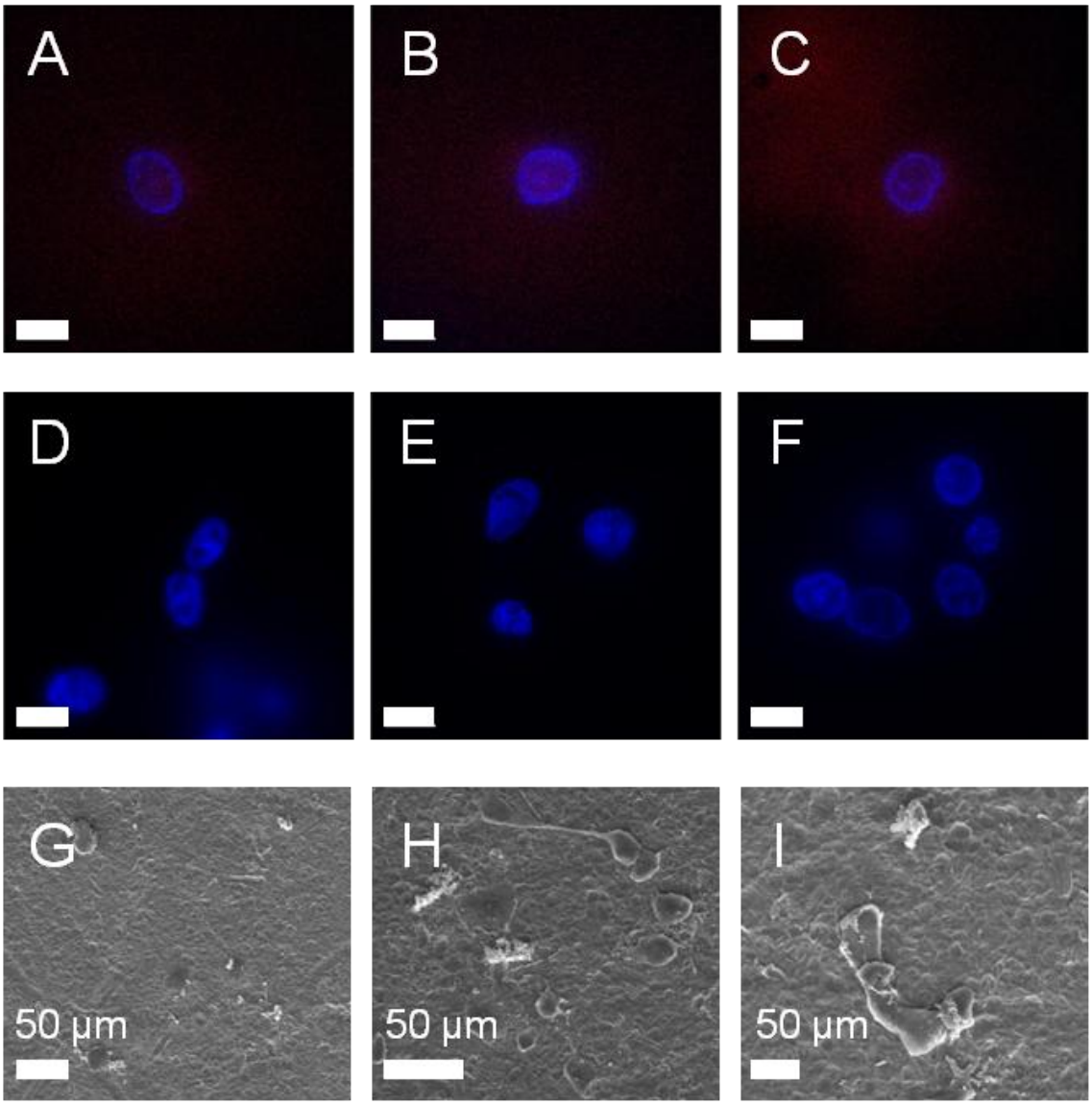

Figure 22: Studying the effects of cell adhesion during fluorescence imaging. MG63 cells were imaged in Teflon® coated chamber slides. **(A)-(C)** Fluorescence MB639 imaging of MG63 cells in a Teflon® coated chamber slide. Scale bar represents 15µm. **(D)-(F)** Fluorescence imaging of the Teflon® coated chamber slide after the disk was removed. Scale bar represents 15µm. **(G)-(I)** SEM of the sample imaged fluorescently in a Teflon® coated chamber slide.

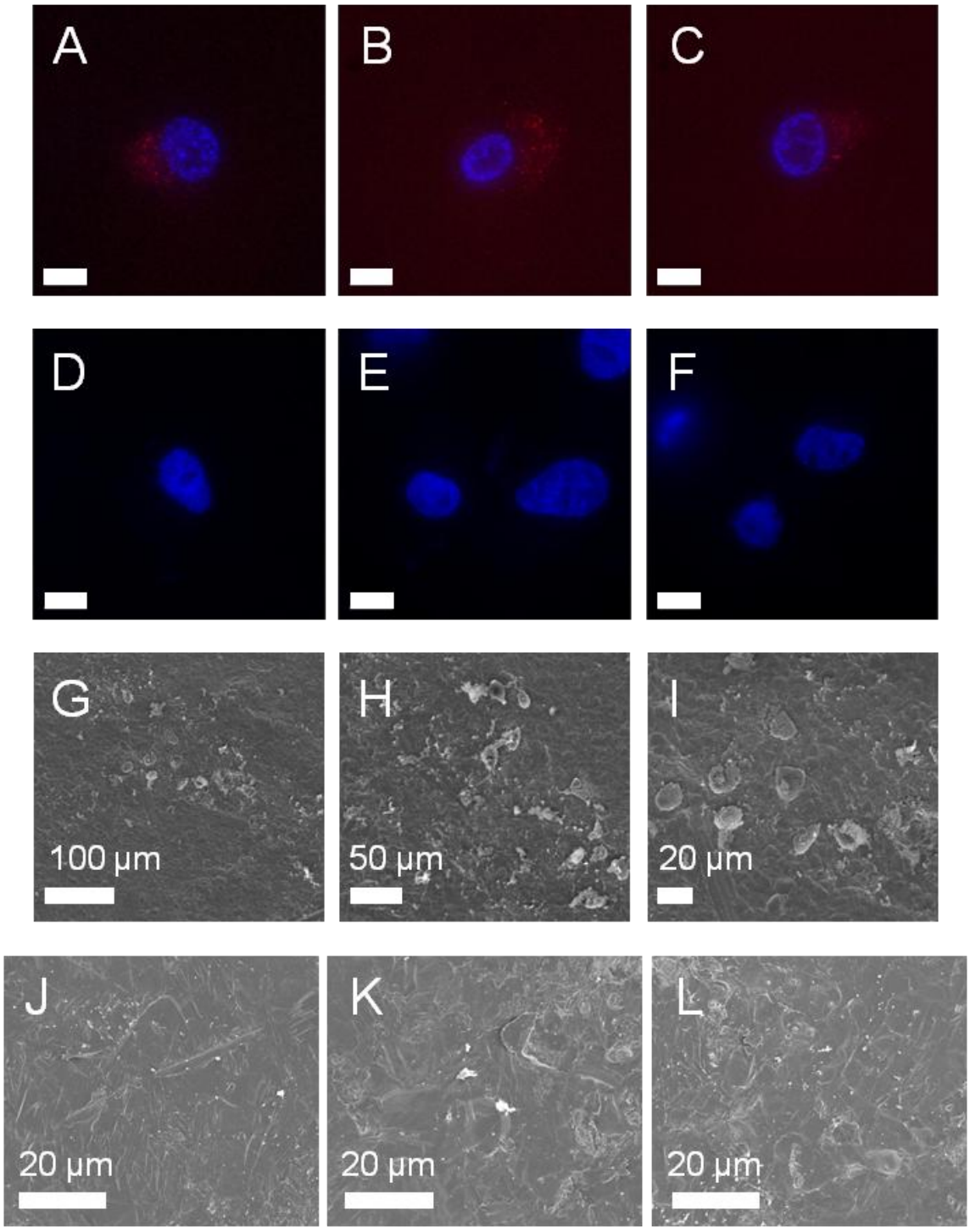

Figure 23: Studying the effects of cell adhesion during fluorescence imaging. MG63 cells were imaged in Sigmacote® coated chamber slides. **(A)-(B)** Fluorescence MB639 imaging of MG63 cells in a Sigmacote® coated chamber slide. Scale bar represents 15µm. **(C)-(F)** Fluorescence imaging of the Sigmacote® coated chamber slide after the disk was removed. Scale bar represents 15µm. **(G)-(I)** SEM imaging of the sample imaged fluorescently in a Sigmacote® coated chamber slide. **(J)-(L)** FIB/SEM imaging of the sample imaged fluorescently in a Sigmacote® coated chamber slide.

After investigating the cause of cell detachment and the possibility of cell fixation before fluorescence imaging, fluorescence imaging was continued without doing lipid raft staining in order to alleviate cell detachment. After MB639 was imaged in cells, and only cell debris was seen on the disk on the SEM, the set-up for fluorescence imaging was observed to find a potential cause for cell detachment. Because the DeltaVision is an inverted microscope, the disk must be imaged with the cells facing downward, where they are in contact with the bottom of the glass chamber slide (Figure 20A). Cells have been shown to attach within 1 – 1.5 hours after seeding.[64,65] Therefore, it is possible that the cells attach to the glass during the fluorescence imaging and then may break apart or detach from the titanium disk when the disk and insert are removed from the chamber slide (Figure 19B). Only one other study has reported imaging molecular beacons on surfaces other than glass,[39] and in this study the samples were not imaged on the SEM after the fluorescence imaging, so this problem has not been studied previously. Rinsing the samples less before fixation and fixing the cells before removing the disk from the chamber slide did not improve the number of cells on the disk surface, so coatings were tested to prevent cell attachment to the glass.

Fluorocarbons are hydrophobic and have been used to pattern glass slides to prevent cell adhesion and control cell positioning and cell migration.[66-68] However, when Teflon® spray was used to coat the chamber slides before fluorescence imaging, cells were seen attached to the glass after the disk was removed from the chamber slide, and few cells were seen on the SEM. While a thicker coating may prevent cell attachment, the transparency of the chamber slides could not be maintained upon the application of more Teflon®, and the chamber slides must be transparent for fluorescence imaging. Sigmacote®, a solution of silicone in heptane, has been used to form a thin silicone film on glass to prevent cell adhesion.[69,70] In a study by Lee et al., hybridoma cells

maintained viability and a significantly lower attachment percentage when cultured in Sigmacote® coated T flasks for three days.[69] While our results demonstrated that Sigmacote® coating did not abolish cell adhesion to the chamber slide, it did reduce the number of cells attached to the glass compared to when chamber slides were coated with Teflon® and more cells were also seen on the SEM compared to previous experiments.

Studying the Effects of using a Spacer during Fluorescence Imaging

Although coating the chamber slides to prevent cell adhesion during imaging improved the number of cells on the disk after fluorescence imaging, spacers to lift the disk and insert off the surface of the chamber slide were tested to see if this would completely prevent cells from attaching to the chamber slide because they would not be in contact with the glass (Figure 24). Aluminum foil and polycarbonate spacers were first tested using disks with no cells. Laser etchings could not be seen at all using the 60X Plan Apo N lens with the aluminum foil spacer (Figure 25A). However, they could be clearly seen using the Olympus LUC 60X Plan FLN lens with both the aluminum foil spacer and the polycarbonate spacer (Figure 25B, C).

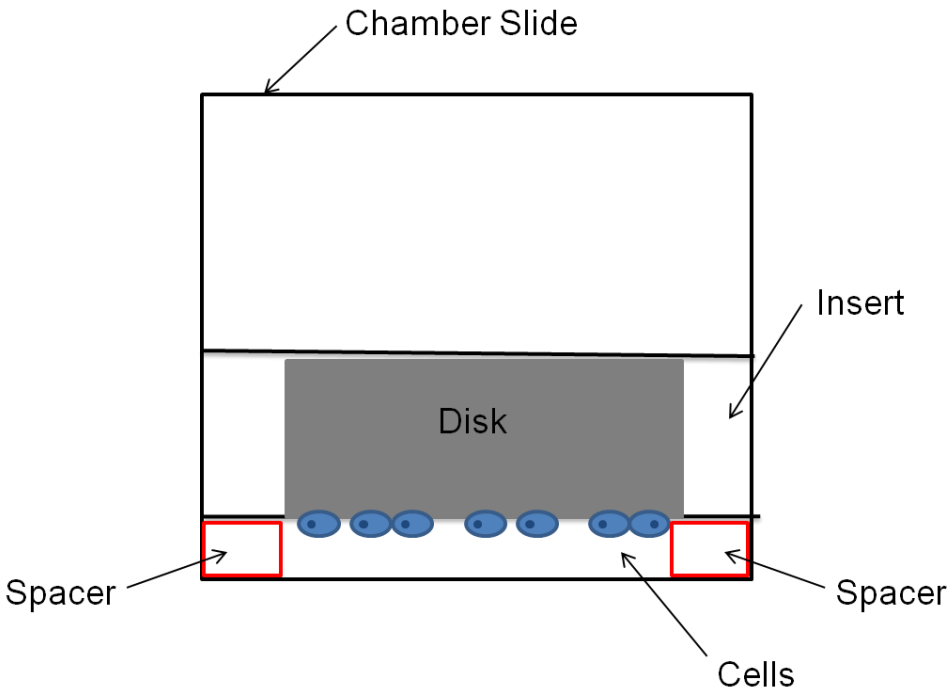

Figure 24: Schematic of fluorescence imaging set up when using spacers. The aluminum foil spacers or polycarbonate spacers are placed in the chamber slide before the insert and disk are inserted in the chamber slide so that the cells on the disk do not come in contact with the glass.

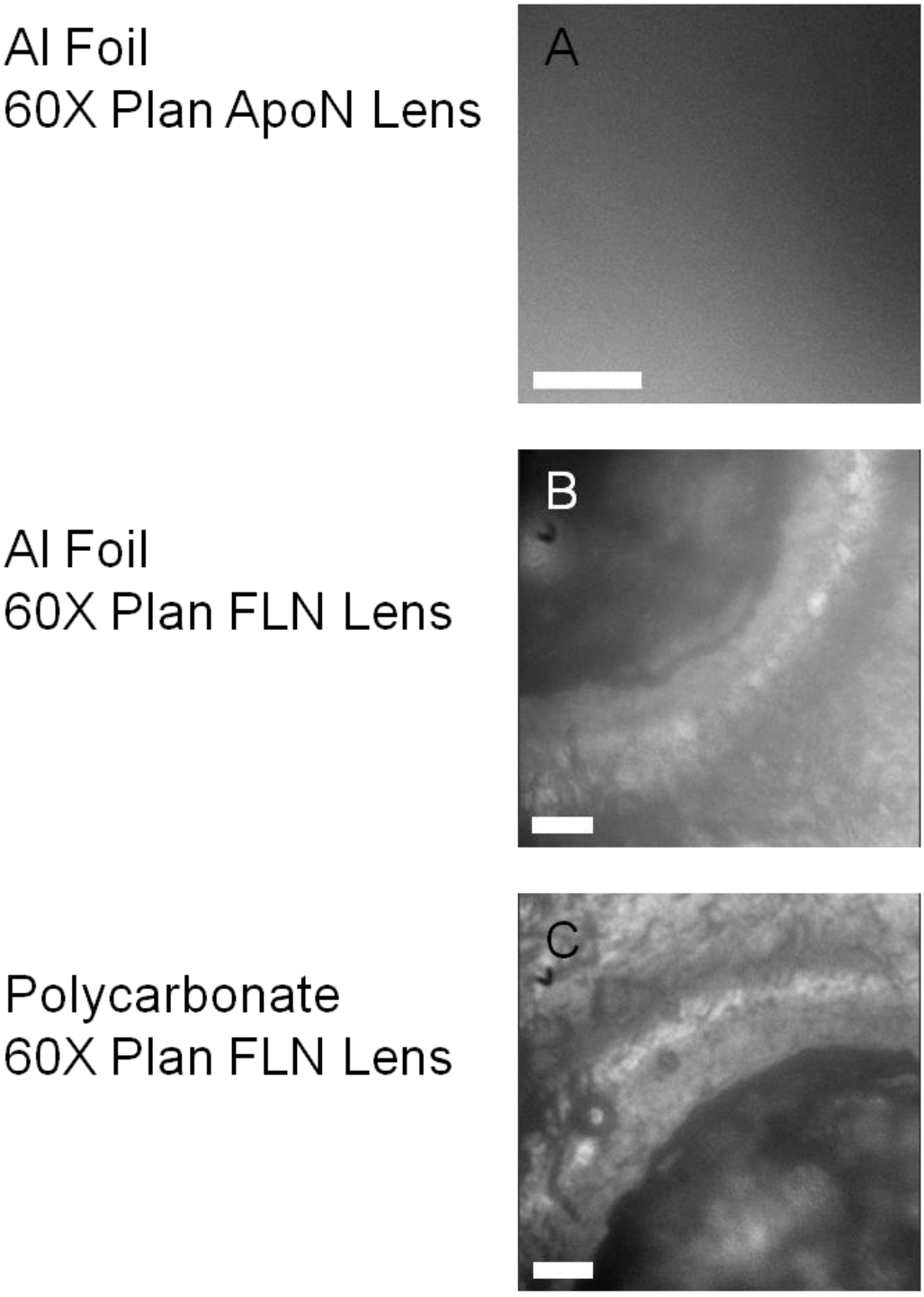

Figure 25: Visualization of laser etchings using a spacer to raise the disk in the fluorescence imaging set-up. **(A)** Etching viewed with the 60X Plan Apo N lens using an aluminum foil spacer. **(B)** Etching viewed with the 60X Plan FLN lens using an aluminum foil spacer. **(C)** Etching viewed with the 60X Plan FLN lens using a polycarbonate spacer.

When the polycarbonate spacer was used during beacon imaging, cells were imaged using the 60X and 40X Plan FLN lenses (Figure 26A, B, D, E). However, none of the cells could be completely focused on, so all cell images were not crisply focused and did not clearly show the beacon signal. The laser etchings were imaged using both lenses (Figure 26C, F). On the SEM, many more cells were imaged on the surface than from any other technique to prevent cell adhesion to the glass during fluorescence imaging (Figure 26G - I). Cells seen on the SEM were rounded with few filopodia connecting to the disk.

When the aluminum foil spacer was used during beacon imaging, cells were imaged using the 60X and 40X Plan FLN lenses (Figure 27A, B, D, E). At 60X, cells could not be completely focused on (Figure 27A, B), however at 40X the focus was crisper (Figure 27D, E). The beacon signal could not be clearly seen with either lens. The laser etchings were imaged using both lenses (Figure 27C, F). On the SEM, fewer cells were seen on the surface than when the polycarbonate spacer was used (Figure 27G - I). Any cells seen on the disks were rounded.

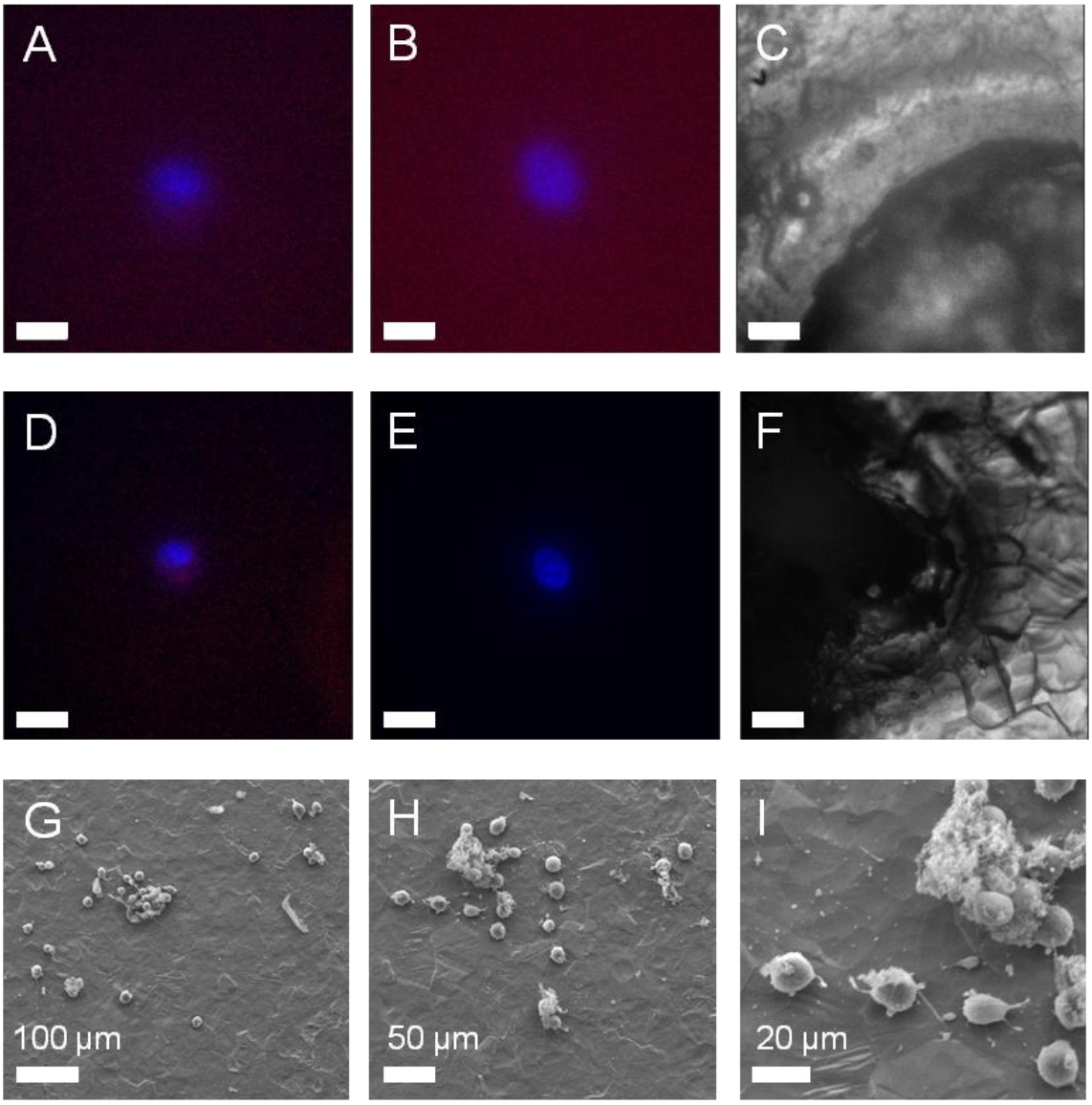

Figure 26: Studying the effects of using a polycarbonate spacer during fluorescence imaging. During fluorescence imaging, a 200µm spacer was used to raise the disk. **(A)-(B)** Fluorescence MB639 imaging of MG63 cells and imaging of an etching using the 60X Plan FLN lens. Scale bar represents 15µm. **(C)** Fluorescence and imaging of an etching using the 60X Plan FLN lens. Scale bar represents 15µm. **(D)-(E)** Fluorescence MB639 imaging of MG63 cells and imaging of an etching using the 40X Plan FLN lens. Scale bar represents 15µm. **(F)** Fluorescence and imaging of an etching using the 40X Plan FLN lens. Scale bar represents 15µm. **(G)-(I)** SEM imaging of the fluorescently imaged sample.

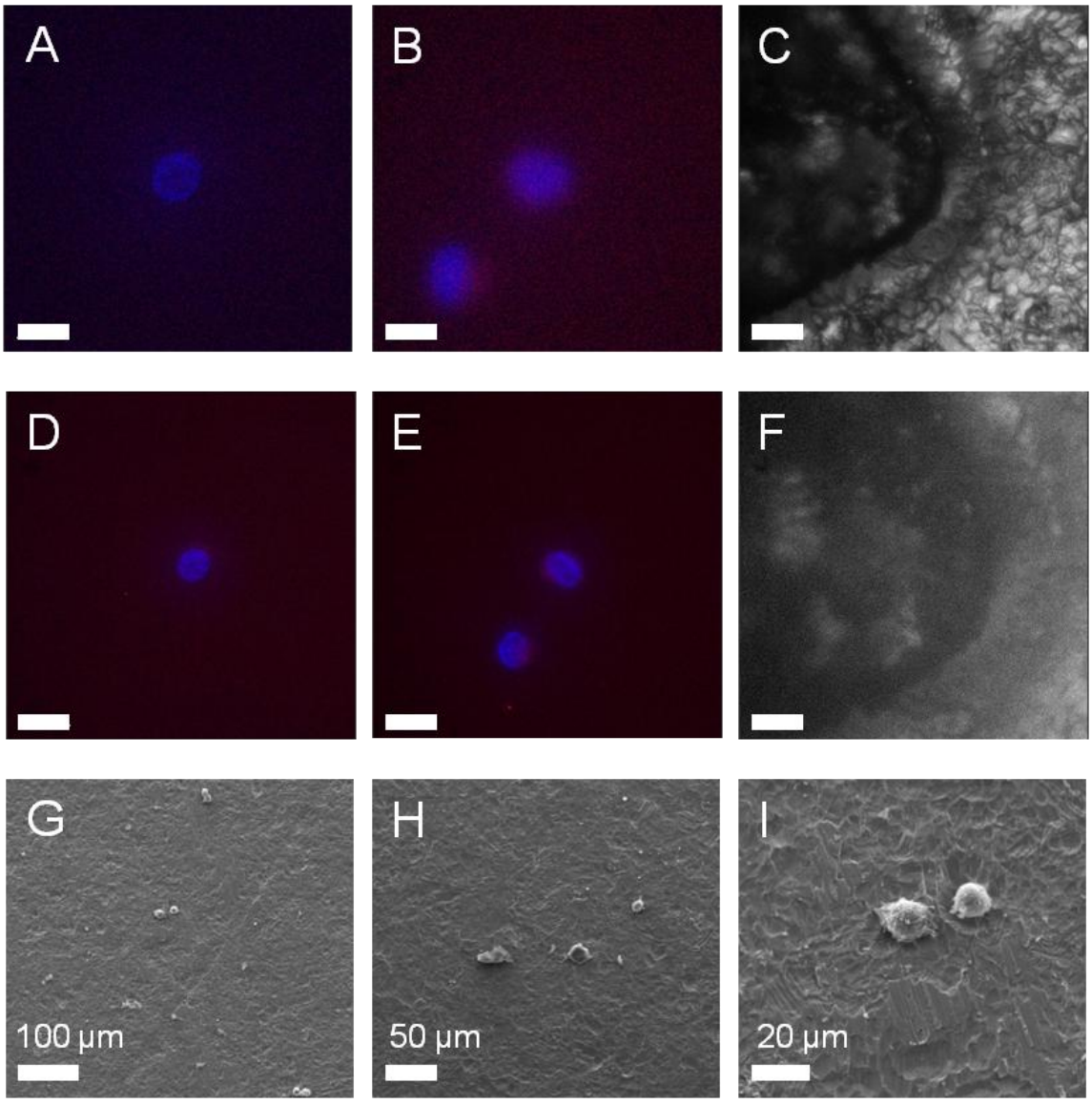

Figure 27: Studying the effects of using an aluminum foil spacer during fluorescence imaging. During fluorescence imaging, a 10µm spacer was used to raise the disk. **(A)-(B)** Fluorescence MB639 imaging of MG63 cells and imaging of an etching using the 60X Plan FLN lens. Scale bar represents 15µm. **(C)** Fluorescence and imaging of an etching using the 60X Plan FLN lens. Scale bar represents 15µm. **(D)-(E)** Fluorescence MB639 imaging of MG63 cells and imaging of an etching using the 40X Plan FLN lens. Scale bar represents 15µm. **(F)** Fluorescence and imaging of an etching using the 40X Plan FLN lens. Scale bar represents 15µm. **(G)-(I)** SEM imaging of the fluorescently imaged sample.

To prevent cells from adhering to the chamber slide during fluorescent images, two spacers were tested to raise the disk off the surface of the chamber slide. A test was first conducted to see if the laser etchings could be imaged when the disk was raised 10µm with an aluminum foil spacer or 200µm with a polycarbonate spacer. The etchings could not be seen with the 60X Plan Apo N lens when the disk was raised by the aluminum foil spacer. This is because this lens has a working distance of approximately 0.2mm, which is the thickness of the glass chamber slides used during fluorescence imaging, and therefore this lens does not have the ability to focus if the disk is not touching the glass. The 60X Plan FLN lens has a working distance of 1.5 – 2.2mm, and therefore the etchings could be seen using this lens when the disk was raised with an aluminum foil spacer and a polycarbonate spacer. While using the polycarbonate spacer did prevent cell adhesion to the glass during imaging, the cells could not be focused upon clearly and the beacon signal could not be clearly seen; cells also could not be focused upon clearly when imaged with the aluminum foil spacer. This inability to obtain well focused fluorescent images was most likely due to the reduction in the numerical aperture of the lenses. The 60X Plan Apo N lens has a numerical aperture of 1.42 while the 40X and 60X Plan FLN lenses had numerical apertures of 0.6 and 0.7, respectively, so the Plan FLN lenses were less sensitive.

FIB Milling and Transmission Electron Microscopy

After investigating methods to prevent cells from attaching to the glass chamber slides during fluorescence imaging, molecular beacon imaging was performed with samples in Sigmacote® coated chamber slides, and the FIB was used to serial section and mill TEM sections from cells with high and low β1 molecular beacon intensity. High molecular beacon intensity cells were those with intensities above $1.4x10^8$ and low intensity cells were those with intensities under $9.0x10^7$ (Table 1). TEM sections from

the one low β1 molecular beacon intensity cell (Figure 28A, B) and one high β1 molecular beacon intensity cell (Figure 29A, B) were milled on the FIB for TEM observation. The low β1 molecular beacon intensity section thinned unevenly during FIB milling, however portions of this section were still available for TEM observation (Figure 28C). An overview image of the section in the TEM showed areas along the top edge of the section that were electron transparent (Figure 28D). The regions of the section appeared to be a crystalline metal, presumably titanium (Figure 28E-G). Striations in the electron transparent regions were an artifact of FIB milling. A TEM section was also milled from a high β1 molecular beacon intensity cell (Figure 29A, B). During TEM observation of the high β1 molecular beacon intensity section (Figure 29C), a possible interface between platinum and titanium was seen (Figure 29D, E). The middle section of this interface thinned more quickly than the metal on either side, and is possibly where a portion of the cell was prior to milling (Figure 29 F, G).

Table 1: Molecular beacon intensity of cells milled on the FIB.

Molecular Beacon Intensity		
Cell	TEM Section	Serial Sectioning
High β1 MB Intensity	1.403×10^8	2.555×10^8
Low β1 MB Intensity	8.589×10^7	5.008×10^7

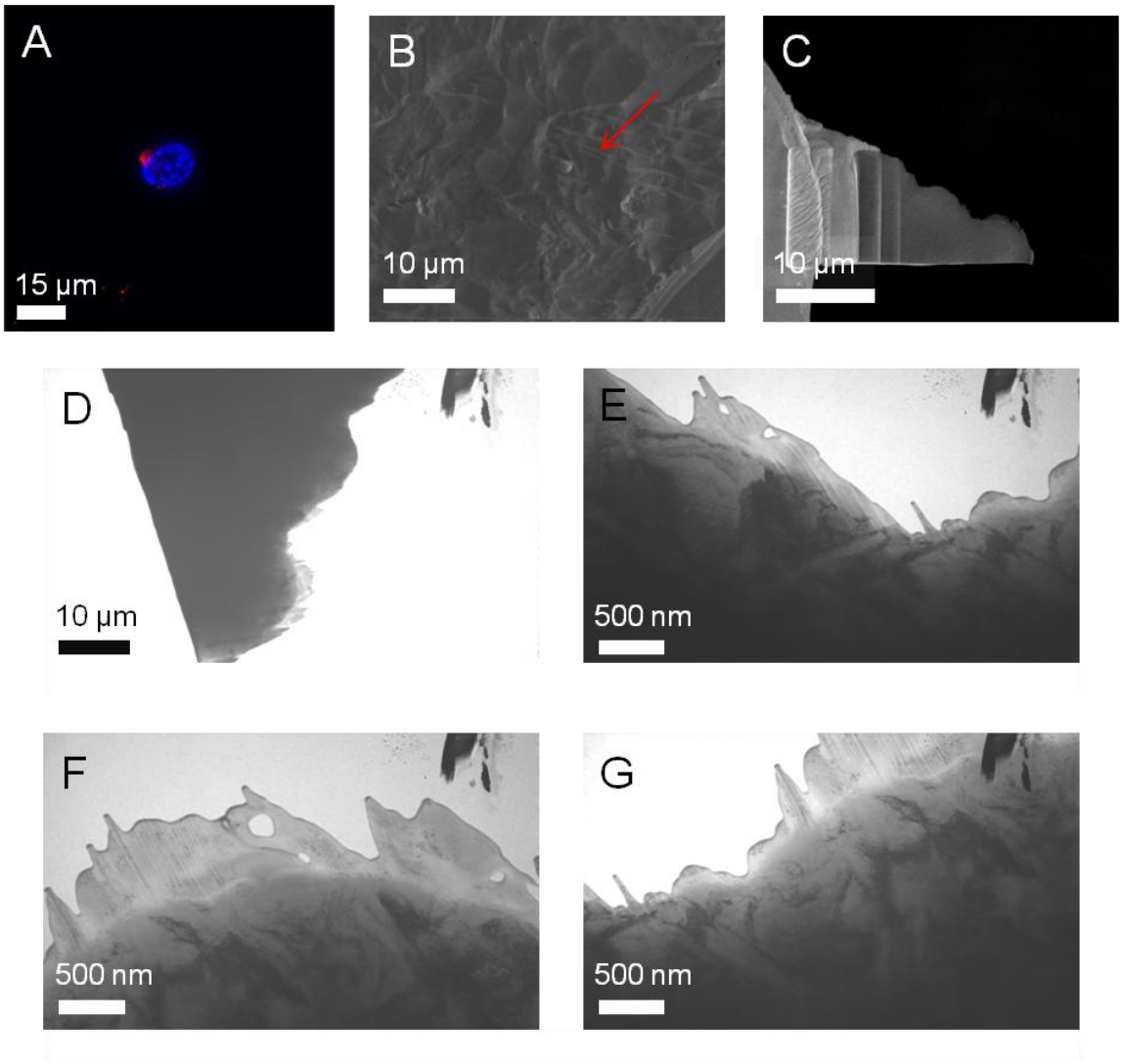

Figure 28: Milling and visualizing a low β1 molecular beacon intensity cell. **(A)** The low β1 molecular beacon intensity MG63 cell image fluorescently. (**B)** The high β1 molecular beacon cell located on the FIB. **(C)** TEM cross section milled on the FIB. **(D)** TEM overview image of the cross section. **(E)** TEM image of the cross section. **(F)** TEM image of the cross section. **(G)** TEM image of the cross section.

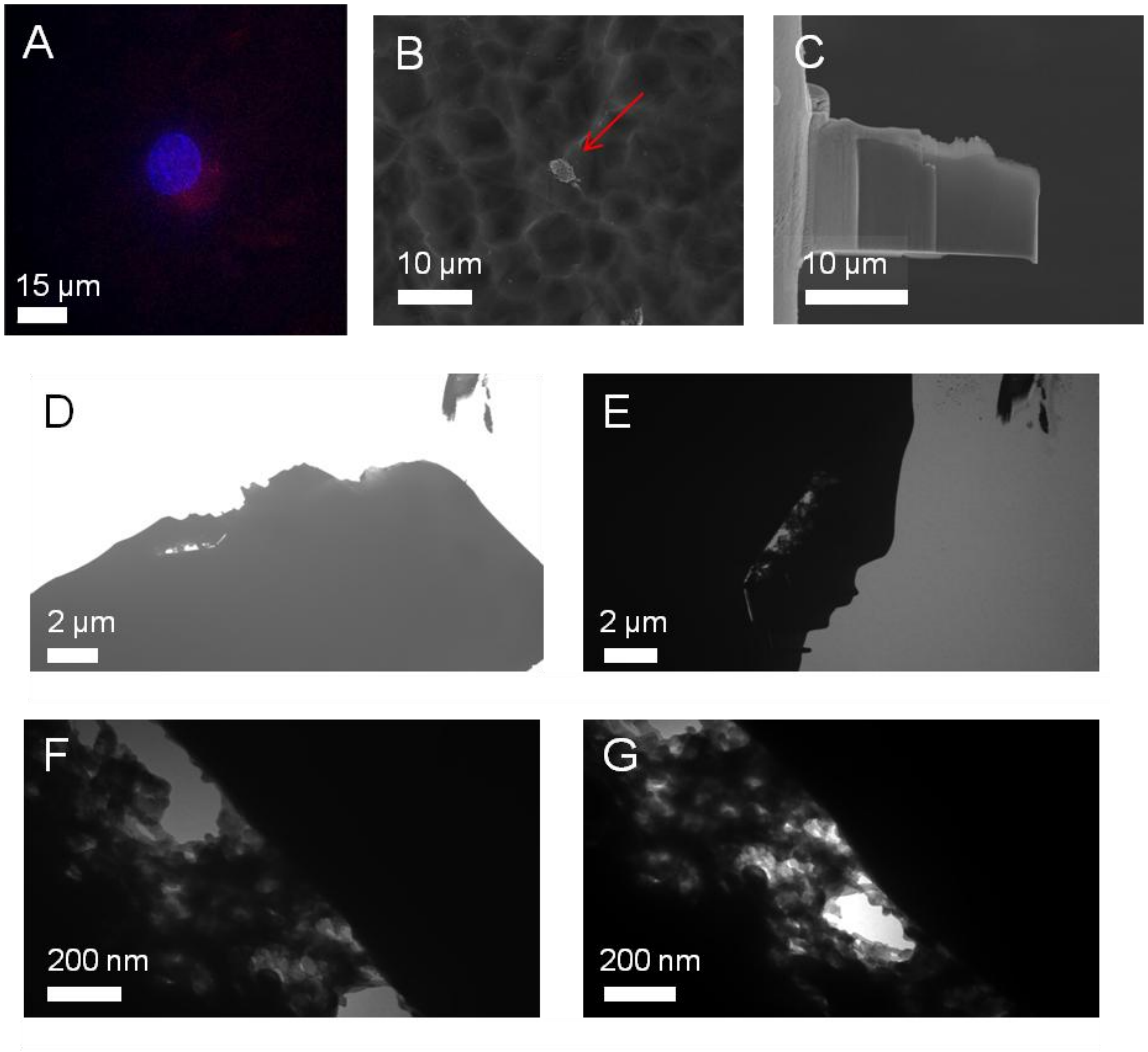

Figure 29: Milling and visualizing a high β1 molecular beacon intensity cell. **(A)** The high β1 molecular beacon intensity MG63 cell image fluorescently. **(B)** The high β1 molecular beacon cell located on the FIB. **(C)** TEM cross section milled on the FIB. **(D)** TEM overview image of the cross section. **(E)** TEM image of the cross section. **(F)** TEM image of the cross section. **(G)** TEM image of the cross section.

One low β1 molecular beacon intensity cell (Figure 30A, B) and one high β1 molecular beacon intensity cell (Figure 31A, B) were also serial sectioned on the FIB for

simultaneous SEM observation of the cell-substrate interactions. In milling through the low β1 molecular beacon intensity cell, the cell was not in continual contact with the substrate. Areas were seen where the cell was in contact with the titanium substrate, and the locations of contact varied throughout the cell (Figure 30C-F). In milling through the high β1 molecular beacon intensity cell, the cell was not in continual contact with the substrate; varying contact between the cell and the substrate could also be seen (Figure 31C-F). There appeared to be larger areas of contact between the high molecular beacon intensity cell and the substrate than with the low molecular beacon intensity cell and substrate. Three-dimensional (3D) reconstructions for both the high and low β1 molecular beacon intensity cells were done to represent a projection of the cell taken from all of the serial sectioning images (Figure 30G, 31G). The cell periphery in contact with the surface and the number of contact regions between the cells and the surfaces were calculated from the serial sectioning images (Figure 32A – D). The low β1 molecular beacon intensity cell had a higher distance in contact with the surface and number of contact points with the surface when normalized to the number of images (Figure 33A, C). However, the high β1 molecular beacon intensity cell had a higher distance in contact with the surface and number of contact points with the surface when normalized to the cell volume (Figure 33B, D).

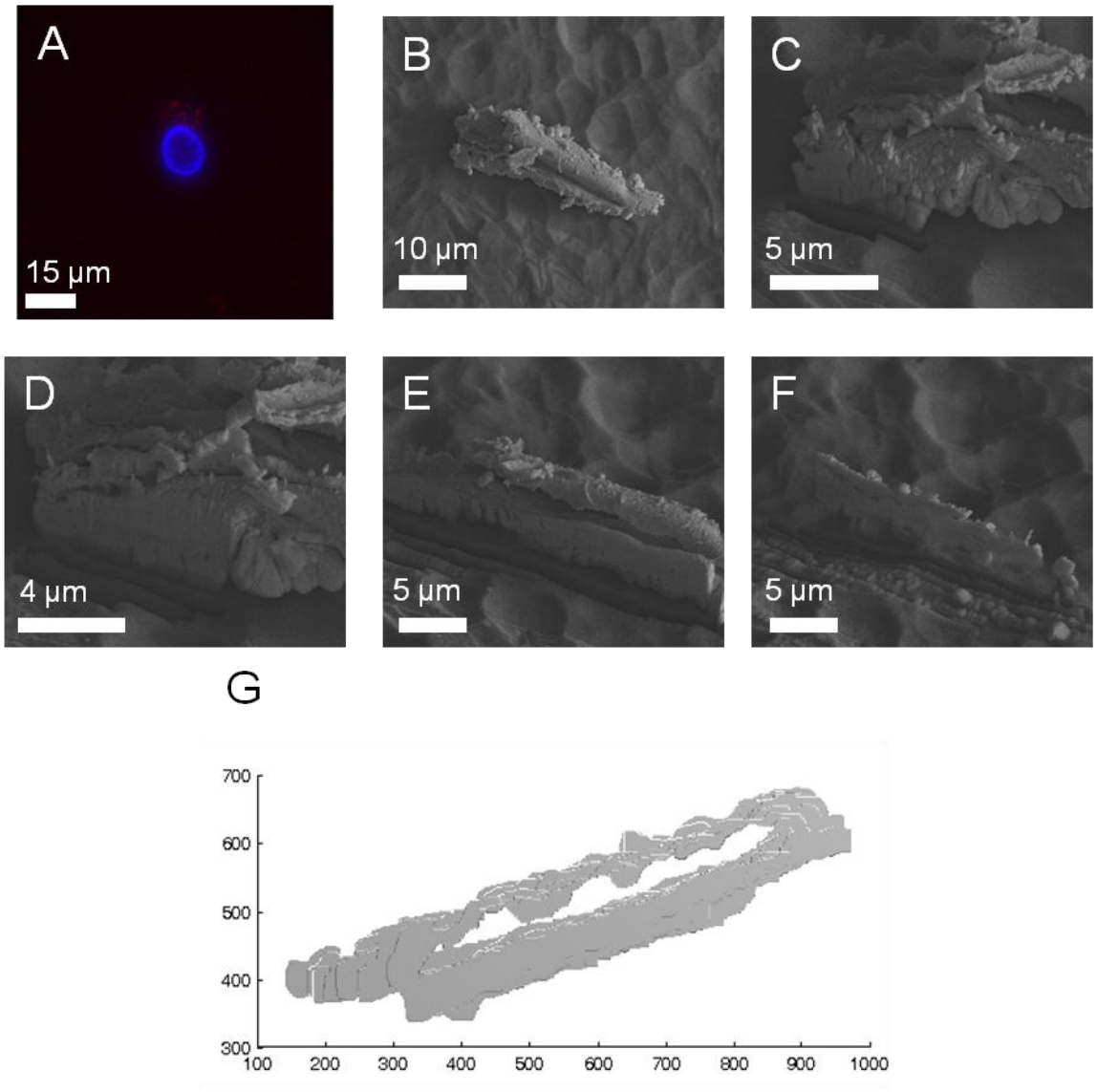

Figure 30: FIB serial sectioning through a low β1 molecular beacon intensity cell. **(A)** The low β1 molecular beacon intensity MG63 cell image fluorescently. **(B)** The same cell identified on the FIB using the coordinates system. **(C)-(F)** Serial sectioning through the cell. **(G)** 3D reconstruction of the low β1 molecular beacon intensity cell.

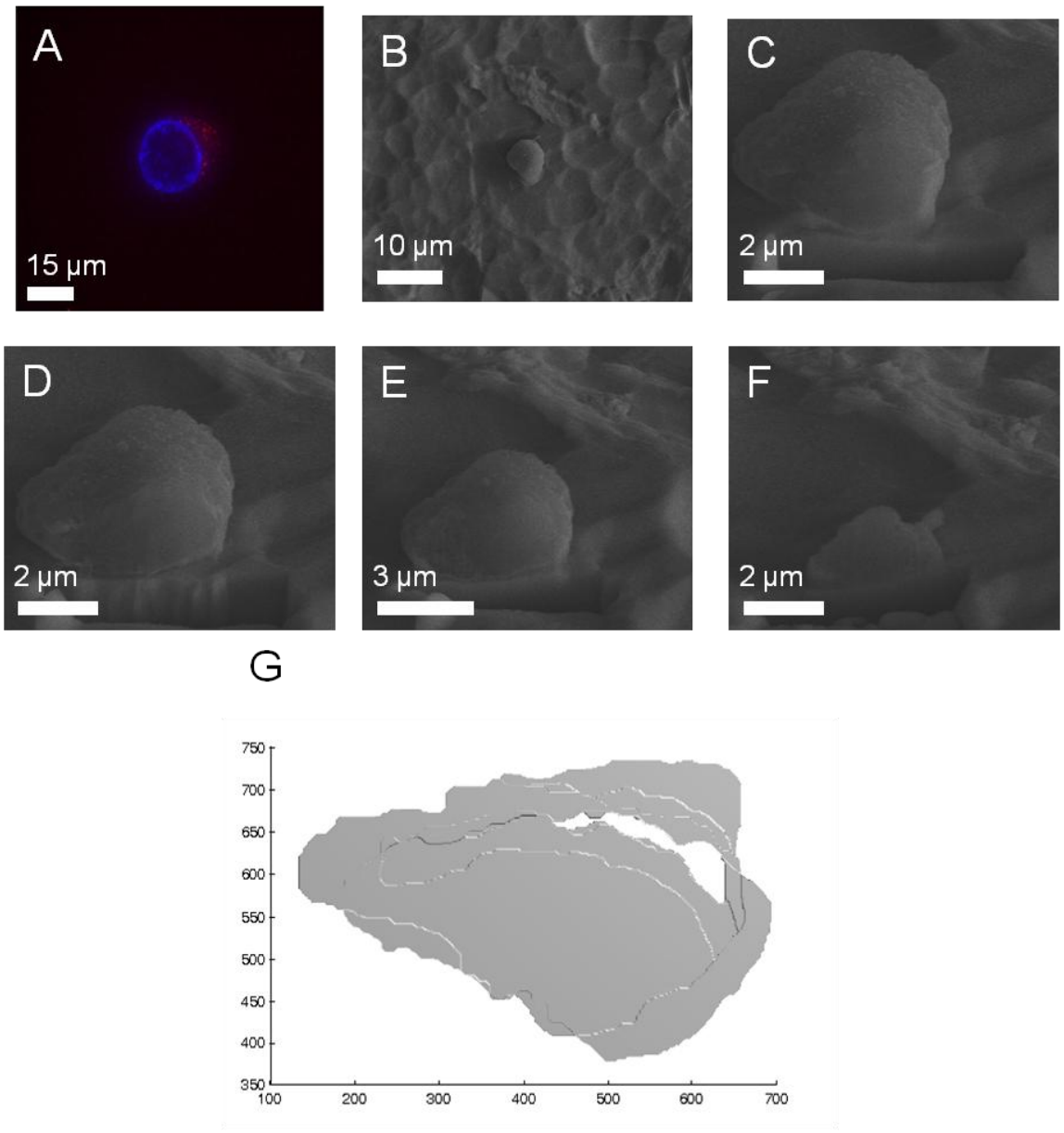

Figure 31: FIB serial sectioning through a high β1 molecular beacon intensity cell. **(A)** The high β1 molecular beacon intensity MG63 cell image fluorescently. **(B)** The same cell identified on the FIB using the coordinates system. **(C)-(F)** Serial sectioning through the cell. **(G)** 3D reconstruction of the high β1 molecular beacon intensity cell.

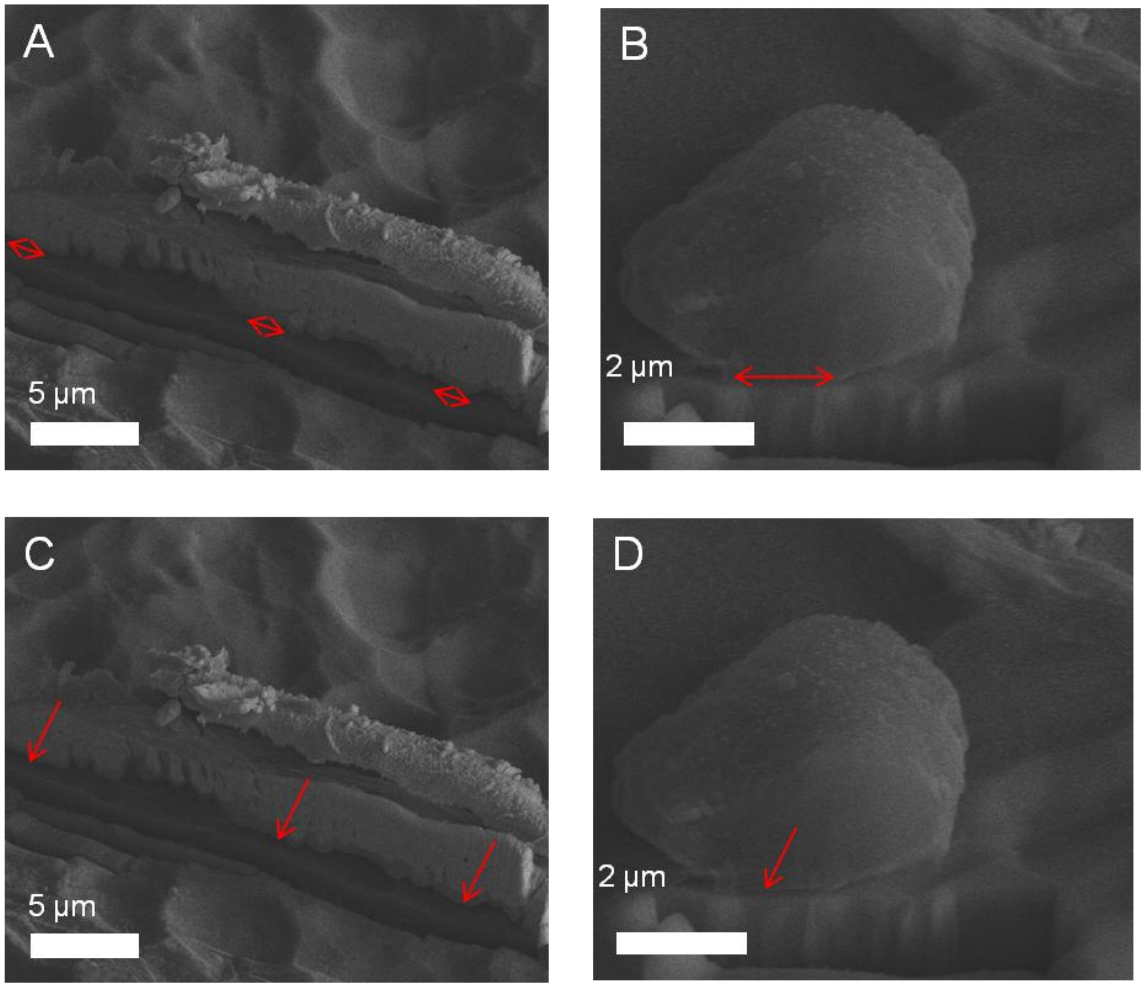

Figure 32: Schematic of parameters quantified in serial sectioning images. **(A)** Cell periphery in contact with the disk surface for the low β1 molecular beacon intensity cell. **(B)** Cell periphery in contact with the disk surface for the high β1 molecular beacon intensity cell. **(C)** Number of contact regions between the cell and the surface for the low β1 molecular beacon intensity cell. **(D)** Number of contact regions between the cell and the surface for the high β1 molecular beacon intensity cell.

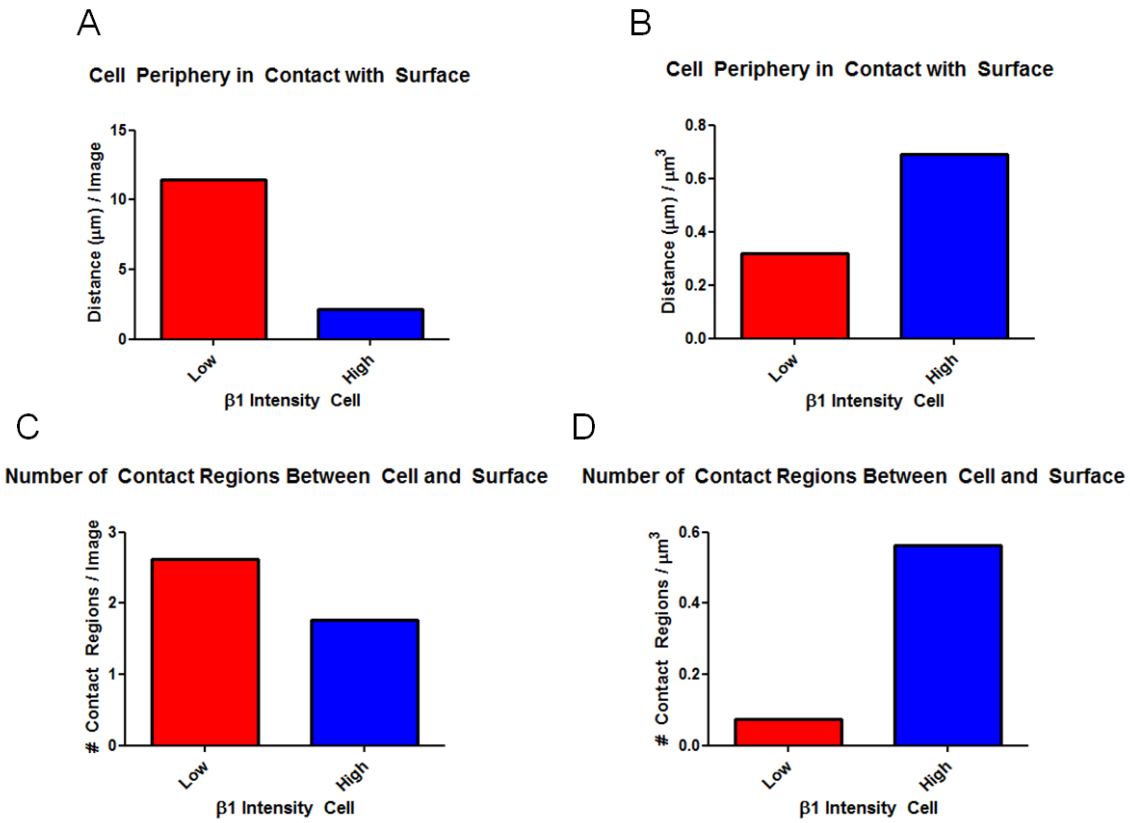

Figure 33: Analysis of high and low β1 molecular beacon intensity cell serial sectioning. **(A)** Cell periphery in contact with the surface normalized to the number of images. **(B)** Cell periphery in contact with the surface normalized to the cell volume. **(C)** Number of contact regions between the cells and the surfaces normalized to the number of images. **(D)** Number of contact regions between the cells and the surfaces normalized to cell volume.

A control cell that was not imaged fluorescently was also serial sectioned. The cell appeared to be flat upon the surface, and was attached to the titanium with a few major extensions (Figure 34A). Serial sectioning through the cell showed that the cell was not in continual contact with the surface but instead contact with the surface, and extensions from the cell body to the substrate could be seen (Figure 34B-F). A 3D reconstruction for the control cell was done to represent a projection of the cell taken from all of the serial sectioning images (Figure 34G).

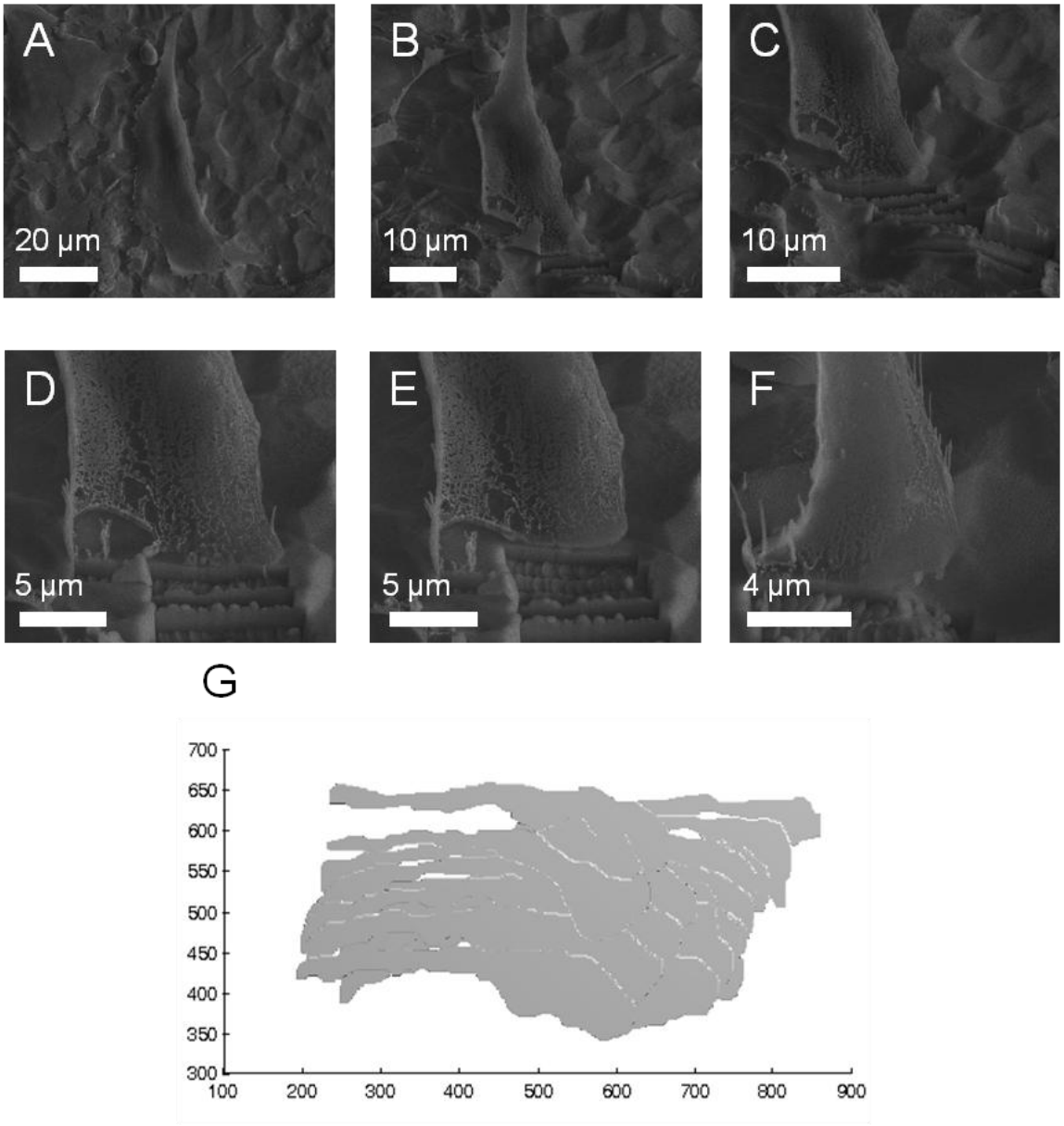

Figure 34: FIB serial sectioning through a control cell. **(A)** The control MG63 cell. **(B)-(F)** Serial sectioning through the cell. **(G)** 3D reconstruction of the control cell.

After observing the cell-substrate interface with a control cell, cells cultured on PT and SLA disks were serial sectioned to determine how the cells attached to the surfaces with different morphologies (Figure 35A, F and 36A, F). Cells on PT disks that were serial sectioned showed that the cells were not in continual contact with the substrate (Figure 35B-D, G-I). Cells on PT surfaces appeared to lay flat on the surfaces, with few extensions attaching to the substrates. Cells on SLA disks also were not in continual contact with the surface (Figure 36B-D, G-I). However, in contrast to cells on PT disks, cells on SLA disks appear to tent over the surface microstructure. Regions of contact between the cells and the surface on PT (Figure 37A, B) and SLA (Figure 37C, D) were observed in serial sectioning images, however no finite points of contact between the cell and the surface were seen. 3D reconstructions for these cells were done to represent a projection of the cell taken from all of the serial sectioning images (Figure 35E, J, 36E, J). The cell periphery in contact with the surface and the number of contact regions between the cells and the surfaces were calculated from the serial sectioning images (Figure 38A – D). Analysis of these images showed no difference in the distance of contact between the cells and the surface on PT and SLA (Figure 39A-C). Cells cultured on SLA had a higher number of points in contact with the surface than cells cultured on PT when normalized to the number of images (Figure 39D) but not when normalized to cell area or volume (Figure 39E, F).

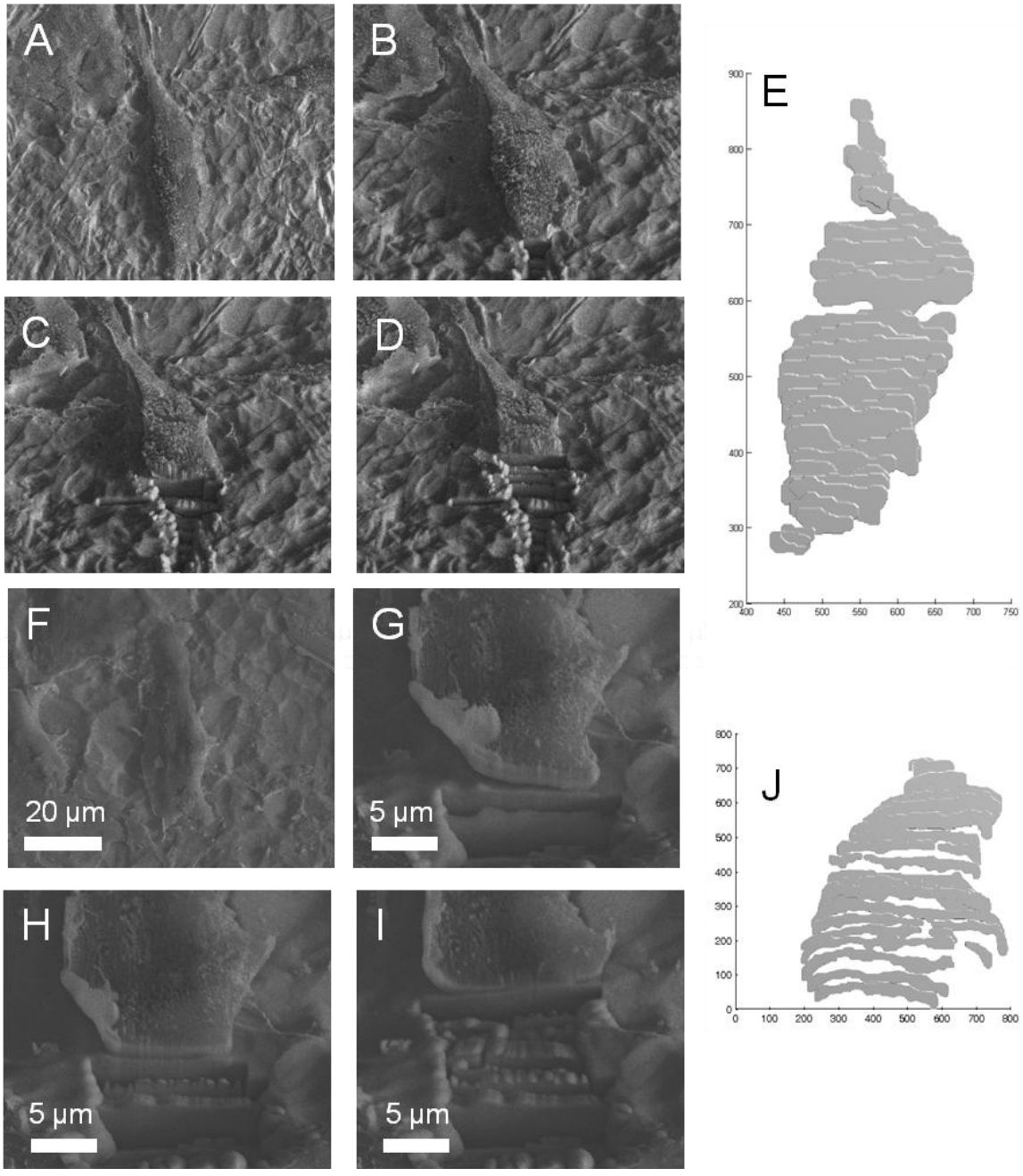

Figure 35: FIB serial sectioning through two cells on PT disks. **(A)** An MG63 cell on a PT disk. **(B)–(D)** Low magnification serial sectioning through the cell. **(E)** 3D reconstruction of the cell. **(F)** An MG63 cell on a PT disk. **(G)–(I)** High magnification serial sectioning through the cell. **(J)** 3D reconstruction of the cell.

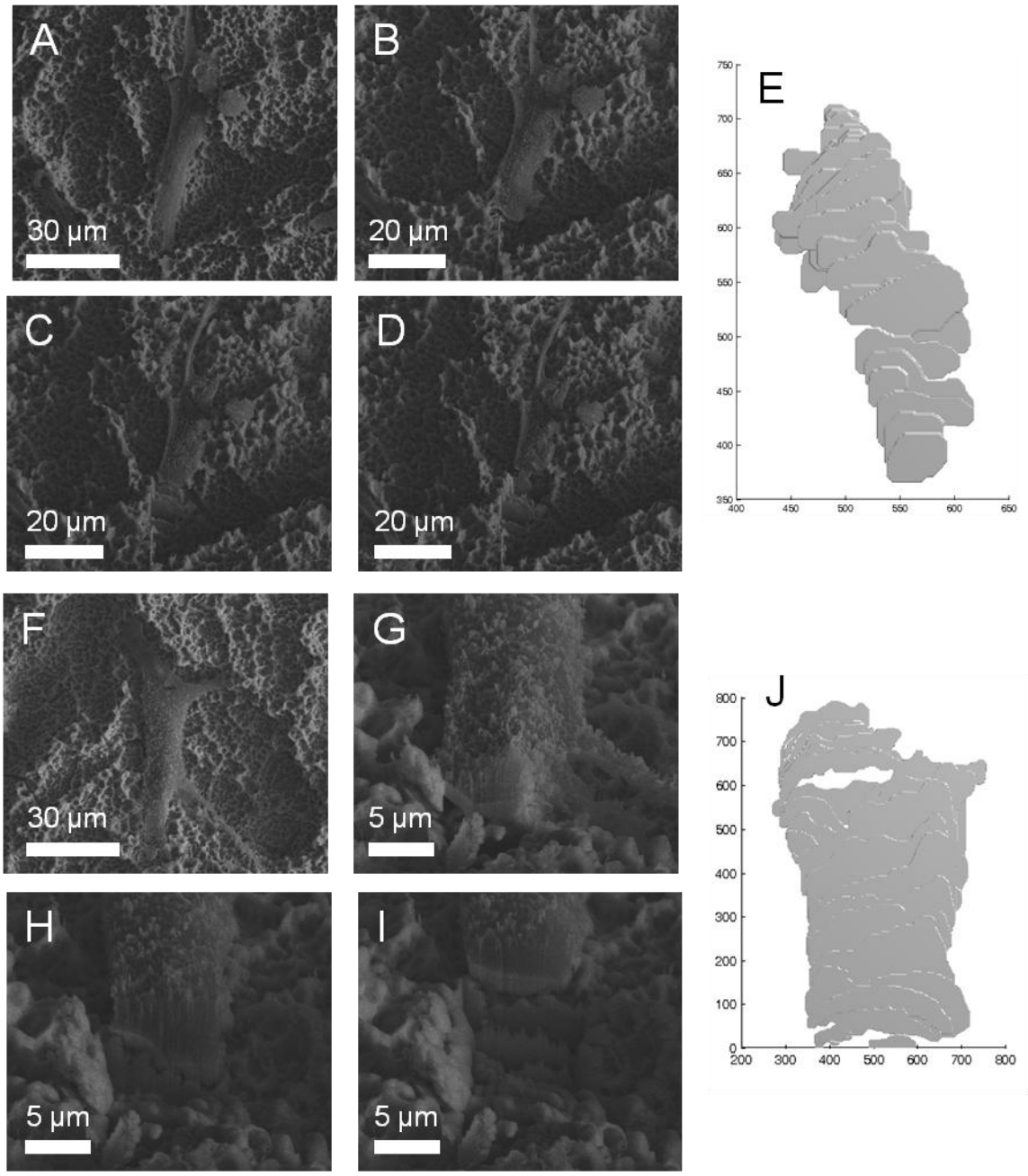

Figure 36: FIB serial sectioning through two cells on SLA disks. **(A)** An MG63 cell on a SLA disk. **(B)–(D)** Low magnification serial sectioning through the cell. **(E)** 3D reconstruction of the cell. **(F)** An MG63 cell on a SLA disk. **(G)–(I)** High magnification serial sectioning through the cell. **(J)** 3D reconstruction of the cell.

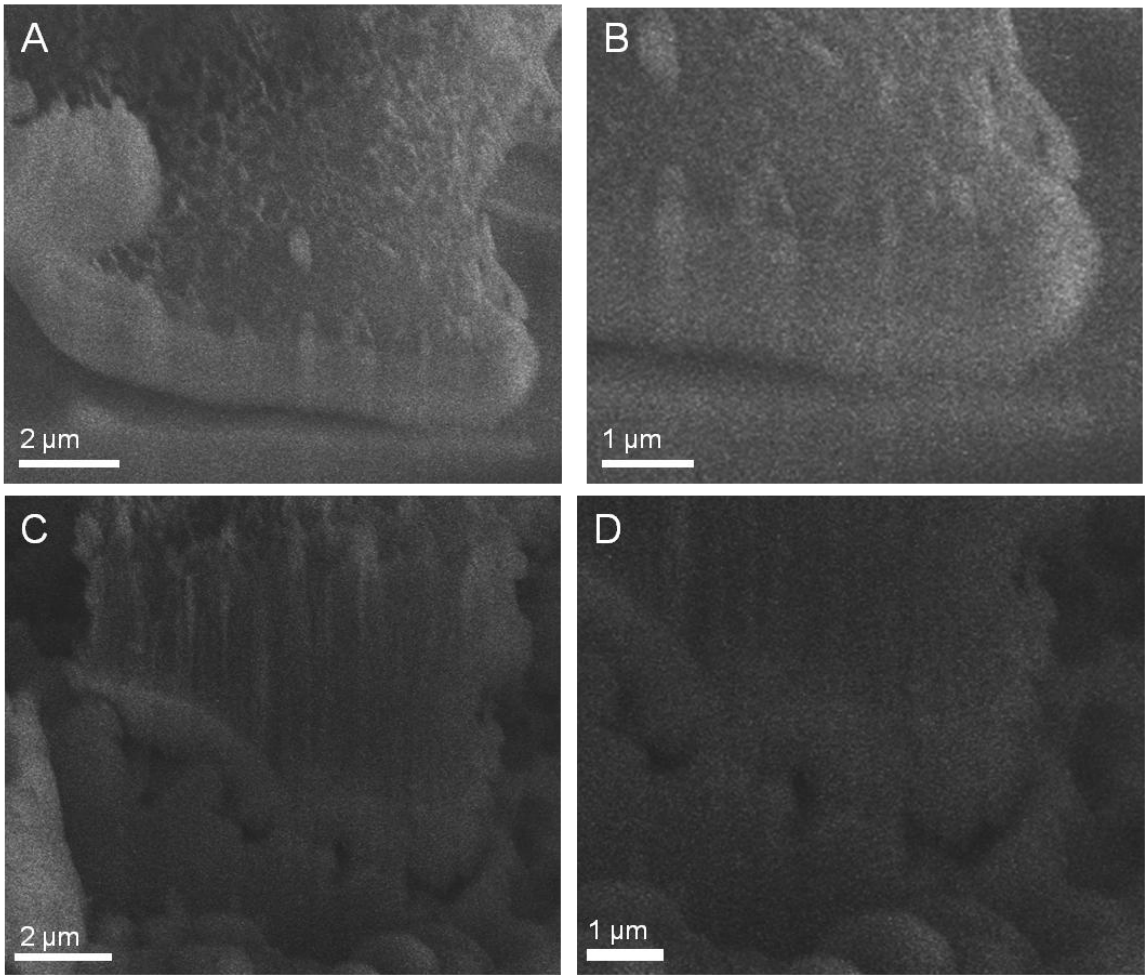

Figure 37: Visualization a contact region of cells on PT and SLA disks. **(A)-(B)** Contact region between a cell and the surface of a PT disk. **(C)-(D)** Contact region between a cell and the surface of a SLA disk.

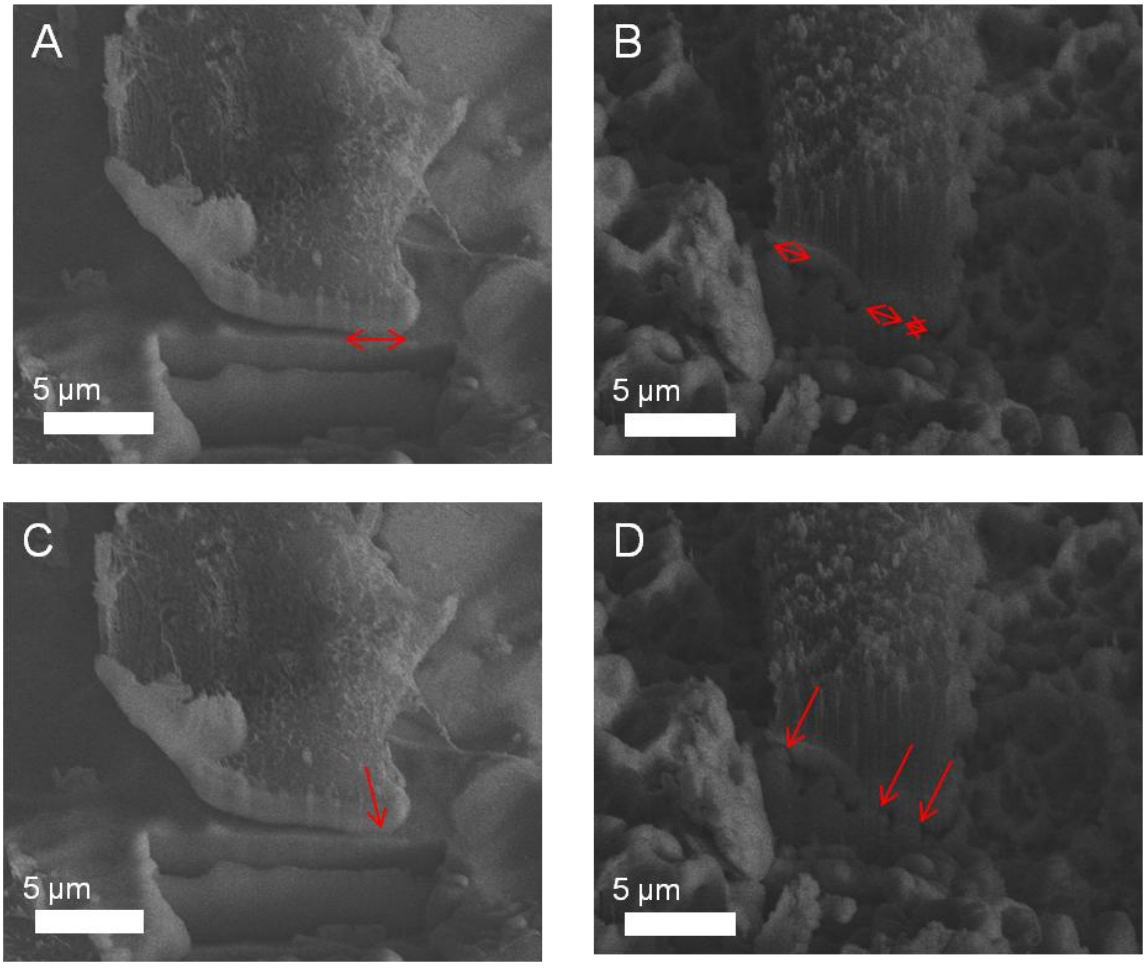

Figure 38: Schematic of parameters quantified in serial sectioning images. **(A)** Cell periphery in contact with the disk surface for a cell on a PT disk. **(B)** Cell periphery in contact with the disk surface for a cell on a SLA disk. **(C)** Number of contact regions between the cell and the surface for a cell on a PT disk. **(D)** Number of contact regions between the cell and the surface for a cell on a SLA disk.

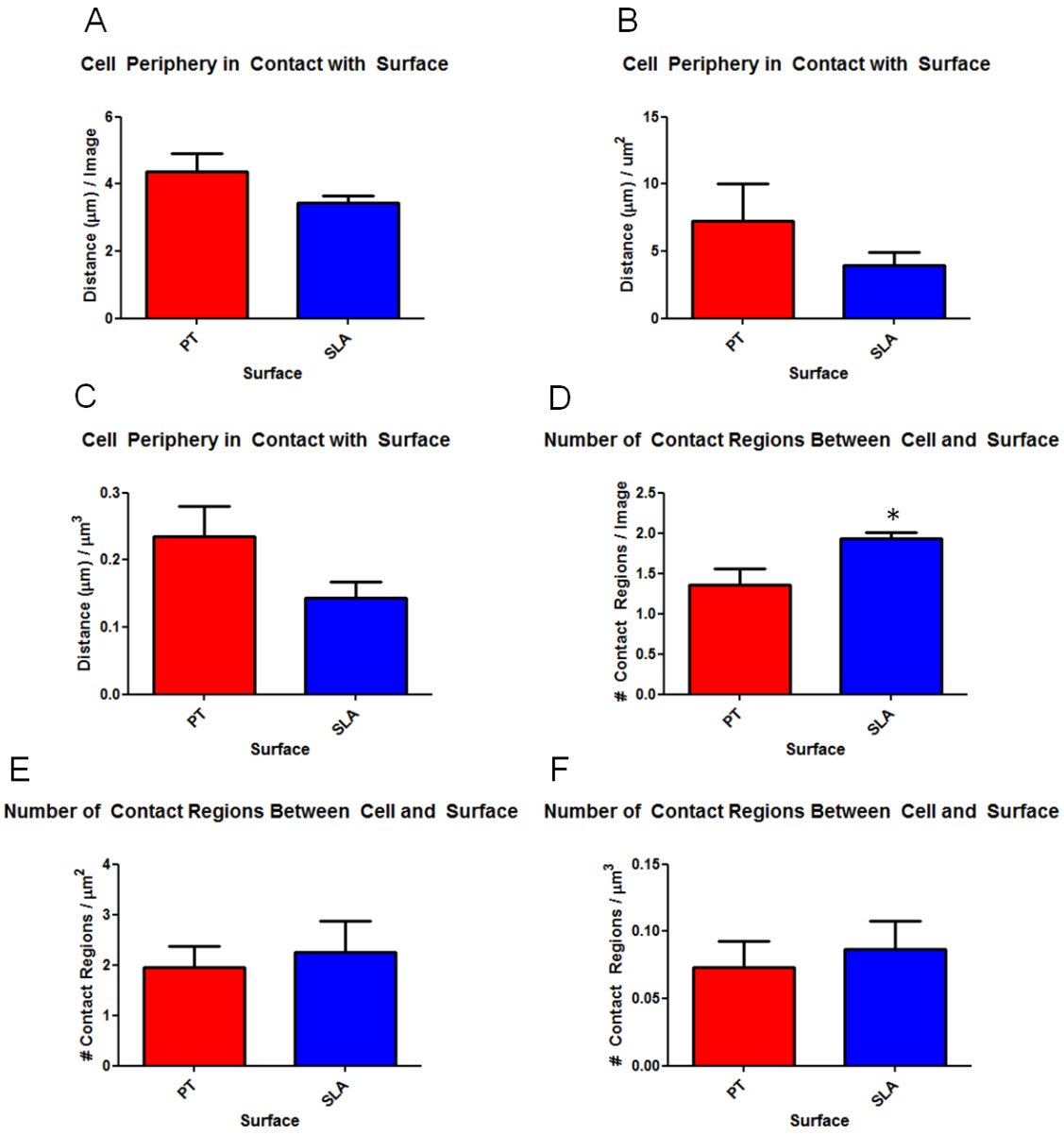

Figure 39: Analysis of cells serial sectioned on PT and SLA disks. **(A)** Cell periphery in contact with the surface normalized to the number of images. **(B)** Cell periphery in contact with the surface normalized to the cell area. **(C)** Cell periphery in contact with the surface normalized to the cell volume. **(D)** Number of contact regions between the cells and the surface normalized to the number of images. **(E)** Number of contact regions between the cells and the surface normalized to cell area. **(F)** Number of contact regions between the cells and the surface normalized to cell volume.

Diverse studies have shown the FIB is a useful tool for sectioning and imaging of tissues[45,46] and cell-substrate interfaces.[47-50] Previous TEM results of cells cultured on titanium foils or PLGA fibers on glass showed clear boundaries at the cell-substrate interfaces.[48,50] Our TEM results did not show a clear cell-substrate boundary like previous studies have. For the low β1 molecular beacon intensity cell, it is possible that the cell-substrate interface was milled away because the sample did not thin evenly as an artifact of the FIB milling. In these images, only striations along the edge of the sample can be seen, and Drobne et al. showed that this effect is caused by an interaction between the ion beam and the sample.[71] The titanium oxide layer on the surface of a dental implant has been viewed in bright field TEM in a study by Jarmar et al.,[44] however this oxide layer was only visible in scanning TEM images and EDX maps in a study of human osteoblasts on titanium foil.[50] In our results, TEM images from the high β1 molecular beacon intensity cell showed a possible interface where presumably organic matter was milled away at a faster rate than the titanium and the platinum, however, no oxide layer was identified. The technique for milling TEM sections, as well as the technology for molecular beacon imaging, would have to be optimized for conclusive results to be drawn correlating β1 molecular beacon intensity and surface properties. The traditional technique for milling TEM sections, which was employed in our study, is limiting because the high currents used to mill the initial trenches cause the organic material to mill away at a faster rate than the titanium substrate or protective platinum coating. Because FIB serial sectioning showed the cell-substrate interface, it would be possible to optimize an alternate, hybrid method for milling TEM sections. In this alternate method, serial sectioning through a cell could be done until a contact was seen between the cell and the substrate. Serial sectioning could then be done from the other side of the cell, narrowing out this region with an identified point of contact

between the cell and the substrate. Narrow, deeper trenches could then be milled around this region, for the TEM section to be removed from the disk.

A low β1 molecular beacon intensity cell, a high β1 molecular beacon intensity cell, and a control cell (that was not fluorescently imaged) were also serial sectioned to image cell-substrate interactions. Studies by Martinez et al. and Bittermann et al. showed that the cell-substrate interface is not homogeneous, but that the cell has contact points with the substrate.[47,48] In contrast, Edwards et al. showed that cells on titanium foils had "continuous attachment" to the substrate. Our results were consistent with Martinez and Bittermann, where the cells were not in continual contact with the titanium. This could especially be seen in cross sectional images of the control cell, where extensions from the cell attached it to the substrate. We also noted that the high β1 molecular beacon intensity cell appeared to have larger areas of contact with the titanium substrate than the low β1 molecular beacon intensity cell. The high β1 molecular beacon intensity cell did have a higher distance of the cell periphery in contact with the surface and number of contact regions with the surface when normalized to the cell volume. This was not seen when these values were normalized to the number of images, possibly because the low β1 molecular beacon intensity cell was larger in size than the β1 molecular beacon intensity cell. However, it would be necessary to optimize the molecular beacon imaging process to prevent cell adhesion to the chamber slide before milling additional cells and drawing further conclusions.

After noting that the cell-substrate interface was clearly visible when a control cell was milled, cells on PT and SLA disks were milled to determine how cells attach to surfaces with different morphologies. While PT is a smooth surface (R_a<0.2μm), SLA is a microrough surface with R_a=3-4μm.[16] MG63 cells cultured on SLA surfaces have a higher β1 integrin expression than cells on PT surfaces[10], and cells cultured on SLA

surfaces exhibit a more differentiated phenotype than cells on PT surfaces.[16,23] Consistent with previous studies and our other serial sectioning results, cells on both surfaces were not in continual contact with the substrate.[47,48] However, when we zoomed in to regions of contact between the cell and surface, we were unable to see any finite contact points to the surface. In order to do so, high-resolution SEM images at much higher should be obtained in future studies. Cells on SLA surfaces appeared to tent over the surface microsturcture, and had more regions of contact between with the substrates than cells cultured on PT surfaces when this was normalized to the number of images, although the distance of cell periphery in contact with the substrate was not different for cells on PT versus SLA. No difference was seen when the number of contact regions was normalized to cell area or volume, and there are three possible explanations for this. First, for our study, we used n=4, and upon performing a larger serial sectioning study, these results may gain significance. Also, depending on the size of the cell, they were imaged at different magnifications, and even with normalization, this may affect results. Finally, for the cells milled at higher magnifications, only a portion of the cell was milled instead of the entire cell. While this may also affect our results, it was necessary to maintain the cell in one field of view for the purposes of later creating the 3D reconstructions.

CHAPTER 5

CONCLUSIONS

This study developed a method for correlating integrin β1 expression with surface characteristics under individual cells. In aim 1, we first developed a template so that the location of individual cells could be coordinated on the fluorescence microscope and the FIB. This was done by creating a system of laser etchings on the titanium disks, where the corners of the etchings could be used as reference points. Fluorescent membrane stains were studied to aid in confirming cell identity on the SEM. However, after studying the process of cell staining, molecular beacon delivery, and sample fixation and drying, it was determined that fluorescent stains could not be used with the molecular beacon delivery process. We also determined that cells were adhering to the glass chamber slide used to hold the disks during fluorescence imaging. Several methods to prevent this were tested, and for the rest of our work, molecular beacon imaging was done in Sigmacote® coated chamber slides for samples to then be prepared for FIB milling.

In aim 2, TEM sections under high and low β1 molecular beacon intensity cells were milled, and high and low β1 molecular beacon cells were serial sectioned. No clear cell-substrate interface was seen, and the technique needs to be optimized before further use. In serial sectioning through cells, contact points between the cell body and the substrate could be seen. The high β1 molecular beacon intensity cell had larger areas of contact with the titanium substrate and more points of contact with the substrate than the low β1 molecular beacon intensity cell. Further optimization of the method for fluorescence molecular beacon imaging would need to be done before milling additional

cells after fluorescence imaging and drawing additional conclusions. Cells cultured on PT and SLA disks were also serial sectioned, showing that cells on SLA surfaces appeared to tent over the surface microsturcture, with many regions of contact between the cells to the surface, while cells on PT surfaces laid flat upon the surface with fewer points of contact with the surface. No difference was seen in the distance of cell periphery in contact between the cells and the surface when cells were studied on PT or SLA surfaces.

Much work could be done in the future using the method developed in this project. As the problem of cell adhesion to the chamber slide during fluorescence imaging is the most limiting factor, I would suggest performing a test where cells are inserted in the chamber slides with spacers for the length of imaging time and then observed on the SEM to ensure that using a spacer would solve this cell adhesion problem. All of our results have led us to believe this would be the most promising solution to improve the fluorescence imaging before SEM. Upon confirmation of this hypothesis, Olympus manufactures a high working distance lens that also has a high numerical aperture, which would most likely allow a spacer to be used during fluorescence imaging. The process for fluorescence imaging could also be improved by investigating methods for molecular beacon delivery that are less damaging than using SLO. It would also be important for the accuracy of the coordinate system to be improved by placing the laser etchings closer to areas where cells will be identified. Additionally, the process for milling TEM sections could be improved by using a hybrid technique of serial sectioning and traditional TEM sample preparation. This would allow for sections to be analyzed using high-resolution TEM to enable surface characteristics, such as morphology, crystal structure, and composition, to be further correlated with integrin β1 molecular beacon intensity. Additionally, the template for coordinating cells

could possibly be used with other fluorescence techniques for cell imaging, such as immunocytochemsitry, instead of live cell molecular beacon imaging. Using appropriate protocols for immunocytochemsitry would allow for correlation of the levels of the desired protein target with substrate characteristics under individual cells.

In conclusion, this work established a method to correlate integrin β1 expression with surface characteristics under individual cells. This study was the first study developed to investigate individual cell behavior with the substrate surface characteristics under the individual cells instead of looking at the average behavior of a cell culture. While previous studies have determined differences in titanium surfaces that lead to a more differentiated osteoblastic phenotype, the surfaces are not uniform, and the results report an average of all cells on the surfaces. The method developed in this study allows for determination of the substrate surface characteristics that positively affect integrin β1 expression in individual cells. The method developed also has the possibilities to be optimized to improve the cell attachment problems during molecular beacon imaging, to optimize the TEM sample preparation process for additional material analyses to be conducted, and to use the template for locating cells in other fluorescent analysis of cell behavior.

REFERENCES

1. Branemark PI, Hansson BO, Adell R, et al. Osseointegrated implants in the treatment of the edentulous jaw. Experience from a 10-year period. *Scand J Plast Reconstr Surg Suppl.* 1977;16:1-132.

2. Albrektsson T, Branemark PI, Hansson HA, Lindstrom J. Osseointegrated titanium implants. Requirements for ensuring a long-lasting, direct bone-to-implant anchorage in man. *Acta Orthop Scand.* 1981;52(2):155-170.

3. Albrektsson T, Johansson C. Osteoinduction, osteoconduction and osseointegration. *Eur Spine J.* Oct 2001;10 Suppl 2:S96-101.

4. Cochran DL, Schenk RK, Lussi A, Higginbottom FL, Buser D. Bone response to unloaded and loaded titanium implants with a sandblasted and acid-etched surface: a histometric study in the canine mandible. *J Biomed Mater Res.* Apr 1998;40(1):1-11.

5. Cochran DL, Buser D, ten Bruggenkate CM, et al. The use of reduced healing times on ITI implants with a sandblasted and acid-etched (SLA) surface: early results from clinical trials on ITI SLA implants. *Clin Oral Implants Res.* Apr 2002;13(2):144-153.

6. Karoussis IK, Salvi GE, Heitz-Mayfield LJ, Bragger U, Hammerle CH, Lang NP. Long-term implant prognosis in patients with and without a history of chronic periodontitis: a 10-year prospective cohort study of the ITI Dental Implant System. *Clin Oral Implants Res.* Jun 2003;14(3):329-339.

7. Bachle M, Kohal RJ. A systematic review of the influence of different titanium surfaces on proliferation, differentiation and protein synthesis of osteoblast-like MG63 cells. *Clin Oral Implants Res.* Dec 2004;15(6):683-692.

8. Lim YJ, Oshida Y, Andres CJ, Barco MT. Surface characterizations of variously treated titanium materials. *Int J Oral Maxillofac Implants.* May-Jun 2001;16(3):333-342.

9. Zinger O, Zhao G, Schwartz Z, et al. Differential regulation of osteoblasts by substrate microstructural features. *Biomaterials.* May 2005;26(14):1837-1847.

10. Olivares-Navarrete R, Raz P, Zhao G, et al. Integrin alpha2beta1 plays a critical role in osteoblast response to micron-scale surface structure and surface energy of titanium substrates. *Proc Natl Acad Sci U S A.* Oct 14 2008;105(41):15767-15772.

11. Zhao G, Schwartz Z, Wieland M, et al. High surface energy enhances cell response to titanium substrate microstructure. *J Biomed Mater Res A.* Jul 1 2005;74(1):49-58.

12. Lossdorfer S, Schwartz Z, Wang L, et al. Microrough implant surface topographies increase osteogenesis by reducing osteoclast formation and activity. *J Biomed Mater Res A.* Sep 1 2004;70(3):361-369.

13. Schwartz Z, Lohmann CH, Oefinger J, Bonewald LF, Dean DD, Boyan BD. Implant surface characteristics modulate differentiation behavior of cells in the osteoblastic lineage. *Adv Dent Res.* Jun 1999;13:38-48.

14. Olivares-Navarrete R, Hyzy SL, Hutton DL, et al. Direct and indirect effects of microstructured titanium substrates on the induction of mesenchymal stem cell differentiation towards the osteoblast lineage. *Biomaterials.* Apr 2010;31(10):2728-2735.

15. Gittens RA, McLachlan T, Olivares-Navarrete R, et al. The effects of combined micron-/submicron-scale surface roughness and nanoscale features on cell proliferation and differentiation. *Biomaterials.* May 2011;32(13):3395-3403.
16. Zhao G, Raines AL, Wieland M, Schwartz Z, Boyan BD. Requirement for both micron- and submicron scale structure for synergistic responses of osteoblasts to substrate surface energy and topography. *Biomaterials.* Jun 2007;28(18):2821-2829.
17. Wang CY, Zhao BH, Ai HJ, Wang YW. Comparison of biological characteristics of mesenchymal stem cells grown on two different titanium implant surfaces. *Biomed Mater.* Mar 2008;3(1):015004.
18. Oonishi H, Yamamoto M, Ishimaru H, et al. The effect of hydroxyapatite coating on bone growth into porous titanium alloy implants. *J Bone Joint Surg Br.* Mar 1989;71(2):213-216.
19. Wang L, Zhao G, Olivares-Navarrete R, et al. Integrin beta1 silencing in osteoblasts alters substrate-dependent responses to 1,25-dihydroxy vitamin D3. *Biomaterials.* Jul 2006;27(20):3716-3725.
20. Siebers MC, ter Brugge PJ, Walboomers XF, Jansen JA. Integrins as linker proteins between osteoblasts and bone replacing materials. A critical review. *Biomaterials.* Jan 2005;26(2):137-146.
21. Sinha RK, Tuan RS. Regulation of human osteoblast integrin expression by orthopedic implant materials. *Bone.* May 1996;18(5):451-457.
22. Postiglione L, Di Domenico G, Ramaglia L, et al. Behavior of SaOS-2 cells cultured on different titanium surfaces. *J Dent Res.* Sep 2003;82(9):692-696.
23. Raz P, Lohmann CH, Turner J, et al. 1alpha,25(OH)2D3 regulation of integrin expression is substrate dependent. *J Biomed Mater Res A.* Nov 1 2004;71(2):217-225.
24. Xiao G, Wang D, Benson MD, Karsenty G, Franceschi RT. Role of the alpha2-integrin in osteoblast-specific gene expression and activation of the Osf2 transcription factor. *J Biol Chem.* Dec 4 1998;273(49):32988-32994.
25. Vihinen P, Riikonen T, Laine A, Heino J. Integrin alpha 2 beta 1 in tumorigenic human osteosarcoma cell lines regulates cell adhesion, migration, and invasion by interaction with type I collagen. *Cell Growth Differ.* Apr 1996;7(4):439-447.
26. Cutler SM, Garcia AJ. Engineering cell adhesive surfaces that direct integrin alpha5beta1 binding using a recombinant fragment of fibronectin. *Biomaterials.* May 2003;24(10):1759-1770.
27. Keselowsky BG, Wang L, Schwartz Z, Garcia AJ, Boyan BD. Integrin alpha(5) controls osteoblastic proliferation and differentiation responses to titanium substrates presenting different roughness characteristics in a roughness independent manner. *J Biomed Mater Res A.* Mar 1 2007;80(3):700-710.
28. Tyagi S, Kramer FR. Molecular beacons: probes that fluoresce upon hybridization. *Nat Biotechnol.* Mar 1996;14(3):303-308.
29. Tan W, Wang K, Drake TJ. Molecular beacons. *Curr Opin Chem Biol.* Oct 2004;8(5):547-553.
30. Kim Y, Sohn D, Tan W. Molecular beacons in biomedical detection and clinical diagnosis. *Int J Clin Exp Pathol.* 2008;1(2):105-116.
31. Wang K, Tang Z, Yang CJ, et al. Molecular engineering of DNA: molecular beacons. *Angew Chem Int Ed Engl.* 2009;48(5):856-870.
32. Nitin N, Santangelo PJ, Kim G, Nie S, Bao G. Peptide-linked molecular beacons for efficient delivery and rapid mRNA detection in living cells. *Nucleic Acids Res.* 2004;32(6):e58.

33. Cheung CY, Murthy N, Stayton PS, Hoffman AS. A pH-sensitive polymer that enhances cationic lipid-mediated gene transfer. *Bioconjug Chem.* Nov-Dec 2001;12(6):906-910.
34. Yin D, Tang JG. Gene therapy for streptozotocin-induced diabetic mice by electroporational transfer of naked human insulin precursor DNA into skeletal muscle in vivo. *FEBS Lett.* Apr 20 2001;495(1-2):16-20.
35. Sokol DL, Zhang X, Lu P, Gewirtz AM. Real time detection of DNA.RNA hybridization in living cells. *Proc Natl Acad Sci U S A.* Sep 29 1998;95(20):11538-11543.
36. Faria M, Spiller DG, Dubertret C, et al. Phosphoramidate oligonucleotides as potent antisense molecules in cells and in vivo. *Nat Biotechnol.* Jan 2001;19(1):40-44.
37. Bhakdi S, Tranum-Jensen J, Sziegoleit A. Mechanism of membrane damage by streptolysin-O. *Infect Immun.* Jan 1985;47(1):52-60.
38. Findlay I. Single cell PCR : theory, practice, and clinical applications. *Methods Mol Med.* 1998;16:233-263.
39. Lennon FE, Hermann CD, Olivares-Navarrete R, et al. Use of molecular beacons to image effects of titanium surface microstructure on beta1 integrin expression in live osteoblast-like cells. *Biomaterials.* Jul 29 2010.
40. Volkert CA, Minor, A.M. (eds). Focused Ion Beam Microscopy and Micromachining. *Mrs Bull.* 2007;32:389-395.
41. Orloff J. High-resolution focused ion beams. *Rev Sci Instrum.* 1993;64(5):1105-1130.
42. Munroe PR. The application of focused ion beam microscopy in the material sciences. *Materials Characterization.* 2009;60:2-13.
43. Li J, Malis T, Dionne S. Recent advances in FIB-TEM specimen preparation techniques. *Materials Characterization.* 2006;57:64-70.
44. Jarmar T, Palmquist A, Branemark R, Hermansson L, Engqvist H, Thomsen P. Technique for preparation and characterization in cross-section of oral titanium implant surfaces using focused ion beam and transmission electron microscopy. *J Biomed Mater Res A.* Dec 15 2008;87(4):1003-1009.
45. Drobne D, Milani M, Ballerini M, et al. Focused ion beam for microscopy and in situ sample preparation: application on a crustacean digestive system. *J Biomed Opt.* Nov-Dec 2004;9(6):1238-1243.
46. Drobne D, Milani M, Zrimec A, Leser V, Berden Zrimec M. Electron and ion imaging of gland cells using the FIB/SEM system. *J Microsc.* Jul 2005;219(Pt 1):29-35.
47. Martinez E, Engel E, Lopez-Iglesias C, Mills CA, Planell JA, Samitier J. Focused ion beam/scanning electron microscopy characterization of cell behavior on polymer micro-/nanopatterned substrates: a study of cell-substrate interactions. *Micron.* 2008;39(2):111-116.
48. Bitterman A.G. BCaHH. Imaging of Cell-to-Material Interfaces by SEM after in situ Focused Ion Beam Milling on Flat Surfaces and Complex 3D-Fibrous Structures. *Adv Eng Mater.* 2009;11(11):B182 - B188.
49. Engqvist H, Svahn F, Jarmar T, et al. A novel method for producing electron transparent films of interfaces between cells and biomaterials. *J Mater Sci Mater Med.* Jan 2008;19(1):467-470.
50. Edwards HK, Fay MW, Anderson SI, Scotchford CA, Grant DM, Brown PD. An appraisal of ultramicrotomy, FIBSEM and cryogenic FIBSEM techniques for the sectioning of biological cells on titanium substrates for TEM investigation. *J Microsc.* Apr 2009;234(1):16-25.

51. Cooper JA. Effects of cytochalasin and phalloidin on actin. *J Cell Biol.* Oct 1987;105(4):1473-1478.
52. Barak LS, Yocum RR, Nothnagel EA, Webb WW. Fluorescence staining of the actin cytoskeleton in living cells with 7-nitrobenz-2-oxa-1,3-diazole-phallacidin. *Proc Natl Acad Sci U S A.* Feb 1980;77(2):980-984.
53. Harder T, Scheiffele P, Verkade P, Simons K. Lipid domain structure of the plasma membrane revealed by patching of membrane components. *J Cell Biol.* May 18 1998;141(4):929-942.
54. Milev MP, Brown CM, Mouland AJ. Live cell visualization of the interactions between HIV-1 Gag and the cellular RNA-binding protein Staufen1. *Retrovirology.* 2010;7:41.
55. Maser MD, Trimble JJ, 3rd. Rapid chemical dehydration of biologic samples for scanning electron microscopy using 2,2-dimethoxypropane. *J Histochem Cytochem.* Apr 1977;25(4):247-251.
56. Svitkina TM, Verkhovsky AB, Borisy GG. Improved procedures for electron microscopic visualization of the cytoskeleton of cultured cells. *J Struct Biol.* Nov-Dec 1995;115(3):290-303.
57. Walev I, Hombach M, Bobkiewicz W, Fenske D, Bhakdi S, Husmann M. Resealing of large transmembrane pores produced by streptolysin O in nucleated cells is accompanied by NF-kappaB activation and downstream events. *FASEB J.* Feb 2002;16(2):237-239.
58. Rowin ME, Xue V, Irazuzta J. Hypothermia attenuates beta1 integrin expression on extravasated neutrophils in an animal model of meningitis. *Inflammation.* Jun 2001;25(3):137-144.
59. Lopez-Hernandez FJ, Ortiz MA, Piedrafita FJ. The extrinsic and intrinsic apoptotic pathways are differentially affected by temperature upstream of mitochondrial damage. *Apoptosis.* Aug 2006;11(8):1339-1347.
60. Yan F, Wu X, Crawford M, et al. The search for an optimal DNA, RNA, and protein detection by in situ hybridization, immunohistochemistry, and solution-based methods. *Methods.* Dec 2010;52(4):281-286.
61. Leser V, Drobne D, Pipan Z, Milani M, Tatti F. Comparison of different preparation methods of biological samples for FIB milling and SEM investigation. *J Microsc.* Feb 2009;233(2):309-319.
62. Zenklusen D, Singer RH. Analyzing mRNA expression using single mRNA resolution fluorescent in situ hybridization. *Methods Enzymol.* 2010;470:641-659.
63. Chen AK, Davydenko O, Behlke MA, Tsourkas A. Ratiometric bimolecular beacons for the sensitive detection of RNA in single living cells. *Nucleic Acids Res.* Aug 1 2010;38(14):e148.
64. Li CY, Gao SY, Terashita T, et al. In vitro assays for adhesion and migration of osteoblastic cells (Saos-2) on titanium surfaces. *Cell Tissue Res.* Jun 2006;324(3):369-375.
65. Wang HL, Miyauchi M, Takata T. Initial attachment of osteoblasts to various guided bone regeneration membranes: an in vitro study. *J Periodontal Res.* Oct 2002;37(5):340-344.
66. Leclair AM, Ferguson SS, Lagugne-Labarthet F. Surface patterning using plasma-deposited fluorocarbon thin films for single-cell positioning and neural circuit arrangement. *Biomaterials.* Feb 2011;32(5):1351-1360.
67. De Silva MN, Paulsen J, Renn MJ, Odde DJ. Two-step cell patterning on planar and complex curved surfaces by precision spraying of polymers. *Biotechnol Bioeng.* Apr 5 2006;93(5):919-927.

68. Kearns VR, Doherty PJ, Beamson G, Martin N, Williams RL. Friction transfer of polytetrafluoroethylene (PTFE) to produce nanoscale features and influence cellular response in vitro. *J Mater Sci Mater Med.* Jul 2010;21(7):2213-2226.

69. Lee GM, Huard TK, Palsson BO. Effect of Anchorage Dependency on Growth Rate and Monoclonal Antibody Production of Hybridoma Cells. *Biotechnology Letters.* 1988;10(5):307-312.

70. Chapeau C, Gagnon C. Nitrocellulose and polyvinyl coatings prevent sperm adhesion to glass without affecting the motility of intact and demembranated human spermatozoa. *J Androl.* Jan-Feb 1987;8(1):34-40.

71. Drobne D, Milani M, Leser V, Tatti F. Surface damage induced by FIB milling and imaging of biological samples is controllable. *Microsc Res Tech.* Oct 2007;70(10):895-903.